Title

Genetic Analysis of Mycobacterium tuberculosis Response to Stressors During Infection

Author

Dinshaw, Kayla Maree

Publication Date

2024

Peer reviewed|Thesis/dissertation

Genetic Analysis of *Mycobacterium tuberculosis* Response to Stressors During Infection

By

Kayla Dinshaw

A dissertation submitted in partial satisfaction of the

requirements for the degree of

Doctor of Philosophy

in

Molecular and Cell Biology

in the

Graduate Division

of the

University of California, Berkeley

Committee in charge:

Professor Sarah A. Stanley, Chair
Professor Arash Komeili
Professor Daniel Portnoy
Professor David Savage

Summer 2024

Abstract

Genetic Analysis of *Mycobacterium tuberculosis* Response to Stressors During Infection

By

Kayla Dinshaw

Doctor of Philosophy in Molecular and Cell Biology

University of California, Berkeley

Professor Sarah A. Stanley, Chair

Mycobacterium tuberculosis (Mtb) is a bacterial pathogen that establishes a pulmonary infection in the lung, and a quarter of the world's population is estimated to be latently infected with Mtb. The genetics behind Mtb's ability to survive in its primary niche, the phagosome of macrophages, is still under investigation. In chapter one, I introduce the history of Mtb forward genetics and discuss how laboratory techniques for forward genetics in Mtb have progressed over time. Then, I discuss mechanisms that are important for Mtb survival in the macrophage, including resistance against oxidative stress, nitrosative stress, and acidic pH. This chapter also reviews how Mtb acquires and metabolizes nutrients, specifically carbon and nitrogen sources.

In the second chapter, I present how a prokaryotic organelle, an encapsulin nanocompartment, is important for defense against oxidative stress in Mtb. Encapsulin nanocompartments are a method of compartmentalization in bacteria and archaea that are comprised of a proteinaceous cell surrounding an enzymatic cargo protein. Much of the previous work on encapsulin nanocompartments has been characterizing their biochemical properties rather than elucidating the contribution of nanocompartments to bacterial physiology. We show that Mtb assembles encapsulin nanocompartments containing the peroxidase DyP, which can detoxify hydrogen peroxide. A mutant lacking the DyP nanocompartment in Mtb is attenuated at acidic pH in the presence of hydrogen peroxide, and the DyP nanocompartment mutant is susceptible to pyrazinamide in broth and a murine mouse model.

Next, in chapter 3, the investigation of encapsulin nanocompartments is expanded to nontuberculosis mycobacteria, including *Mycobacterium smegmatis* (M. smeg) and *Mycobacterium abscessus* (M. abs). M. smeg and M. abs are predicted to encode the DyP nanocompartment in addition to a nanocompartment encoding a cysteine desulfurase (CyD). Genetic deletion nanocompartments in M. smeg and M. abs are largely unable to recapitulate the phenotypes observed in Mtb. However, M. smeg nanocompartment mutants have unique colony morphologies that are not observed in Mtb. Chapter 3 also investigates remaining hypotheses about Mtb nanocompartments, including the ability of Mtb DyP to use lipid peroxides as a substrate. We also explore the

possibility that KatG, a catalase peroxidase in Mtb, acts redundantly with Mtb DyP in infection models.

In chapter 4, random barcode-transposon site sequencing (RB-TnSeq), a technique for high-throughput forward genetics, is used to uncover the function of unknown genes in Mtb. RB-TnSeq is a pooled, transposon-mutant based method wherein each transposon contains a unique twenty nucleotide barcode, which bypasses steps of laborious protocols used for standard TnSeq screens. We exposed an RB-TnSeq library in Mtb to a chemical library of carbon sources, nitrogen sources, and stress compounds. From the genetic screen data for Mtb growth on carbon sources, we find that the Nuo complex, one of the three NADH dehydrogenases encoded by Mtb, is specifically required for growth on propionate and asparagine. Additionally, we explore the possibility of D-lactate to act as a carbon source for Mtb. Finally, we identify novel mutants that confer resistance to pretomanid, a recently approved tuberculosis antibiotic. Broadening our knowledge concerning Mtb genetics and how the bacterium survives in the face of immunological stressors *in vivo* is critical for furthering the development of novel bacterial therapeutics.

Table of contents

Abstract……..1
Table of contents……..……i
List of figures and tables……..……iii
Acknowledgements……..……iv

Chapter 1: Overview of Mycobacterium tuberculosis pathogenesis 1
1.1 Introduction to tuberculosis 1
1.2 History of forward genetics in Mtb 1
1.3 Survival of Mtb in host cells 3
1.3.1 Resistance against oxidative, nitrosative, and acid stress 3
1.3.2 Metabolism of carbon sources 4
1.3.3 Metabolism of nitrogen sources 5

Chapter 2: A nanocompartment system contributes to defense against oxidative stress in M. tuberculosis 7
2.1 Abstract 7
2.2 Introduction 7
2.3 Results 8
2.4 Discussion. 12
2.5 Materials and Methods 15
2.6 Acknowledgments. 19
2.7 Figures 20

Chapter 3: Analysis of nanocompartments in nontuberculosis mycobacteria 26
3.1 Abstract 26
3.2 Introduction 26
3.3 Results 28
3.3.1 Broth phenotypes in M. smeg nanocompartment mutants 28
3.3.2 M. smeg nanocompartment mutant colony morphology 29
3.3.3 Macrophage infections with M. smeg nanocompartment mutants 30
3.3.4 M. abs nanocompartment mutant phenotypes 30
3.3.5 Biochemistry of Mtb DyP 31
3.3.6 KatG and DyP redundancy in Mtb 32
3.4 Discussion 32
3.5 Materials and Methods 36
3.6 Figures 39

Chapter 4: Random barcode transposon-site sequencing in Mycobacterium tuberculosis to reveal the functions of unknown genes 48

4.1 Abstract 48
4.2 Introduction 48
4.3 Results 50
4.3.1 High-throughput fitness data with Mtb RB-TnSeq library 50
4.3.2 The nuo operon is required for growth on propionate 51
4.3.3 D-lactate as a potential carbon source for Mtb 52
4.3.4 Mutants in Rv1633-Rv1634 confer resistance to pretomanid 53
4.4 Discussion 53
4.5 Materials and Methods 55
4.6 Figures 59
Chapter 5: Summary of results and future directions 73
5.1 Characterization of mycobacterial nanocompartments 73
5.1.1 Summary of results 73
5.1.2 Future directions 73
5.2 Random-barcode transposon site sequencing in Mycobacterium tuberculosis 74
5.2.1 Summary of results 74
5.2.2 Future directions 75
References 76

List of figures and tables

Chapter 2

Figure 1. Mtb produces endogenous nanocompartments that package a peroxidase… 20
Figure 2. Nanocompartments protect Mtb from oxidative stress environments……..…...21
Figure 3. Susceptibility of Mtb nanocompartment mutants to oxidative and acid stress is mediated by free fatty acids……..….22
Figure 4. Nanocompartment mutants are attenuated for survival in macrophages and are more susceptible to pyrazinamide treatment……..23
Figure S1 Nanocompartment purification and complementation strategies……..…..24
Figure S2. SDS-PAGE analysis of DyP purified from *E. coli*……...……25

Chapter 3

Figure 1. In vitro M. smeg nanocompartment phenotypes ……..…..…39
Figure 2. Colony morphologies in M. smeg nanocompartment mutants……..…...41
Figure 3. Macrophage infection with M. smeg nanocompartment mutants……..…..43
Figure 4. Nanocompartment mutant phenotypes in M. abs……...….44
Figure 5. Lipid peroxides as a substrate for Mtb DyP…….……..46
Figure 6. Testing redundancy of DyP and KatG during Mtb infection…….……47

Chapter 4

Figure 1. RB-TnSeq screens, specific phenotypes, and cofitness……..……59
Figure 2. Comparison of TnSeq and BarSeq fitness…….……61
Figure 3. Nuo mutants are attenuated on propionate and asparagine…….……..62
Figure 4. Mutants attenuated for growth on lactate…….……..63
Figure 5. Rv133-Rv1634 confers resistance to pretomanid……...…..64
Figure S1. Protocol for construction of RB-TnSeq library in Mtb……...…..65
Table 1: Carbon source RB-TnSeq experiments …….……66
Table 2: Nitrogen source RB-TnSeq experiments…….……70
Table 3: Antibiotic/stress RB-TnSeq experiments…….……72

Acknowledgements

First, I would like to thank my thesis advisor, Sarah Stanley, for her mentorship and guidance throughout my PhD. I'm thankful to have a PI who has provided me with so much support and encouragement while training me to become a better scientist. Thank you to my thesis committee, Arash Komeili, Dan Portnoy, and David Savage as well as the Cox and Vance labs for your insightful comments and helpful feedback on my thesis work.

I would also like to thank my previous science mentors before starting graduate school at UC Berkeley. Ann Miller and the rest of the lab at the University of Michigan, thank you for teaching me how to be a scientist and instilling the confidence in me to go to graduate school. Stuart Yuspa, Brandi Carofino, and the rest of the lab NIH, thank you for your mentorship and sharing your breadth of knowledge with me. I owe it to you all for preparing me for graduate school.

Next, I would like to thank all Stanley lab members – both past and present – for making my time in the Stanley lab so fun and keeping me sane. I have learned so much from everyone. My undergraduate students, Thomas and Samantha, it was a joy to work with you, and thank you for your hard work and dedication to the lab.

To the 2018 Berkeley MCB cohort, thank you for providing a layer of sanity to graduate school. I feel lucky to have entered UC Berkeley with such a supportive and fun environment.

To my non-graduate school friends from high school, college, D.C., thank you for providing me with an additional layer of sanity, laughter, and always being a quick phone call away.

To my classmate, friend, and partner Costa, thank you for supporting me at every step.

Lastly, to my parents and to my twin brother Brandog, thank you for your unwavering and unconditional support.

Chapter 1: Overview of Mycobacterium tuberculosis pathogenesis

1.1 Introduction to tuberculosis

Mycobacterium tuberculosis (Mtb) is the bacterium that causes the disease tuberculosis. Until the COVID-19 pandemic, tuberculosis was the number one cause of mortality from a single infectious agent[1]. In 2022, the number of deaths from tuberculosis were almost two times those from HIV/AIDS[1]. Mtb is estimated to latently infect one-quarter of the world's population and around 5-10% of those individuals will progress to active disease[2]. Mtb is spread through aerosols, thus tuberculosis typically presents as a pulmonary infection, although Mtb can infect other tissues such as the central nervous system, bone, kidneys, and lymph nodes[3].

The genus *Mycobacterium* consists of over 170 species, traditionally categorized into "fast" and "slow" growers, with Mtb belonging to the slow growers[4]. Although most tuberculosis infections are a result of infection with Mtb, tuberculosis can be the result of infection by any other member of the Mycobacterium tuberculosis complex, which includes *Mycobacterium bovis*, *Mycobacterium africanum*, *Mycobacterium microti*, *Mycobacterium caprae*, *Mycobacterium pinnipedii,* and *Mycobacterium canettii*. Nontuberculosis mycobacteria (NTMs) consist of all mycobacteria except those that cause tuberculosis (*Mycobacterium tuberculosis* complex) and leprosy (*Mycobacterium leprae*). NTMs are environmental bacteria, often residing in soil and water, that can infect and cause severe disease in immunocompromised hosts. In contrast, Mtb is an obligate human pathogen and does not have an environmental or animal reservoir but is thought to have evolved from an environmental mycobacterium[5,6]. It is hypothesized that a key step towards adaptation in human hosts was the step-wise adaptation to survive in protozoa such as amoebae[6]. Amoebae often ingest environmental bacteria and share features with professional phagocytes such as macrophages[7], the primary niche of Mtb.

The genomic features of Mtb that enable its unique adaptation to human hosts are largely unknown. Sequencing of mycobacterial strains have revealed that known virulence factors such as the ESX-1 type VII secretion system, PhoPR two-component system, DosR/S/T regulon, proline-glutamic acid (PE) family, and proline-proline-glutamic acid (PPE) family are present in NTMs[5,8]. Therefore, it is unlikely that one genomic feature is responsible for Mtb human adaptation. Nonetheless, there is much to uncover considering Mtb genetics and how it evolved into a successful human pathogen.

1.2 History of forward genetics in Mtb

The common Mtb lab strain H37Rv, first isolated in 1905, has a 4.4 megabase GC-rich genome containing about 4000 genes[9]. Interestingly, the assembled genome sequence published in 1998 revealed that a large fraction of the Mtb genome is dedicated to lipid metabolism and biosynthesis when compared to bacteria such as *Escherichia coli*[9]. Yet, genes for glycolysis, the pentose phosphate pathway, and the tricarboxylic acid and glyoxylate cycles are all still present[9]. In addition, it was clear that Mtb has the genetic components to synthesize essential amino acids, vitamins, and co-factors[9]. The assembled genome also revealed 10% of the Mtb genome is dedicated to the PE and PPE gene families, which contain Pro-Glu and Pro-Pro-Glu motifs near the N-terminus, respectively. Precise functions were attributed to 40% of predicted proteins, 44% of proteins had some similarity to other proteins, and 16% of the Mtb genome had no known protein function and was hypothesized to have a unique mycobacterial function[9]. While

whole genome sequencing of Mtb was informative, the exact function of many genes remained elusive.

An early technique for forward genetics in Mtb was signature-tagged mutagenesis (STM). In STM, transposons insert into the Mtb genome and disrupt gene function. Each transposon has a unique DNA signature-tag that can be distinguished by PCR-amplification and hybridization to a master dot-blot filter. Signature-tagged mutagenesis was low-throughput and typically conducted in pools of 48-96 mutants. The input and output transposon pools are compared to evaluate drop out of transposon mutants during the condition of interest, most commonly a mouse infection model[10]. STM in mouse infections with Mtb revealed the first genetic evidence for the importance of lipids in Mtb virulence. Mutants in genes such as *pps*, *fadD26*, *fadD28*, and *mmpL7*, which are involved in biosynthesis or transport of the cell-wall associated lipid phthiocerol dimycocerosate (PDIM) were not able to grow in mice[11,12]. Follow up STM studies demonstrated that *mmpL8* is required for sulfolipid-1 production and also required for full virulence in mice, likely due to its ability to transport other unidentified molecules[13]. STM conducted with Mtb in a macrophage infection uncovered mutants in ABC transporters that were impaired in binding to host cells[14].

The next development in forward genetics came with transposon site hybridization (TraSH), where transposon mutagenesis was combined with microarray hybridization. TraSH libraries contained around 200,000 mutants, a significant increase in the number of transposon mutants analyzed by STM[15]. TraSH was used in Mtb to determine essential genes *in vitro*[15] and genes required for growth *in vivo* in macrophages[16] and in mice[17].

With advances in next generation sequencing, TraSH evolved into transposon site sequencing (TnSeq), where transposon libraries are characterized with Illumina sequencing[18]. TnSeq allows for single-base pair resolution sequencing of transposon insertions along with quantification of their relative abundance[18]. Compared to TraSH, TnSeq provides higher resolution and thus a more precise categorization of essential genes in vitro[18,19]. Currently, TnSeq screens have been conducted in many conditions related to Mtb biology, including, but not limited to, diverse mouse models[20], cholesterol catabolism[18], acid and oxidative stress[21], hypoxia[22], and tuberculosis antibiotics[23].

While TnSeq has proven to be a useful technique in Mtb for uncovering gene function, there are some caveats. Protocols for TnSeq are often laborious and require many steps. Mtb must be plated on solid agar and incubated for 18-21 days after which time colonies are scraped and resuspended in liquid medium for genomic DNA extraction. Next steps involve DNA shearing, end repair, A-tailing of DNA fragments, and adaptors are ligated with multiple purification steps in between[24]. Transposon junctions are PCR-amplified and subjected to next generation sequencing[24]. The sequencing reads then require a computationally intensive alignment back to the genome[25]. In chapter 4, we investigate a more high throughput method of conducting transposon insertion screens in Mtb by using a barcoded transposon library (RB-TnSeq)[26]. Barcoded transposons are simply PCR-amplified prior to sequencing, allowing for high-throughput genetic screens[26].

More recently, CRISPR has been adapted for use in mycobacteria[27,28]. While the CRISPRi with commonly-used Cas9 from *Streptococcus pyogenes* has poor efficiency in mycobacteria, CRISPRi using the CRISPR1 Cas9 from *Streptococcus thermophilus* results in robust knockdown efficiency[28]. This enabled development of a robust CRISPRi screening platform in Mtb[29]. The Mtb CRISPRi library was first used to assay the

contribution of genes annotated as essential to *in vitro* growth and found that "essential" genes are highly variable in their degree of essentiality for *in vitro* growth[29]. A follow up study used the Mtb CRISRPi platform to screen for chemical-genetic interactions of nine tuberculosis antibiotics at a range of concentrations[30]. CRISPRi has overcome the challenge for investigating essential genes in mycobacteria, which transposon-based methods are unable to accomplish.

Despite advances in technology, much of the genome of Mtb remains poorly annotated. Annotations include "conserved hypothetical", genes described as "predicted" or "possible", and genes described by something that is not function ("phosphate-starvation induced" or "threonine rich")[31]. The poorly annotated genome could be attributed to the challenges of working with Mtb in the laboratory given its slow doubling time and necessity for BSL-3 facilities. More high-throughput and comprehensive methods such as TnSeq, RB-TnSeq, and CRISPRi have and will continue to expand our knowledge of Mtb gene function.

1.3 Survival of Mtb in host cells

1.3.1 Resistance against oxidative, nitrosative, and acid stress

Mtb is an intracellular pathogen that primarily resides in the phagosome of macrophages. Upon infection, macrophages initiate an arsenal of host defenses. These include the assembly of the NADPH oxidase on the phagosomal membrane to generate a respiratory burst of superoxide (O_2-), the induction of NOS2 to generate nitric oxide (NO), and the acidification of the phagolysosome by the vacuolar ATPase[32]. Superoxide generated by NADPH oxidase can dismutate to hydrogen peroxide (H_2O_2) and hydroxyl radicals[33]. Superoxide reaction with nitric oxide forms peroxynitrite (ONOO-), which has enhanced reactivity[34]. These oxidative and nitrosative stressors damage DNA, protein, and lipids, but Mtb has evolved various mechanisms of resistance to grow inside of macrophages.

In Mtb, two superoxide dismutates, SodA and SodC, catalyze the reaction of superoxide to hydrogen peroxide and molecular oxygen. SodA and SodC have been demonstrated to function extracellularly or on the surface of the bacteria, and thus likely detoxify superoxide in the phagosomal lumen[35–37]. To detoxify peroxides, Mtb encodes ~15 putative peroxidases[38]. The catalase-peroxidase KatG can detoxify hydrogen peroxide[39,40] as well as peroxynitrite[41]. AhpC and AhpD, alkylhydroperoxide reductases, have the ability to use hydrogen peroxide and alkylhydroperoxides as substrates *in vitro*[42], and AhpC can detoxify peroxynitite[43]. In chapter 2, we demonstrate that a bacterial nanocompartment containing the peroxidase DyP reduces hydrogen peroxide and is important for defense against oxidative stress in acidic conditions[21].

Mycothiol is a small molecular weight thiol that acts as reducing agent in actinobacteria, including mycobacteria[44]. Produced in millimolar quantities, mycothiol is functionally equivalent to glutathione, found in eukaryotes and other bacteria[44], and thus, is important for maintaining intracellular redox homeostasis[45]. Mtb contains other macromolecules that can scavenge reactive oxygen species. For example, lipoarabinomannan, a cell-wall associated glycolipid, scavenges cytotoxic oxygen free radicals[46].

Mtb's thick cell wall can not only act as a radical scavenger but also functions as a strong barrier against various insults, including protons. Because Mtb primarily resides in the phagosome and phagolysosome, understanding defense against acidic pH has

relevance to Mtb biology. In resting macrophages, Mtb has the ability to inhibit phagosome-lysosome fusion[47] and resides in a mildly acidic phagosome at a pH of ~6.2[48]. Upon activation of macrophages with the cytokine IFN-γ, the phagolyosomal compartment becomes acidified and reaches pH values between 4.5-5[49]. This acidic pH may activate host enzymes such as acid-dependent lysosomal hydrolases[50] and potentiate the toxicity of reactive oxygen and reactive nitrogen species[49]. Notably, Mtb maintains a neutral intracellular pH in the presence of acidic external pH[51]. If protons do cross the cell wall, intracellular neutral pH is thought to be maintained by the action of proton pumps, amino acid decarboxylation, and ammonia production[49].

Acid-sensitive mutants in Mtb have been identified, yet exact mechanisms of acid resistance are unknown. These genes include a magnesium transporter (*mgtC*), a pore-forming protein (*ompA*), a unadecaprenol pyrophosphate phosphatase (*bacA*), and a membrane bound serine protease (*Rv3671c*)[49,51–53]. Depending on the gene, these mutants tend to be susceptible to other types of stress, including oxidative stress, nitrosative stress, detergents, and antibiotics[52]. Gene expression analysis using microarrays at an acidic pH of 5.5 revealed that genes involved in fatty acid metabolism are upregulated at low pH[54]. Further microarray gene-expression analysis was conducted in Mtb-infected macrophages with and without the vacuolar ATPase inhibitor concanamycin A to evaluate the intracellular acid-responsive Mtb transcriptome[55]. Many of the induced genes are regulated by the PhoPR two-component system, which is involved in regulation of lipid biosynthesis genes. In line with these gene expression datasets, it was discovered that Mtb can grow as low as a pH of 4.5 in the presence of lipids[56].

1.3.2 Metabolism of carbon sources

To multiply during infection, Mtb must acquire and metabolize nutrients from the host. Mtb is considered to have a large metabolic capacity and versatility, especially in regards to lipid metabolism, and contains the genetic components for glycolysis, the pentose phosphate pathway, tricarboxylic acid, glyoxylate cycle, methylcitrate cycle, and methylmalonyl-CoA pathway[9]. Mtb differs from many bacteria in its ability to co-catabolize carbon sources. For instance, when given both glucose and acetate, glucose was fluxed through the glycolysis pathway, and acetate simultaneously incorporated through gluconeogenesis[57]. *In vitro*, Mtb generates the most biomass when grown on glycerol[57]. Although glycerol is a major component of the liquid media used for laboratory growth of Mtb, it is not considered to be an important carbon source during infection. Glycerol kinase (*glpK*), which converts glycerol to glycerol 3-phosphate, is not required for Mtb growth in a mice[58].

Mtb also grows on sugars *in vitro*, such as glucose and trehalose. The *in vivo* environment faced by Mtb is not thought to be especially sugar rich, and Mtb does not upregulate sugar metabolism genes in macrophages or mice[59,60]. Trehalose is not produced by mammalian cells, but Mtb releases trehalose-containing glycolipids that are re-imported by the bacteria. The LpqY-SugA-SugB-SugC carbohydrate transporter was shown to be required for growth in a mouse model of infection, highlighting the importance of trehalose recycling[61]. Mtb encodes two genes for glucokinase, *ppgK* and *glkA*, which convert glucose to glucose-6-phosphate, the first committed step in glucose metabolism. *ppgK* and *glkA* double mutants are attenuated in a chronic stage of infection, suggesting

that glucose phosphorylation may be important late in infection[62]. Mtb has also demonstrated the ability to grow on amino acids as a primary carbon source, although much of the research on amino acid metabolism is conducted in the context of nitrogen utilization[63].

The primary carbon sources thought to be important during infection are lipids, including fatty acids and cholesterol. In the in 1950's, it was shown that Mtb collected from mouse lungs had increased metabolic activity when cultured on lipids[64]. Accordingly, lipid metabolism genes are upregulated in mouse infection models[59], including the fatty acid transporter *mce1*, which is also important for growth *in vivo*[17]. Growth on fatty acids in bacteria requires β-oxidation to generate acetyl-CoA, which is shuttled into the TCA cycle. To prevent loss of carbon in the TCA cycle, the glyoxylate shunt converts isocitrate into succinate and glyoxylate. When isocitrate lyase (*icl*), an enzyme of the glyoxylate shunt was deleted, Mtb was attenuated for virulence in activated macrophages and mouse infection[65,66]. Metabolism of odd-chain fatty acids, branched-chain fatty acids, and cholesterol generates a three-carbon molecule propionyl-CoA. Because propionyl-CoA is toxic to cells, it must be detoxified by either the methylcitrate cycle, methylmalonyl-CoA pathway, or shuttled into lipid biosynthesis. Mutants in the methylcitrate cycle, *prpC* and *prpD*, are attenuated in a bone marrow macrophage infection but not in a mouse infection[67]. Interestingly, *icl,* present in two different isoforms, also appears to function as a methylcitrate lyase in the methylcitrate cycle in addition to its role as an isocitrate lyase in the glyoxylate cycle. Lastly, gluconeogenesis is another metabolic pathway required growth on lipids. Phosphoenolpyruvate carboxykinase (PEPCK), encoded by *pckA*, catalyzes the first committed step of gluconeogenesis, and a deletion of PEPCK is not able to persist in macrophages or mice[62]. Due to the overlap of enzymes in functioning in multiple metabolic pathways, it is still unclear which exact carbon sources Mtb is utilizing *in vivo*. However, infections of mice with enzymatic mutants have been informative in understanding which metabolic pathways and categories of macromolecules may be important during infection.

1.3.3 Metabolism of nitrogen sources

In addition to carbon, Mtb must acquire nitrogen from the host due to its importance for amino acids, nucleotides, organic co-factors, and cell wall components[68]. Interestingly, Mtb encodes the biosynthetic machinery for all essential amino acids and nucleotides[9]. While most bacteria seem to prefer ammonium as a nitrogen source, it is thought that Mtb may prefer amino acids[69,70]. Nonetheless, Mtb can import and use ammonium, which likely enters the cell through the transporter Amt and is converted into glutamine, as Mtb is thought to assimilate ammonium mainly through the glutamine synthetase and glutamine oxoglutarate aminotransferase sytem[68,71]. Another inorganic nitrogen source used by Mtb is nitrate, which is transported into the cell by NarK2, reduced to nitrite by the nitrate reductase NARGHJI, and then reduced to ammonium by NirBD[68,72].

Amino acids enter the bacterial cell through amino acid transporters and subsequently undergo a deamination reaction to release ammonium. For instance, AnsP1 and AnsP2 transport aspartate and asparagine, respectively, and the deamination of asparagine is catalyzed by the asparaginase AnsA[68]. Host radiolabelled carbon spectral analysis revealed that Mtb uptakes alanine, aspartate, asparagine, glutamate, and glutamine from the host, yet some amino acids, such as valine, are primarily synthesized

by the bacterium[73]. In line with these results, host ^{15}N-labelled asparagine and aspartate were imaged inside the bacterium in macrophages[74,75]. Further supporting the hypothesis that Mtb acquires amino acids from the host, the expression of host amino acid transporters, such as SLC1A2 that imports glutamate and aspartate, are upregulated upon Mtb infection[76]. Given that both carbon and nitrogen metabolism in Mtb are required for establishing and maintaining an infection, future studies uncovering the complex metabolic network of Mtb will be informative for developing future antimicrobial therapies.

Chapter 2: A nanocompartment system contributes to defense against oxidative stress in *M. tuberculosis*

This work has been published in eLife
Lien KA*, Dinshaw K*, Nichols RJ, Cassidy-Amstutz C, Knight M, Singh R, Eltis LD, Savage DF, Stanley SA. 2021. A nanocompartment system contributes to defense against oxidative stress in Mycobacterium tuberculosis. *Elife* **10**. doi:10.7554/eLife.74358

2.1 Abstract

Encapsulin nanocompartments are an emerging class of prokaryotic protein-based organelle consisting of an encapsulin protein shell that encloses a protein cargo. Genes encoding nanocompartments are widespread in bacteria and archaea, and recent works have characterized the biochemical function of several cargo enzymes. However, the importance of these organelles to host physiology is poorly understood. Here, we report that the human pathogen *Mycobacterium tuberculosis* (Mtb) produces a nanocompartment that contains the dye-decolorizing peroxidase DyP. We show that this nanocompartment is important for the ability of Mtb to resist oxidative stress in low pH environments, including during infection of host cells and upon treatment with a clinically relevant antibiotic. Our findings are the first to implicate a nanocompartment in bacterial pathogenesis and reveal a new mechanism that Mtb uses to combat oxidative stress.

2.2 Introduction

The success of *M. tuberculosis* as a human pathogen results from its ability to avoid, resist or subvert immunological mechanisms that are effective against most pathogens. *M. tuberculosis* has a remarkable ability to withstand the microbicidal arsenal of host macrophages, including the low pH of the lysosome and a diverse array of toxic reactive oxygen species produced by the host respiratory burst. However, relatively little is known about the molecular mechanisms of resistance to these toxic insults.

Upon phagocytosis of a pathogen, macrophages and neutrophils unleash a potent microbicidal arsenal, including a respiratory burst that leads to the rapid release of reactive oxygen species (ROS) that kill and degrade most microbes [77–79]. The production of ROS is initiated when NADPH oxidase assembles on pathogen-containing phagosomes and initiates a series of reactions that produce superoxide, hydrogen peroxide, hyperchlorous acid, lipid peroxides, and other toxic reactive molecules. Importantly, *M. tuberculosis* is highly resistant to oxidative stress, enabling the bacterium to survive within macrophages and neutrophils and establish chronic infection[80]. Although some oxidative defense mechanisms have been characterized[81–83], the *M. tuberculosis* genome encodes a large number of enzymes that could participate in defense against oxidative stress that remain uncharacterized. For example, *M. tuberculosis* encodes ~15 peroxidases, a class of enzymes with diverse functions that form the front line of oxidative defense in bacteria[38,84]. It is unclear why *M. tuberculosis* encodes such a diversity of peroxidases, and little is known about what individual roles these enzymes may play in both resistance to oxidative stress and in normal bacterial physiology. One possibility is that specific peroxidase genes may participate in defense against different types of ROS generated during the respiratory burst. One of the most intriguing peroxidases encoded by *M. tuberculosis* is DyP, a member of the dye-decolorizing peroxidase family of proteins.

DyP enzymes are unique amongst peroxidases in that some family members have been shown to have optimal activity at pH 4-5[84–86]. Furthermore, DyP is the only *M. tuberculosis* peroxidase predicted to be packaged inside a proteinaceous organelle known as a bacterial nanocompartment[87].

Bacterial cells were long thought to lack compartmentalization of function. However, the identification of organelle-like structures including microcompartments, anammoxosomes, magnetosomes and, most recently, encapsulin nanocompartments have revolutionized our understanding of bacterial cell biology[88–90]. Characterized nanocompartments are proteinaceous shells that are 24 to 45 nm in diameter and comprised of 60-240 subunits of a single protomer[91,92]. This shell surrounds ("encapsulates") an enzymatic cargo protein[92]. Although putative encapsulin systems have been identified in >900 bacterial and archaeal genomes[93,94], very little is known about their physiological function. Based on genomic organization, encapsulin systems are often predicted to compartmentalize enzymes involved in oxidative stress defense, iron storage, and anaerobic ammonium oxidation[93]. However, the function of an encapsulin system has only ever been demonstrated in a single bacterial species, *Myxococcus xanthus*[94], and the physiological role of nanocompartments is largely unexplored.

Here we demonstrate that a *M. tuberculosis* nanocompartment containing DyP is crucial for resisting oxidative stress at low pH. Mutants lacking the nanocompartment are highly attenuated when exposed to H_2O_2 at pH 4.5, the pH of the lysosome. We show that this attenuation is linked to fatty acid metabolism in the bacteria. Further, we show that encapsulation of the DyP enzyme promotes its function, the first report to demonstrate a role for encapsulation in endogenous bacterial physiology. Finally, we show that the *M. tuberculosis* nanocompartment system is required for full growth in macrophages, and for resistance to the antibiotic pyrazinamide, demonstrating the importance of this system for a globally significant pathogen.

2.3 Results

The *Mycobacterium tuberculosis* genome encodes the predicted encapsulin gene *Rv0798c/*Cfp29[95] in a two-gene operon with *Rv0799c*, the dye-decolorizing peroxidase DyP (Figure 1A). Overexpression of the predicted Mtb encapsulin gene in *Escherichia coli* was previously shown to result in the formation of nanocompartment-like structures[96]. Three potential cargo proteins for the nanocompartment were proposed based on a putative shared encapsulation targeting sequence: DyP, FolB, and BrfB. In *E. coli*, overexpression of each protein with Cfp29 resulted in encapsulation. However, this study did not address whether Mtb produces endogenous nanocompartments or identify the specific function of these compartments in Mtb biology. A transposon screen has identified Cfp29 as a gene required for growth in mice[97] and Cfp29 has long been known as an immunodominant T cell antigen in both mice and human TB patients[98]. Taken together, these results suggest that Mtb may produce an encapsulin nanocompartment that is important for pathogenesis.

To confirm the previous finding that heterologous expression of *Rv0798c* and *Rv0799c* in a host species results in the assembly of an encapsulin system, we expressed these genes in *E. coli* and isolated nanocompartments. Clarified protein lysates from *E. coli* were purified by ultracentrifugation and size exclusion chromatography. Assembled

encapsulin nanocompartments are distinguishable by their high molecular weight[92]. Indeed, a fraction from the purification contained a high-molecular weight species >260 kDa observable on an SDS-PAGE gel (Figure S1A). Fractions containing putative nanocompartments were pooled and imaged using transmission electron microscopy, which revealed the presence of icosahedral structures with the expected diameter of ~25 nm (Figure 1B, 1C).

To determine whether Mtb produces nanocompartments under normal laboratory growth conditions, we performed an ultracentrifugation-based nanocompartment isolation strategy using wild-type H37Rv strain bacteria grown to mid-log phase (Figure S1B). Mass spectrometry analysis of the nanocompartment fraction identified both the encapsulin protein Cfp29 and the peroxidase DyP (Figure 1D). TEM analysis confirmed the presence of nanocompartment particles ~25 nm in diameter (Figure 1E). Interestingly, Rv1762c, a protein of unknown function, was consistently identified in purified nanocompartment preparations from Mtb (Figure 1D). We were unable to identify either FolB or BrfB in nanocompartments from Mtb, suggesting that these proteins are not endogenous substrates for encapsulation under normal laboratory growth conditions for Mtb.

Cfp29 ('culture filtrate protein 29') was originally identified in the supernatants of Mtb cells grown in axenic culture[87,99] . As Cfp29 lacks a secretory signal sequence and is part of a large macromolecular complex, it is unclear how a nanocompartment could be actively secreted. However, nanocompartment structures are remarkably stable and it is possible that nanocompartments released from dying bacteria accumulate in culture as they are highly resistant to proteolysis/degradation[92,99].

DyP proteins are known to have low pH optima[77]. To demonstrate that Mtb DyP has a similarly low pH optimum, SUMO-tagged unencapsulated DyP was purified from *E. coli* (Figure S2), and the peroxidase activity was evaluated at a range of pH values using the ABTS (2,2'-azino-bis(3-ethylbenzothiazoline-6-sulfonic acid)) dye-decolorizing assay previously used to characterize DyP proteins[87,100]. Similar to the *Vibrio cholerae* DyP[98], purified Mtb DyP had increased enzymatic activity in low pH environments, with the greatest efficacy at pH 4.0, the lowest pH tested (Figure 1F). We next tested the ability of encapsulated DyP to degrade ABTS across a range of pH values. Similar to free DyP, the encapsulated enzyme had the highest activity at pH ~4.0 (Figure 1G). Taken together, these data demonstrate the stability and functionality of *M. tuberculosis* nanocompartments under acid stress a condition that mimics the host lysosomal environment. The Mtb DyP protein was previously shown to function as a bona fide dye-decolorizing peroxidase[99,100]. Because peroxidases consume H_2O_2, they often participate in defense against oxidative stress[100]. During macrophage infection, the phagocytes initiate an oxidative burst that exposes Mtb to H_2O_2[101,102]. We therefore reasoned that DyP-containing nanocompartments may function to protect Mtb from H_2O_2-induced stress. To test this hypothesis, we created a mutant strain lacking both genes from the nanocompartment operon (Figure 1A, Δoperon). Lysates from Δoperon mutants were used for nanocompartment purification (data not shown) and western blot analysis using an antibody for Cfp29 as a probe (Figure S1C). Data from these analyses revealed that Δoperon mutants cannot produce viable nanocompartments. In addition, we isolated a transposon mutant (*DyP::Tn*) containing an insertion in *DyP*, a mutation that eliminated expression of both Cfp29 and DyP (Figure S1D).

To test whether DyP-containing nanocompartments are required for defense against H_2O_2, we exposed wild-type and *DyP::Tn* Mtb to increasing concentrations of H_2O_2 and monitored bacterial survival. Mutants lacking DyP nanocompartments were more susceptible to H_2O_2 when compared with wild-type bacteria as measured by OD_{600} (Figure 2A) and by plating for CFU (Figure 2B). However, the phenotype was relatively modest. We next reasoned that DyP nanocompartments might be required to resist oxidative stress in acidic environments that more closely mimic the *in* vivo environment. During infection, Mtb bacilli encounter the low pH of the phagolysosome, and *vivo* environment. During infection, Mtb bacilli encounter the low pH of the phagolysosome, and the ability to tolerate low pH is required for Mtb survival in both infected macrophages and mice[103]. We therefore tested the susceptibility of DyP mutants to a combination of H_2O_2 and acid stress (pH 4.5). Wild-type Mtb was able to withstand these conditions and did not significantly decrease in number over a three-day exposure period (Figure 2C). In contrast, the Δoperon mutant was resistant to each stressor individually, but was highly susceptible to H_2O_2 at pH 4.5 (Figure 2C). Thus, DyP-containing nanocompartments are required to protect bacteria from oxidative stress at low pH.

We next sought to determine whether encapsulation of DyP is important for its activity in bacterial cells. To accomplish this, *DyP::Tn* mutants were complemented with constructs expressing DyP alone (pDyP), Cfp29 encapsulin alone (pCfp29), or both proteins (pOperon). As expected, expression of DyP did not restore production of nanocompartments, whereas expression of Cfp29 alone resulted in the formation of empty nanocompartment structures (Figure S1D). Co-expression of both proteins resulted in the formation of DyP-containing nanocompartments in the *DyP::Tn* mutant (Figure S1D). We exposed the full set of complemented mutants to H_2O_2 at pH 4.5 and determined survival after three days by plating for CFU. As expected, *DyP::Tn* was attenuated for survival under these conditions when compared to wild-type bacteria (Figure 2D). Restoring expression of the nanocompartment shell protein in the absence of DyP had no effect on bacterial survival (Figure 2D). Complementation by overexpression of unencapsulated DyP was sufficient to confer almost wild-type levels of resistance to oxidative and acid stress (Figure 2D). However, complementation with both Cfp29 and DyP resulted in enhanced resistance to these stressors when compared to mutants complemented with DyP alone (Figure 2D), suggesting that encapsulation of DyP enhances its function.

In the mutant complemented with DyP alone, it is possible that overexpression of the peroxidase compensates for the lack of encapsulation. We therefore examined the importance of DyP encapsulation in mutant strains in which we deleted *Cfp29* only (Δcfp29). Deletion of *Cfp29* resulted in a ~0.5 log decrease in bacterial viability after three days of exposure to H_2O_2 at pH 4.5, confirming that encapsulation of the peroxidase in the shell protein is important for full protection (Figure 2E). As expected, greater attenuation was observed in the mutant lacking both DyP and Cfp29 (Δoperon). Complementation of the Δcfp29 fully restored resistance (Figure 2F). Taken together, these data demonstrate that encapsulation of DyP has a modest, yet significant impact on protection against oxidative stress in low pH conditions.

We next sought to test whether nanocompartment mutants have altered redox homeostasis in the presence of oxidative stress. We transformed wild-type and mutant strains with Mrx1-roGFP, a fluorescent reporter of redox potential in mycobacteria[101].

Remarkably, the Δoperon mutant had an intracellular environment at baseline that was more oxidizing than wild-type bacteria exposed to H_2O_2 (Figure 2G), indicating a failure of redox homeostasis in mutants lacking the DyP encapsulin system. This oxidizing cellular environment was further enhanced by treatment with H_2O_2 (Figure 2G). We did not observe a difference in the redox state of Δcfp29. Thus, mutants lacking DyP-containing nanocompartments exhibit significant dysregulation of redox homeostasis.

The Mtb genome encodes ~18 putative peroxidase genes, including DyP. To determine whether other bacterial peroxidases participate in the defense against oxidative stress at low pH, we performed a transposon sequencing (Tn-seq) screen[102,103]. To do so, we created a transposon library containing ~100K individual transposon mutants and exposed this library to H_2O_2 at pH 4.5 for three days, at which point the surviving bacteria were plated. Transposon gene junctions were amplified and sequenced from the recovered bacteria and the sequencing data were analyzed using TRANSIT[106–108] (Table S1). These data revealed that of the 18 putative enzymes encoded by Mtb that could be involved in oxidative defense, including peroxidases, catalases, and superoxide dismutases, only 2 genes were required for survival in the culture conditions—*DyP* and *KatG* (Figure 3A). *KatG* encodes a catalase-peroxidase that is important for defense against oxidative stress in the host[104,105]. Coincidentally, KatG is also required for activation of isoniazid (INH), a central component of anti-TB therapy. Approximately 10% of TB cases are caused by INH-resistant bacteria, many of which have loss-of-function mutations in KatG[106]. Importantly, KatG variants that do not activate INH often display a concomitant decrease in peroxidase and catalase activity[107–109]. Both the high proportion of KatG mutant bacteria in the human population and studies of virulence in animals suggest that KatG mutants are still capable of growth *in vivo*[105,110]*.* The fact that both DyP and the KatG mutants are important for survival in oxidative stress at low pH suggests that the DyP nanocompartment may provide redundancy that compensates for a loss of KatG in INH resistant strains of Mtb.

In the Tn-seq data, we observed that mutants involved in lipid or cholesterol metabolism were also attenuated when exposed to H_2O_2 at pH 4.5 (Figure 3B). *M. tuberculosis* biology is highly linked to lipid biology; Mtb granulomas are rich in free fatty acids[111] and the bacteria utilize lipids as a source of nutrition both during macrophage infection *ex vivo* and growth *in vivo*[62,112,113]. In particular, mutants containing transposon insertions in three independent subunits of the Mce1 complex, which is required for import of fatty acids[114], were susceptible to oxidative stress under acidic conditions (Figure 3B). The standard Mtb culture medium, 7H9, contains Bovine Serum Albumin (BSA), which has binding sites for fatty acids and may also serve as a cholesterol shuttle in serum[115,116]. We hypothesized that import of fatty acids might protect bacteria from toxicity of fatty acids carried by albumin in the medium that become toxic under oxidative stress and low pH. We therefore tested whether fatty acids are required for the susceptibility of Δoperon mutants using exposure to acid and oxidative stress in Sauton's broth, a minimal medium that lacks BSA, and found that in the absence of fatty acids the Δoperon mutants persisted to the same degree as wild-type bacteria (Figure 3C). To test whether lipids bound to BSA mediate the susceptibility of DyP mutants to acid and oxidative stress, we cultured wild-type and Δoperon Mtb in media constituted with fatty acid-free BSA and exposed the bacteria to H_2O_2 at pH 4.5 for three days. In the absence of BSA bound lipids, we found that the Δoperon mutant was not susceptible to oxidative stress at low pH (Figure 3D).

7H9 medium prepared with lipid free BSA was then reconstituted with oleic acid, an abundant lipid found in mammalian systems[117]. Reconstitution of fatty acid free medium with oleic acid restored toxicity to nanocompartment mutants under conditions of acid and oxidative stress (Figure 3D). Taken together, these data suggest that the phagosomal lipids used by Mtb as a carbon source may be toxic to bacteria lacking functional nanocompartments under conditions of oxidative stress

We considered the possibility that lipids present in the medium might disrupt Mtb membranes, resulting in altered pH homeostasis, and a drop in cytosolic pH. Interestingly, in acidified medium we found that the intracellular pH of wild-type bacteria dropped from ~pH 7.5 to ~ pH 6.2 and this decrease was dependent on the presence of albumin-bound fatty acids (Figure 3E). These data confirm published results demonstrating that the cytosolic pH of Mtb drops significantly during acid exposure[118]. A lower cytosolic pH would possibly impair the function of many other bacterial enzymes important for resisting oxidative stress and place increasing importance on enzymes that can function in acidic environments, such as DyP (Uchida et al., 2015). Taken together, these data may explain why functional nanocompartments are critical for bacterial survival when Mtb is exposed to acid and oxidative stress in a fatty acid-rich environment.

Our *in vitro* findings that DyP nanocompartments are important for defense against a combination of oxidative stress, low pH, and fatty acids suggested that this system may be important for Mtb survival in the phagosomal environment. Therefore, we sought to determine whether DyP nanocompartments are required for bacterial growth in host cells. We found that both the *DyP::Tn* and Δoperon mutants had impaired growth in murine bone-marrow derived macrophages that was manifest by two days after infection (Figure 4A, 4B). One of the antibiotics used to treat TB infection, Pyrazinamide (PZA), is most effective in low pH environments, such as the phagolysosome. PZA is thought to disrupt the cell wall of Mtb, which leads to acidification of the bacterial cytosol. A recent study in human TB patients demonstrated that the pH of necrotic lung cavities is ~5.5, a finding that may also explain the efficacy of pyrazinamide in treating Mtb infection[118] (Kempker et al., 2017). Since DyP is critical for protection of Mtb against oxidative stress at low pH, we considered whether nanocompartments may mediate Mtb resistance to PZA. To test bacterial susceptibility to PZA, we treated wild-type and Δoperon Mtb with PZA in the presence of H_2O_2 at pH 5.5. We found that mutants lacking the DyP nanocompartment were sensitive to concentrations of PZA that did not impact growth of the wild-type bacteria (Figure 4C). We next set out to test whether mutants lacking the DyP operon are susceptible to PZA treatment *in vivo.* We infected BALB/C mice with wild-type and mutant bacteria by the aerosol route with a dose of ~250 bacteria instilled on day 0 of infection. PZA treatment began on day 14, and continued until day 35, at which time we enumerated CFU in the lungs. We did not find that Δoperon mutants were more attenuated that wildtype bacteria in mouse lungs at 35 days post infection, at least under the conditions examined. However, Δoperon mutants were significantly more susceptible to treatment with PZA *in vivo* (Figure 4D)*,* demonstrating the DyP encapsulin operon is required for endogenous resistance to PZA treatment.

2.4 Discussion.

Here we report that a protein nanocompartment in *M. tuberculosis* encapsulates the dye-decolorizing peroxidase DyP. By demonstrating that the encapsulin system is important

for resisting oxidative stress at low pH, we provide the first evidence that encapsulin systems contribute to oxidative stress in a bacterial pathogen, and only the second demonstration of a functional encapsulin system in any species. Furthermore, we expand our understanding of the importance of encapsulation in enzyme function by demonstrating that the protein shell encapsulating DyP enhances its function *in vivo.* Finally, we demonstrate that the DyP nanocompartment system is essential for the ability of *M. tuberculosis* to grow in host macrophages, and to resist killing by the antibiotic pyrazinamide. These findings are the first demonstration that a nanocompartment system is important for virulence in any bacterial pathogen.

Bacterial protein-based compartments are emerging as functional equivalents of eukaryotic organelles that can sequester enzymatic reactions from the environment of the cytosol. Bacteria appear to have two predominant classes of protein based organelles, the relatively well understood bacterial microcompartment[96], and the more recently discovered bacterial nanocompartment[92]. Rather than using a lipid membrane for compartmentalization, both bacterial microcompartments and nanocompartments consist of a porous protein shell that surrounds enzymatic proteins. Bacterial microcompartments that enable utilization of specialized nutrients including ethanolamine and 1,2 propane diol have previously been implicated in pathogenesis of *Escherichia coli* and *Salmonella enterica* respectively[98]. Nanocompartments, which are 10 times smaller than a typical bacterial microcompartment, have been identified bioinformatically in over 900 bacterial species, however very few studies have addressed the role that nanocompartments play in bacterial physiology. Bioinformatic analysis and the heterologous expression of nanocompartment systems from diverse bacteria in *E. coli* have suggested that these systems might function in iron mineralization, oxidative and nitrosative stress resistance, and anaerobic ammonium oxidation[93]. However the only nanocompartment that has been shown to be important for survival under conditions of stress is the ferritin like protein containing compartment in *Myxococcus xanthus*, which is required for resistance to H_2O_2[106–108]. Our demonstration that an encapsulin system is required for resistance to oxidative stress in *Mycobacterium tuberculosis* significantly broadens the potential role and impact of nanocompartment systems in bacterial physiology.

A previous report examined the *M. tuberculosis* nanocompartment by heterologous expression of the encapsulin gene in *E. coli.* Co-expression with 3 potential substrates identified bioinformatically based on a putative signal sequence suggested that three proteins can be encapsulated by the *M. tuberculosis* nanocompartment: DyP, FolB, and BrfB[119]. Here we show for the first time that *M. tuberculosis* produces this nanocompartment. However, of the three potential cargo proteins, only DyP was identified in encapsulin systems purified from logarithmically growing bacteria. Why is the DyP protein encapsulated? There is almost no understanding of the role of encapsulation in bacterial physiology despite the widespread presence of encapsulins in across bacterial species. In this study, we found that the encapsulin shell protein alone protects the bacteria from oxidative stress at low pH. It is possible that in some circumstances, particularly when the stressor is not maximal, encapsulation of DyP may not be necessary. We expect that further investigation of this nanocompartment system in *M. tuberculosis* and in other bacterial species will reveal additional roles of encapsulins in the bacterial physiology.

We showed that Mtb mutants lacking the DyP encapsulin system have an altered redox balance at baseline, with a significantly more oxidative cytosol than wild type. However, under standard growth conditions, the mutants are not defective. While mutants exhibit a small defect for survival when exposed to H_2O_2 at pH 6.5, they are highly attenuated at low pH in the presence of H_2O_2. Intriguingly, the attenuation of the mutants under these conditions requires the presence of fatty acids bound to BSA in the culture medium. Why is the DyP encapsulin system required for growth under these conditions? It is possible that this system is required for detoxifying an oxidative species other than H_2O_2 itself, such as a lipid peroxide. It is also possible that the low pH compromises the integrity of the cell wall such that oxidative damage is sustained, or that the low pH magnifies the importance of DyP, which has a low pH optimum. Nevertheless, although the exact function of the DyP encapsulin system remains to be elucidated, this system is clearly important for pathogenesis, as mutants fail to grow in host macrophages. Intriguingly, encapsulin systems have been shown to confer stability to the enzymatic cargo under harsh conditions, including heat and protease exposure[92]. Cfp29 was originally identified as a component of short-term culture filtrate present in broth of growing cells, leading to the supposition that this protein is secreted[107–109]. Given that nanocompartments spontaneously assemble inside cells[92,99,120], it is unlikely that a structure the size of a ribosome could be secreted. We speculate that nanocompartments are released from dying cells, and that their extreme stability promotes their accumulation in axenic bacterial culture. Indeed this stability may partially explain why Cfp29 is a known immunodominant antigen for T cells[121]. Taken together, these data suggest the intriguing possibility that nanocompartments released from dying cells *in vivo* could continue to provide defense against oxidative stress for the surviving bacteria.

We found that only 2 peroxidases, KatG and DyP, are required for survival in the presence of H_2O_2 at pH 4.5. These findings raise the possibility that these peroxidases have redundant function *in vivo,* possibly explaining the lack of attenuation we observed in Δoperon mutants in BALB/C mice at 35 days post infection. It is also possible that Δoperon mutants are not attenuated at this timepoint in BALB/C mice, as the TnSeq screen that previously identified Cfp29 as being required for growth in mouse lungs used the C57BL/6 strain[101] . KatG mutants are highly prevalent in the clinic, as loss of function in KatG prevents activation of the INH prodrug. Importantly, many KatG mutants that fail to activate INH are also defective for catalase activity[122]. This raises the intriguing possibility that the DyP nanocompartment system could partially compensate for a loss of KatG catalase activity, enabling these drug resistant mutants to survive *in vivo.* In addition to a potential role for DyP in the context of INH treatment and INH resistant infections, we found that DyP encapsulin mutants are susceptible to treatment with PZA, an antibiotic known to require acidic conditions for efficacy. Thus, we predict that this encapsulin system may limit the efficacy of PZA treatment of patients.

In summary, we have demonstrated that *M. tuberculosis* produces a functional nanocompartment containing the peroxidase DyP. This system is essential for resisting oxidative stress at low pH, conditions that resemble the host lysosome. In addition, the DyP encapsulin system is required for growth in host macrophages, and for resistance to the antibiotic pyrazinamide. Previously encapsulin systems have been primarily studied in the context of heterologous expression in *E. coli* and for bioengineering or structural

studies. Our findings demonstrate the significance of encapsulin nanocompartments in bacterial physiology in the globally significant pathogen *Mycobacterium tuberculosis.*

2.5 Materials and Methods

Mycobacterium tuberculosis bacterial strains and plasmids.

The *M. tuberculosis* strain H37Rv was used for all experiments. The transposon mutants DyP::Tn and Rv1762c::Tn were picked from an arrayed transposon mutant library generated at the Broad Institute. The ΔOperon, ΔCfp29, and ΔDyP strains were made by homologous recombination using the pMSG361 vector[121]. For genetic complementation studies, the region encoding GFP and KanR in pUV15tetORm[122] was substituted via GoldenGate cloning with open reading frames for Rv0798c, Rv0799c, or the whole nanocompartment operon (Rv0798-99c). Expression of the complementation constructs was induced with anhydrotetracycline (200 ng/mL). To measure redox homeostasis, strains were transformed with pMV762-mrx1-roGFP2[45]. To measure intrabacterial pH, strains were transformed with pUV15-pHGFP (Addgene). The transposon mutant library for Tn-Seq was generated in *M. tuberculosis* using the ΦMycoMarT7 transposon donor plasmid.

M. tuberculosis bacterial cell culture.

For infections*, M. tuberculosis* was grown to mid-log phase (OD_{600} = 0.5-1.0) in Middlebrook 7H9 liquid medium supplemented with 10% albumin-dextrose-saline, 0.4% glycerol, and 0.05% Tween-80 or on solid 7H10 agar plates supplemented with Middlebrook OADC (BD Biosciences) and 0.4% glycerol. When specified, Tween-80 was substituted with 0.05% Tyloxapol, and 10% albumin-dextrose-saline was prepared with fatty acid free BSA (Sigma-Aldrich). Sauton's media was prepared with tyloxapol as previously specified[123].

DyP activity assays.

Activity of the encapsulated and unencapsulated DyP was performed using methods adapted from Contreras *et al.* 2014[124]. Briefly, DyP concentration for the encapsulated and unencapsulated DyP was determined by absorbance of the heme prosthetic group at 411 nm. Reactions were performed using 5 nM DyP, 480 nM H_2O_2, and 480 nM 2,2'-azino-bis (3-ethylbenzothiazoline-6-sulfonic acid) (ABTS) in 100mM sodium citrate buffer pH 4-6. Product formation was monitored over 20 minutes via absorbance at 420 nm using a Varian Cary® 50 UV-Vis Spectrophotometer (Agilent).

Nanocompartment Purification from Mtb.

For each purification, 1.5 L of *M. tuberculosis* was grown to mid-log phase in standard 7H9 and washed with PBS. Bacteria were pelleted and lysed in buffer by bead beating (for 50 mL of buffer, PBS with 1 mM PMSF was supplemented with 50 mg lysozyme, 20 U DNaseI, and 100 µg RNase A). Lysates were passaged twice through 0.2 µm filters before removal from the BSL3. Clarified lysates were prepared by centrifugation at 20,000 x *g* for 20 minutes in a JA-20 rotor. Following clarification, 4-5 mL of lysate was layered onto top of 16mL of 38% sucrose and centrifuged for 18 hours at 100,000 x *g* in a type 50.2 Ti rotor. The supernatant was discarded and the pellet was resuspended in 200 µL of PBS. Resuspended pellets were layered on top of a 10-50% discontinuous sucrose

gradient and centrifuged for 21 hours at 100,000 x g in a SW 41 Ti rotor. The gradient was fractionated and aliquots from each fraction were analyzed by SDS-PAGE for the presence of Cfp29.

Expression of Holo-nanocompartment and naked DyP in E. coli.
Plasmids for the expression of the Holo-nanocompartment (DyP-loaded) and naked DyP constructs were designing using Gibson Assembly (NEB). Each construct was cloned into a pET-14-based destination vector containing a T7 promoter. The naked DyP construct contained an N-terminal poly-histidine tag for affinity purification. These constructs were transformed into *E. coli* BL21 (DE3) LOBSTR cells for protein overexpression. Cells were grown in LB media containing 60 µg/mL kanamycin at 37°C with shaking at 250rpm until cultures reached an optical density (OD_{600} = 0.5-0.6). Samples were then induced with 0.5 mM IPTG and grown overnight at 18°C. Liquid cultures were harvested by centrifugation at 5000 x *g* for 20 minutes at 4°C, flash frozen in liquid nitrogen, and then stored at -80°C for future use.

Purification of Holo-nanocompartment complex from E. coli.
Cell pellets (5 g dry cell mass) were thawed at room temperature and resuspended in 50 mL of lysis buffer (20 mM Tris-HCl pH 8, 150 mM NH_4Cl, 20 mM $MgCl_2$) supplemented with 50 mg lysozyme, 20 U DNaseI, 100 ug RNase A. Samples were lysed by three passages through an Avestin EmulsiFlex-C3 homogenizer and clarified via centrifugation (15,000 x g, 30 min, 4°C). The clarified lysate was then spun at 110,000 x *g* for 3 hours at 4 °C. The supernatant was discarded and the resulting pellet was resuspended with wash buffer (20 mM Tris pH 8, 150 mM NH_4Cl, 20 mM $MgCl_2$ supplemented with 1X Cell Lytic B (Sigma-Aldrich). The sample was then spun at 4,000 x *g* at 4°C for 10 min followed by removing the supernatant and resuspension of the pellet in 4 mL of 50 mM Tris-HCl pH 8, 300 mM NaCl. The sample was then incubated at room temperature for 10 minutes to allow for solubilization and then centrifuged at 4000 x *g* at 4°C for 10 minutes to remove insoluble material. The resulting supernatant was then concentrated using Vivaspin® 6 100,000 MWCO concentrator columns (Sartorius). The sample was then purified via size exclusion chromatography using a Superose™ 6 Increase column (GE Life Sciences) and fractions were analyzed by SDS-PAGE using 4-20% Criterion™ polyacrylamide gels (Bio-Rad) and visualized with GelCode Blue stain (ThermoFisher).

Purification of unencapsulated DyP from E. coli.
Cell pellets (5 g dry cell mass) were thawed at room temperature and resuspended in 50 mL of buffer A (25 mM Tris HCl pH 7.5, 150 mM NaCl, 20 mM imidazole) supplemented with 50 mg lysozyme, 20 U DNaseI, 100 µg RNase A. Samples were lysed by three passages through an Avestin EmulsiFlex-C3 homogenizer and clarified via centrifugation (15,000 x g, 30 min, 4°C). The resulting supernatant was then bound to HisPur™ Ni-NTA resin (ThermoFisher Scientific) for 90 minutes at 4°C and then applied to a gravity column. The nickel resin was then washed with 30 resin volumes of buffer B (25 mM Tris-HCl pH 7.5, 150 mM NaCl, 40mM imidazole) prior to eluting with buffer C (25 mM Tris-HCl pH 7.5, 150 mM NaCl, 350 mM imidazole). The eluate was then concentrated using Vivaspin® 20 10,000 MWCO concentrator columns (Sartorius) and desalted into 25mM Tris pH 8, 300mM NaCl using Econo-Pac®10DG desalting columns (BioRad). The SUMO

tag was removed upon addition of SUMO protease at a 1: 300 (SUMO protease: DyP) molar ratio and incubating overnight at 4°C. Purification was finished by size exclusion chromatography with a Superose™ 6 Increase column (GE Life Sciences).

Negative stain Transmission Electron Microscopy.
Nanocompartment samples were diluted to 50 nM and applied to Formvar/ carbon-coated copper grids. The grids were then washed with MilliQ water three times followed by staining with 2% (w/v) uranyl acetate. Grids were examined using the FEI Tecnai 12, 120kV transmission electron microscope, and images were captured with a charge-coupled device (CCD) camera.

Exposure to oxidative and pH stress.
M. tuberculosis was grown to mid-log phase in 7H9 media. Bacteria were diluted to OD_{600} = 0.1 in 10 mL of specified media at pH 4.5-6.5 and H_2O_2 was added to bacterial cultures at specified concentrations. Bacteria were incubated with stressors for 24 or 72 hours. CFUs were enumerated by diluting bacteria in PBS with 0.05% Tween-80 and plating serial dilutions on 7H10 agar.

Measurement of redox homeostasis.
M. tuberculosis strains were transformed with a plasmid expressing mrx1-roGFP2 and grown to mid-log phase in 7H9. Bacteria were diluted to OD_{600} = 0.25 in 200 µL of specified media and added to 96 well plates. Upon addition of H_2O_2 (5 mM), fluorescent emissions were recorded at 510 nm after excitation at 390 nm and 490 nm using a Spectramax M3 spectrophotometer. Values reported are emissions ratios (390 nm/ 490 nm) and were measured 20 minutes following addition of H_2O_2.

Measurement of intrabacterial pH.
M. tuberculosis strains were transformed with a plasmid expressing pHGFP and grown to mid-log phase in 7H9. To prepare standards, 1.5 x 10^8 bacterial cells were pelleted and resuspended in 400 µL lysis buffer (50 mM Tris-HCl pH 7.5, 5 mM EDTA, 0.6% SDS, 1 mM PMSF) before bead beating. Cell debris were pelleted and clarified lysates were kept at 4°C until use, at which point 10 µL of clarified lysate were added to 200 µL of medium with varying pH levels (4.5-8.0). To prepare samples, 1.5 x 10^8 bacterial cells were pelleted and washed with PBS twice before being resuspended in specified media and diluted to OD_{600} = 0.5 in 200 µL of medium and added to 96 wells plates. Upon addition of H_2O_2 (5 mM), fluorescent emissions were recorded at 510 nm following excitation at 395 nm and 475 nm. Values reported were interpolated from 395/475 ratios obtained from the standard curve.

Western blot analysis of Cfp29 expression.
M. tuberculosis strains were grown to mid-log phase in 7H9 medium. Bacteria were pelleted and washed twice with PBS prior to resuspension in lysis buffer (50 mM Tris-HCl pH 7.5, 5 mM EDTA, 0.6% SDS, 1 mM PMSF). Samples were lysed using a bead-beater, and cell debris were pelleted. Clarified lysates were heat-sterilized at 100°C for 15 minutes and frozen prior to use. Total protein lysates were analyzed by SDS-PAGE using precast Tris-HCl 4-20% criterion gels (Bio-Rad). Primary polyclonal antibodies for Cfp29

were generated by GenScript USA Inc via immunization of rabbits with three peptides from the protein sequence. HRP-conjugated goat anti-rabbit IgG secondary antibodies were used (sc-2030; Santa Cruz Biotechnology). Western Lightning Plus-ECL chemiluminescence substrate (Perkin Elmer) was used and blots were developed using a ChemiDoc MP System (Bio-Rad).

Infection of murine macrophages.

Macrophages were derived from bone marrow of C57BL/6 mice by flushing cells from femurs. Cells were cultured in DMEM supplemented with 10% FBS and 10% supernatant from 3T3-M-CSF cells for 6 days, with feeding on day 3. After differentiation, BMDMs continued to be cultured in BMDM media containing M-CSF. For infection, BMDMs were seeded at a density of 5 x 10^4 cells per well in a 96-well dish. BMDMs were allowed to adhere overnight and then infected with DMEM supplemented with 5% FBS and 5% horse serum (BMDMs) at a multiplicity of infection of 1. Following a 4-hour phagocytosis period, infection medium was removed and cells were washed with room temperature PBS before fresh, complete medium was added. For CFU enumeration, medium was removed and cells were lysed in water with 0.5% Triton-X and incubated at 37°C for 10 minutes. Following the incubation, lysed cells were resuspended and serially diluted in PBS with 0.05% Tween-80. Dilutions were plated on 7H10 plates.

Infection of mice.

BALB/C mice were obtained from the Jackson Laboratory, Bar Harbor, ME. Mice were infected at 6 weeks of age with 250 CFUs of *M. tuberculosis* strains by the aerosol route using a Glas-Col (Brazil, Indiana) full body inhalation exposure system. Infections were allowed to proceed for 35 days at which time mice were euthanized and CFU from the lungs enumerated by plating on 7H10 plates. PZA treatment began 14 days after infection. PZA (Acros Organics) was formulated in water and administered 5 days per week, once per day, at 150 mg/kg, by oral gavage. We used G*power to calculate the needed number of animals to power the mouse study, and used 5 mice per group.

Transposon-sequencing screen.

A transposon mutant library in H37Rv was grown to mid-log phase in 7H9. Bacteria were diluted to OD_{600} = 0.1 in 10 mL 7H9 at pH 4.5 with 2.5 mM H_2O_2. Mutants were exposed to these stressors for 72 hours and then diluted to 15,000 CFU/mL in PBS with 0.05% Tween-80. Approximately 30 thousand bacteria were plated onto six 245 mm x 245 mm 7H10 plates supplemented with 0.05% Tween-80 and Kanamycin (50 μg/mL). Control libraries were not exposed to low pH or H_2O_2 and were plated onto 7H10 plates. Colonies grew for 21 days and were collected for genomic DNA isolation. Samples for sequencing were prepared by the University of California, Davis Genome Center DNA Technologies Core by following the protocol outlined by Long et al(Long et al., 2015). PE100 reads were run on an Illumina HiSeq with ~20 million reads per sample. Sample alignment and TRANSIT pre-processing were performed by the University of California, Davis Bioinformatics Group as previously outlined[84] . TRANSIT analysis was performed as specified by DeJesus et al[125]. Resampling analysis was preformed using the reference genome H37RvBD_prot and the following parameters: for global options, 0% of the N- and C- terminus were ignored; for resampling options, 10,000 samples were taken and

normalized using the TTR function. Correction for genome positional bias was performed. Statistical significance was determined by p value ≤ 0.05 and log2 fold change ≤-1 or by p-adjusted value ≤ 0.05.

Ethics

All procedures involving the use of mice were approved by the University of California, Berkeley Institutional Animal Care and Use Committee (protocol no. R353-1113B). All protocols conform to federal regulations, the National Research Council's Guide for the Care and Use of Laboratory Animals, and the Public Health's Policy on Humane Care and Use of Laboratory Animals.

2.6 Acknowledgments.

We thank Tom Ioerger and Michael DeJesus for assistance with TRANSIT analysis and Amit Singh for the kind gift of pMV762-mrx1-roGFP2. We thank Jeff Cox and members of the Cox lab for helpful discussions. This work was supported by funding from the Center for Emerging and Neglected disease for funding to KAL, the National Institute of General Medical Sciences (R01GM129241) to DFS and the National Institute of Allergy and Infectious Diseases (1R01AI143722) to SAS.

2.7 Figures

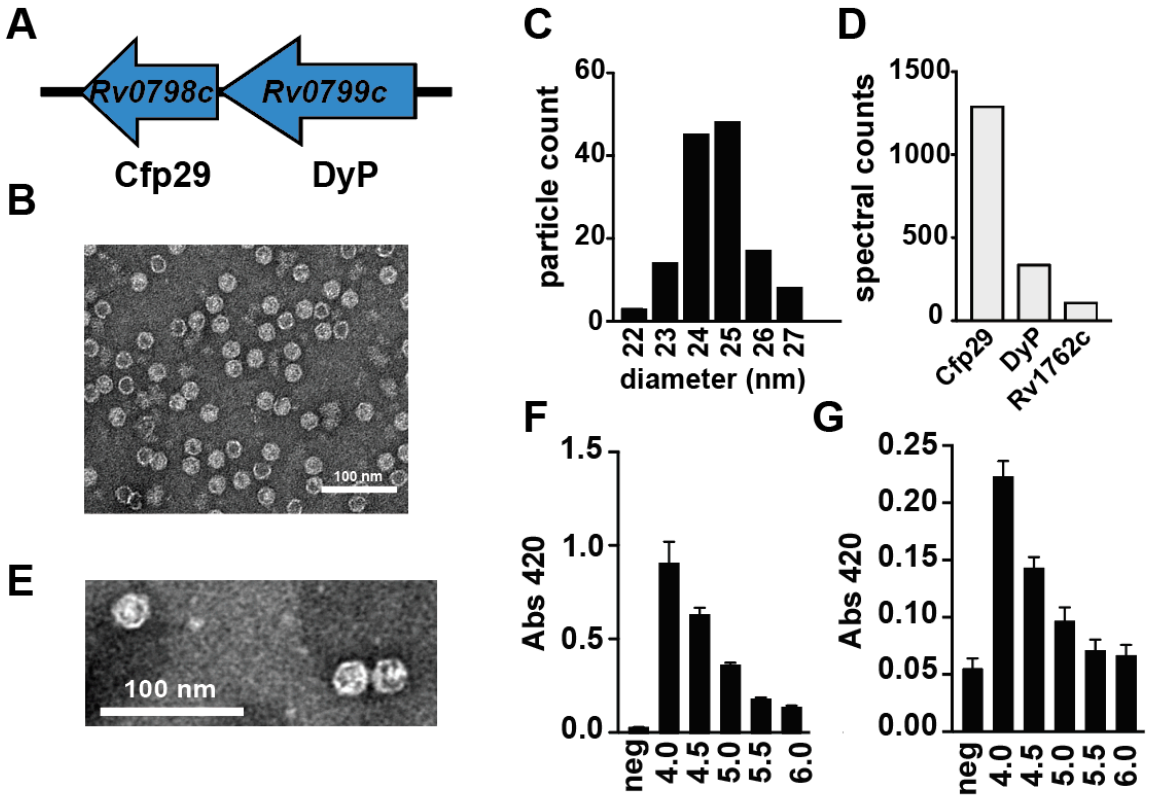

Figure 1. Mtb produces endogenous nanocompartments that package a peroxidase. (A) Schematic of the nanocompartment operon in Mtb which encodes the encapsulin shell protein (Cfp29) and the dye-decoloring peroxidase cargo protein (DyP). (B) TEM of Cfp29 encapsulin proteins purified following heterologous expression of the Mtb nanocompartment operon in *E. coli.* (C) Size distribution of Cfp29 protomers purified from *E. coli*. (D) Peptide counts from mass spectrometry analysis of endogenous nanocompartments purified from Mtb. (E) TEM of endogenous nanocompartments purified from Mtb. (Peroxidase activity of (F) unencapsulated and (G) encapsulated DyP (5 nM) using ABTS (480 nM) as a substrate in the presence of H_2O_2 (480 nM) at varying pH levels (4.0-6.0) as reported by a change in the absorbance at 420 nm. neg=no added enzyme. *$p<0.05$ by student's t-test.

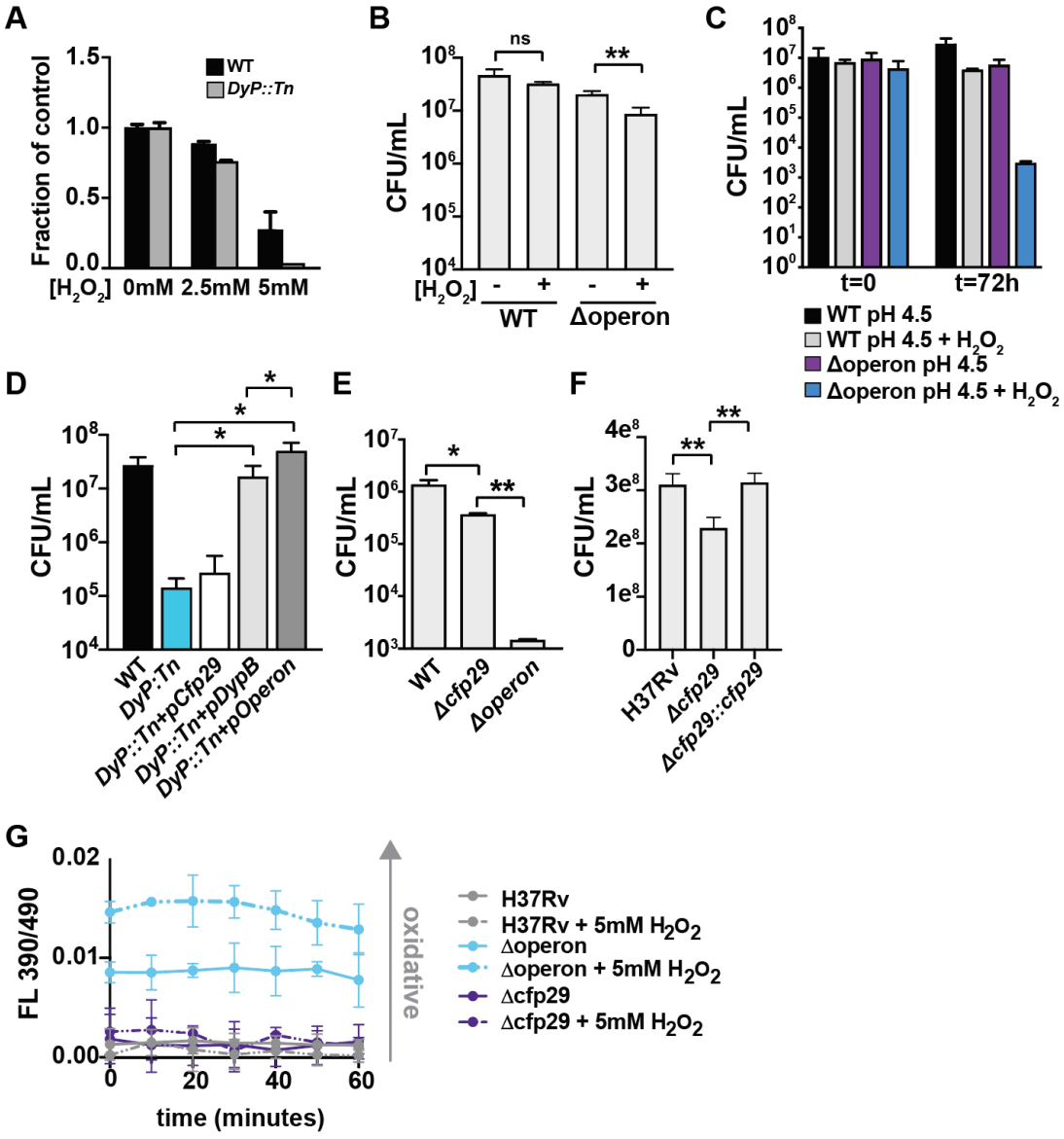

Figure 2. Nanocompartments protect Mtb from oxidative stress in acidic environments. (A) OD_{600} measurements of wild-type and *DyP::Tn* Mtb grown in 7H9 medium following exposure to H_2O_2 for 96 hours. Values reported are normalized to the untreated controls. CFU enumeration of wild-type and Mtb nanocompartment mutants grown in (B) standard 7H9 medium (pH 6.5) and (C, E, F) acidified 7H9 medium (pH 4.5) following exposure to oxidative stress (2.5 mM H_2O_2) for 72 hours. (D), (E), (F) CFU enumeration of wild-type, *DyP::Tn* mutants, and complemented mutants (pCfp29, pDyP, pOperon) following 24 hour exposure to oxidative stress (2.5 mM H_2O_2) in acidified 7H9 medium (pH 4.5). (G) Fluorescence emissions of wild-type and Δoperon Mtb expressing mrx1-roGFP exposed to 5 mM H_2O_2 at pH 4.5 in 7H9 medium for 20 minutes. Data are reported as a ratio of fluorescence emissions following excitation at 490 nm and 390 nm.Figures are representative of at least 2 (E,F) or 3 (A-D;F) independent experiments. p-values were determined using unpaired t test. *p<0.05, **p<0.01.

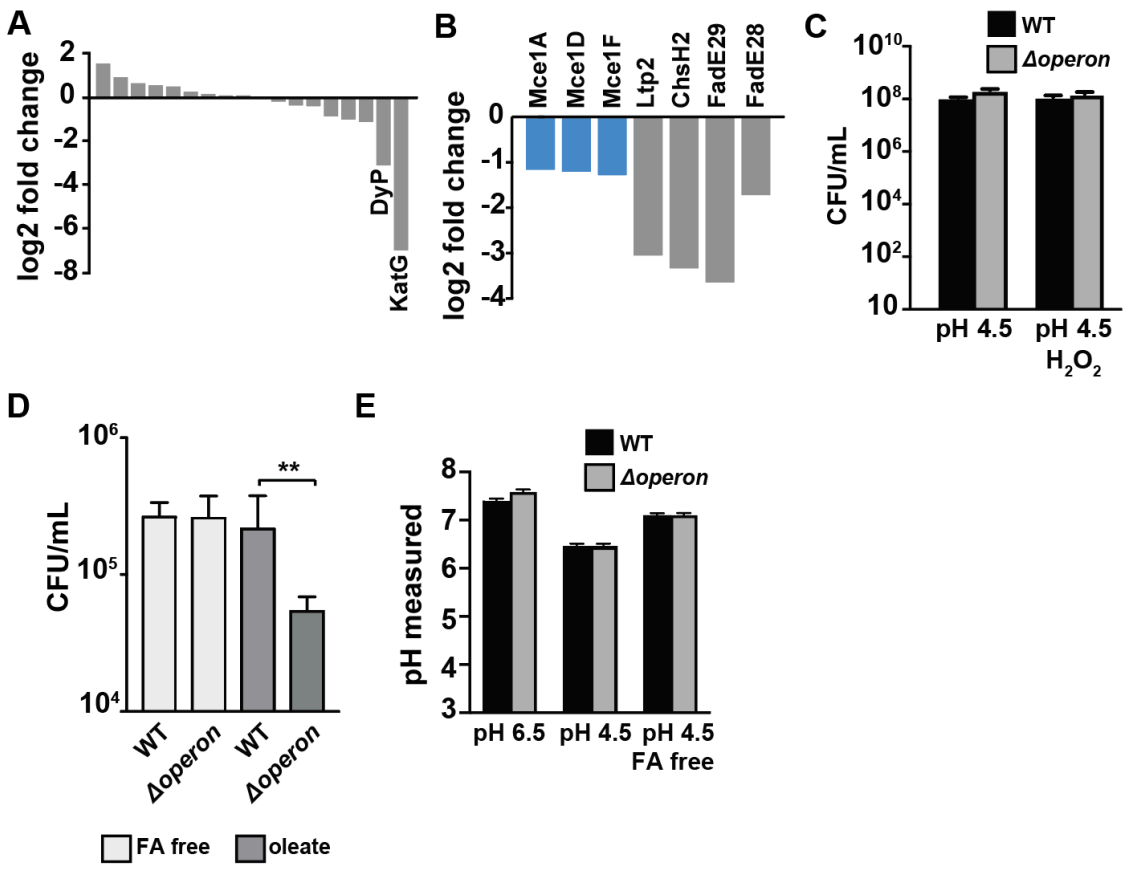

Figure 3. Susceptibility of Mtb nanocompartment mutants to oxidative and acid stress is mediated by free fatty acids. (A) Tn-seq data showing normalized sequence reads per gene for all putative Mtb peroxidases and (B) lipid and cholesterol metabolism Mtb mutants that were significantly attenuated following 72 hour exposure to 2.5 mM H_2O_2 at pH 4.5. (C) CFU enumeration of wild-type Mtb and Δoperon mutants following 24 hour exposure to 2.5 mM H_2O_2 at pH 4.5 in Sauton's minimal medium and (D) 72 hour exposure to 2.5 mM H_2O_2 at pH 4.5 in 7H9 medium prepared using fatty-acid (FA) free BSA +/- oleic acid (150 uM). (E) Intrabacterial pH measurements of wild-type and Δoperon Mtb expressing pUV15-pHGFP following 20 minute exposure to 5 mM H_2O_2 at pH 6.5 or pH 4.5. 7H9 medium was prepared with standard BSA or FA free BSA. Figures are representative of at least 2 (D) or 3 (A-C;E) independent experiments. p-values were determined using an unpaired t test. *p<0.05, **p<0.01.

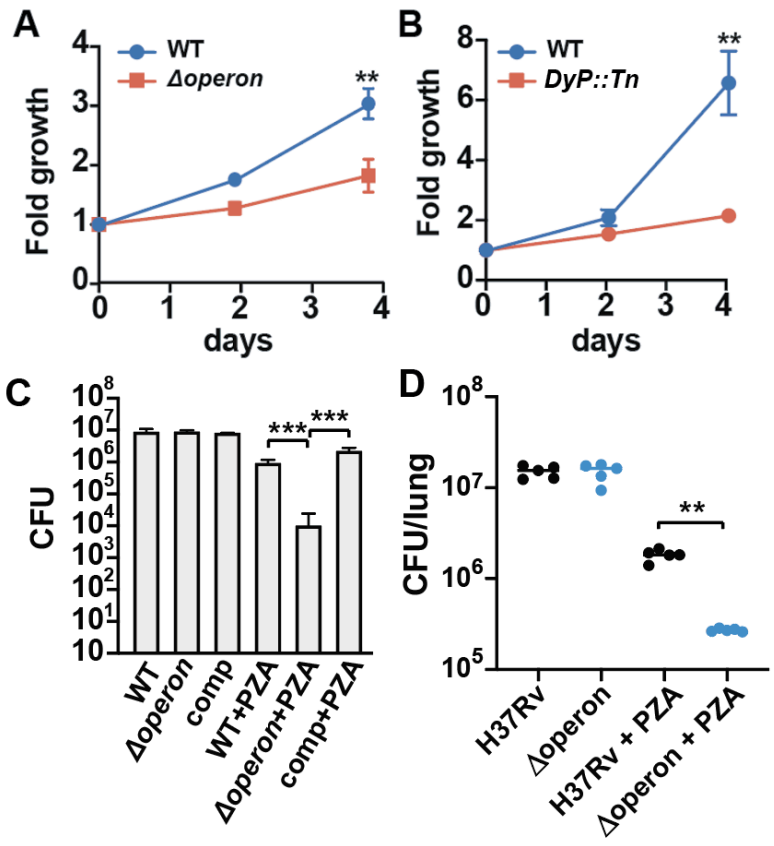

Figure 4. Nanocompartment mutants are attenuated for survival in macrophages and are more susceptible to pyrazinamide treatment. CFU enumeration of wild-type Mtb and (A) Δoperon or (B) DyP::Tn mutants during infection of murine bone marrow-derived macrophages. Macrophages were infected with a bacterial MOI of 1 and CFUs were enumerated immediately following phagocytosis and at days 2 and 4. Error bars are SD from 4 replicate wells. (C) CFU enumeration of wild-type and Mtb Δoperon mutants following 72 hour exposure to pyrazinamide (24 μg/mL) and H_2O_2 (2.5 mM) in acidified 7H9 medium (pH 5.5). Comp=*Δoperon+pOperon*. (D) Infection of BALB/C mice with WT and Δoperon mutant with and without treatment with 150 mg/kg PZA. CFU at 35 days post infection in the lung is shown. Figures are representative of at least 2 independent experiments; p-values were determined using an unpaired t test. **p<0.01; ***p<0.001.

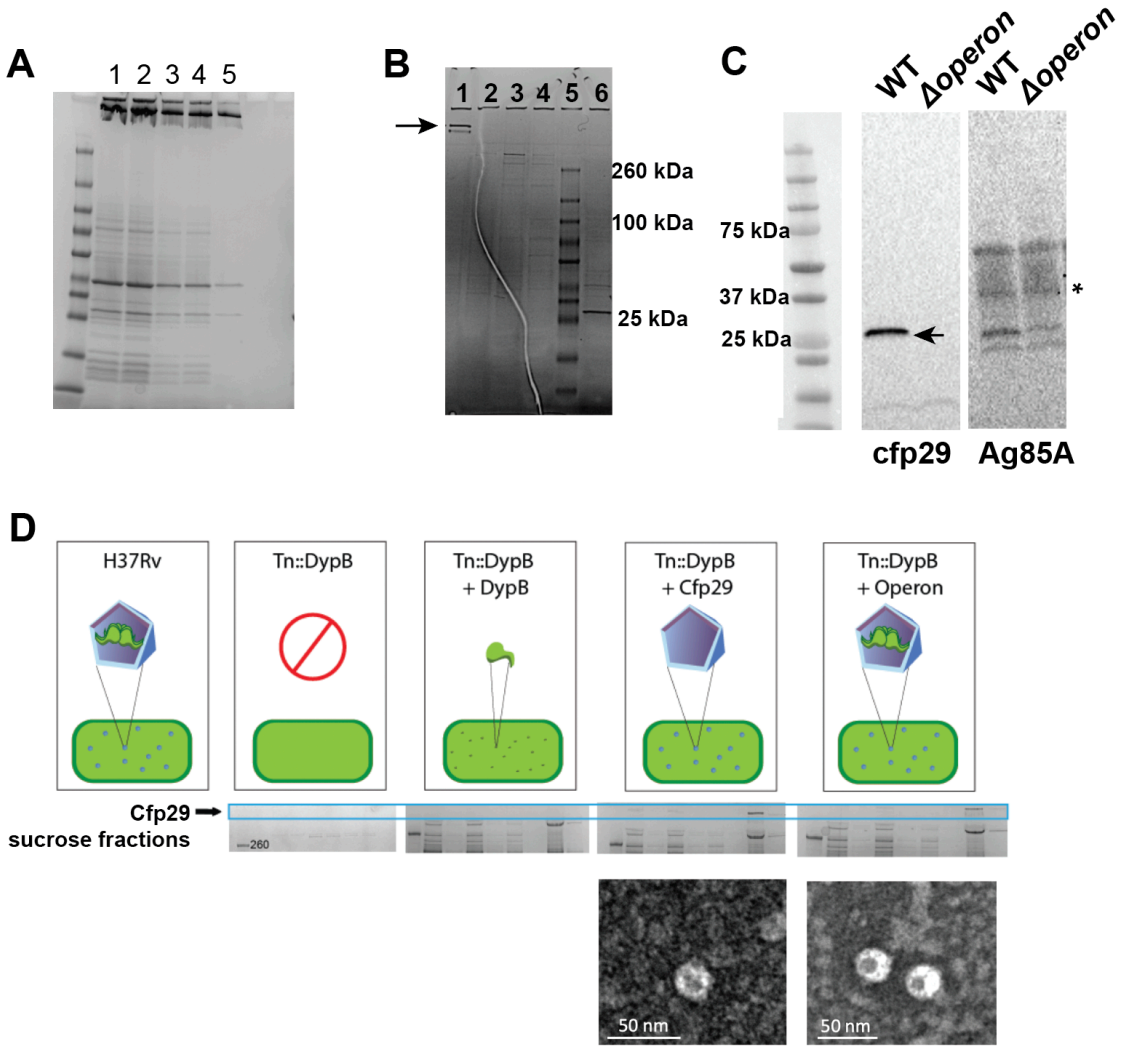

Figure S1. Nanocompartment purification and complementation strategies. (A) Coomassie stained SDS-PAGE of fractions collected during purification of nanocompartments heterologously expressed in *E. coli*: (1) Ultracentrifugation pellet post CellLytic B solubilization (2) Size exclusion chromatography input (3) lane 1 diluted (4) lane 2 diluted (5) encapsulin fraction from size exclusion. (B) Coomassie stained SDS-PAGE of sucrose fractions collected during purification of nanocompartments from wild-type Mtb lysates: (1) Fraction containing assembled encapsulin nanocompartment complexes (5) Ladder (6) Lane 1 boiled in SDS for 30 minutes to dissociate encapsulin nanocompartment into monomers. (C) Western blot for Cfp29 from wild-type Mtb (lane 1) and Δoperon mutant (lane 2) lysates. (D) Complementation strategy schematic for *DyP::Tn* mutants (top). *DyP::Tn* mutants were transformed with ATc-inducible complementation constructs encoding the unencapsulated cargo protein (pDyP), the encapsulin shell protein (pCfp29), or the nanocompartment operon (pOperon). Lysates from each strain were used for nanocompartment purification. Sucrose fractions containing high molecular weight Cfp29 protomers were identified in complemented strains expressing the encapsulin shell and the operon (middle) and were analyzed using TEM (bottom).

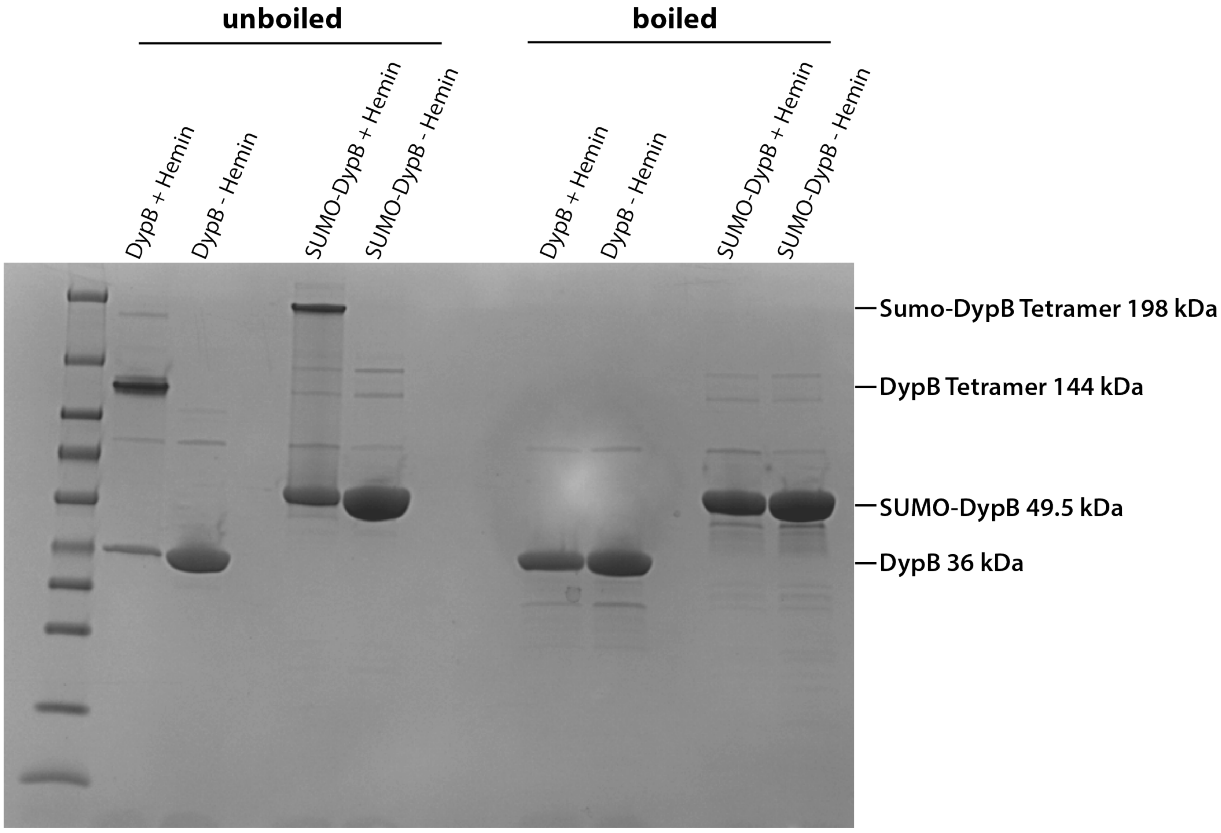

Figure S2. SDS-PAGE analysis of DyP purified from *E. coli*.
DyP samples with or without addition of hemin were analyzed by SDS-PAGE. Samples were loaded either in their unboiled native state (left half) or heat-denatured by boiling at 95°C for 15 minutes. Addition of hemin yields a tetrameric DyP at 144 kDa.

Chapter 3: Analysis of nanocompartments in nontuberculosis mycobacteria

Kayla M. Dinshaw, Thomas S. Kouyate, Samantha Lam, Sarah A. Stanley

3.1 Abstract

Bacteria have long been thought to lack standard membrane-bound organelles and thus lack cellular compartmentalization. However, nanocompartments have arisen as a method of compartmentalization in bacteria and archaea. Nanocompartments are comprised of a proteinaceous shell that surrounds a cargo protein. In *Mycobacterium tuberculosis* (Mtb), a nanocompartment containing the peroxidase DyP is important for defense against oxidative stress. Here, we delete both the DyP nanocompartment and another evolutionarily distinct nanocompartment containing the cysteine desulfurase CyD in the nontuberculosis mycobacterial species *Mycobacterium smegmatis* (M. smeg) and *Mycobacterium abscessus* (M. abs). We find that nanocompartment mutants in M. smeg and M. abs fail to recapitulate phenotypes observed in a nanocompartment mutant in Mtb. Nanocompartment mutants in M. smeg display unique colony morphology that may translate to survival in a macrophage infection. Our data provide insights into the role of nanocompartments in bacterial physiology.

3.2 Introduction

Around 2.4 billion years ago, the “great oxidation event” occurred and oxygen levels on Earth rose significantly[124]. With the rise of oxygen, organisms adapted to the presence of toxic molecules created by oxygen metabolism, known as reactive oxygen species[125]. Reactive oxygen species, such as superoxide (O_2-) and hydrogen peroxide (H_2O_2), can damage proteins, lipids, and DNA. Reactive oxygen species are generally made as a byproduct of metabolism, but immune cells such as phagocytes assemble the protein complex NADPH oxidase on phagosomal membranes to generate a burst of superoxide to inflict damage on invading pathogens. However, pathogens have evolved methods to combat oxidative stress.

We have previously found that a nanocompartment containing a peroxidase called DyP is important for defense against oxidative stress in *Mycobacterium tuberculosis* (Mtb)[123]. Mtb is a human bacterial pathogen that causes the disease tuberculosis. It primarily infects the lungs and spreads through aerosols. Until the covid-19 pandemic, tuberculosis was the number one cause of death from a single infectious agent[126]. Mtb lives in the phagosome of macrophages, where it encounters oxidative stress from the NADPH oxidase and its own aerobic metabolism. To protect itself against oxidative stress, Mtb produces the low molecular weight thiol called mycothiol, used as a reducing agent equivalent, to maintain intracellular redox homeostasis[125]. Mtb also encodes two superoxide dismutases that convert superoxide to hydrogen peroxide. Additionally, Mtb is predicted to encode numerous peroxidases. Our previous work in Mtb demonstrates that the peroxidase DyP can utilize hydrogen peroxide as a substrate and provide protection against oxidative stress at acidic pH[126].

An interesting feature of Mtb DyP is that it is the cargo protein encapsulated within a nanocompartment. Nanocompartments are a method of compartmentalization in bacteria and archaea, comprised of a proteinaceous shell (encapsulin) that resembles an icosahedral viral capsid and surrounds a cargo protein. Nanocompartments have been identified in over 900 bacterial and archaeal species. Encapsulins can vary from 25 to 35

nanometers in diameter and contain either 60 or 180 protomers[93]. The protomers are encoded by one gene and are thought to self-assemble to form the protein shell. Interestingly, nanocompartments may have a common theme of defense against oxidative stress. Cargo proteins, which typically contain a C- or N-terminal cargo loading peptide, are predicted to be involved in oxidative stress defense, iron storage, and anaerobic ammonium oxidation[93].

Mtb DyP is in a two gene operon with its shell protein Cfp29. Electron microscopy and mass spectrometry analysis of nanocompartments from Mtb revealed that DyP and Cfp29 form nanocompartments[127]. DyP is a dye-decolorizing peroxidase, a family of heme peroxidases that were named for their ability to decolorize industrial dyes[128]. We found that purified encapsulated and unencapsulated DyP is able to reduce hydrogen peroxide[129]. We also found that mutant in Mtb lacking the DyP nanocompartment is attenuated at acidic pH in the presence of hydrogen peroxide[127]. The nanocompartment mutant in Mtb is also susceptible to pyrazinamide both in broth and in a mouse model of infection[128].

In this study, we used the nontuberculosis mycobacterial species *M. smegmatis* (M. smeg) and *M. abscessus* (M. abs) to further characterize the function of nanocompartments. M. smeg is a nonpathogenic saprophytic mycobacterium that is commonly used as a model for studying Mtb. M. smeg and Mtb share ~2800 orthologs with over 50% amino acid identity[129]. M. abs is an environmental mycobacterium that often lives in the soil and water and can cause opportunistic infections in immunocompromised human hosts, especially in patients with cystic fibrosis[130]. M. abs is intrinsically antibiotic resistant to many tuberculosis antibiotics[134], requiring at least twelve months of combinatorial antibiotic therapy[131]. Unlike Mtb, M. smeg and M. abs do not require a biosafety level-3 facility for research and are fast growing, with doubling times around 3-4 hours compared to 22 hours in Mtb. Both M. smeg and M. abs are predicted to encode homologs of the DyP/Cfp29 nanocompartment in Mtb. However, both M. smeg and M. abs are predicted to encode a second nanocompartment that Mtb does not – an evolutionarily distinct nanocompartment encoded by the genes CyD and SrpI[131].

SrpI is the shell protein predicted to encapsulate CyD, a cysteine desulfurase. Cysteine desulfurases catalyze the conversion of L-cysteine to L-alanine, mobilizing a sulfur for sulfur-containing biomolecules[132,133]. Cysteine desulfurases are important for thio-cofactors, such as iron sulfur clusters, tRNA modifications, DNA phosphorothioation, thiamine, and biotin[21]. In the context of oxidative stress, iron sulfur clusters are easily damaged by the oxidation of iron, and the subsequent repair of these iron sulfur clusters requires sulfur mobilization. In the cyanobacterium *Synechococcus elongatus*, the gene encoding SrpI was found to have upregulated mRNA under sulfur starvation and was given the name sulfur regulated plasmid-encoded gene-I (SrpI)[134]. Another study revealed that SrpI encapsulates CyD to form a functional nanocompartment, whose protein level is upregulated by sulfur starvation[135].

The exact role of the SrpI/CyD nanocompartment has not been well-characterized, especially in mycobacteria. The SrpI/CyD nanocompartment is not predicted to be encoded in a subset of mycobacteria more closely related to Mtb, including the entire Mycobacterium tuberculosis complex, *Mycobacterium bovis*, *Mycobacterium ulcerans*, and *Mycobacterium marinum*. However, SrpI was identified in bacterial membrane fractions of the pathogenic species Mycobacterium leprae[136], the causative agent of

leprosy. SrpI was originally named and is annotated in mycobacterial genomes as major membrane protein 1 (MMP1). This is likely an artifact, as methods used to isolate bacterial membranes are also likely to isolate high molecular weight nanocompartments. Here, we will refer to MMP1 as SrpI. SrpI is a significant antigen in human leprosy[135–137], and vaccination of mice with cellular fractions containing SrpI was protective against infection against Mycobacterium leprae[138]. Vaccination of cattle with an attenuated strain of *Mycobacterium avium* subspecies *paratuberculosis* revealed that SrpI is a dominant vaccine-elicited antigen[139,140]. Thus, much of the work on SrpI in mycobacteria has been in the context of vaccine development rather than its endogenous function.

Here, we generate nanocompartment mutants in M. smeg and M. abs and evaluate phenotypes in the presence of oxidative stress and during macrophage infection. We find that it is difficult to discern phenotypes at acidic pH in M. smeg due to a strong inoculum effect, and M. abs nanocompartment mutants fail to recapitulate our observations of the nanocompartment mutant in Mtb. M. smeg nanocompartment mutants display unique colony morphology which may correlate with survival in macrophages. Lastly, we show that Mtb DyP cannot use lipid peroxides as a substrate and has non-redundant function with the catalase-peroxidase KatG. Our data broadens our knowledge about the endogenous role of nanocompartments.

3.3 Results

3.3.1 Broth phenotypes in M. smeg nanocompartment mutants

In M. smeg, the DyP/Cfp29 operon is encoded by MSMEG_5829/MSMEG_5830, and the SrpI/CyD operon is encoded by MSMEG_4537/MSMEG_4538 (Figure 1A). We generated single knockouts of each nanocompartment operon (Δ*dyP operon* or Δ*cyD operon)* as well as a double nanocompartment knockout (Δ*dyPop*Δ*cyDop*) in M. smeg by oligo recombineering followed by Bxb1 Integrase targeting (ORBIT)[141]. Mutants were confirmed to have the endogenous locus knocked out and replaced by the ORBIT integrating plasmid by PCR and sequencing. For the DyP operon, we re-confirmed the knockout by western blotting with an antibody raised to Mtb Cfp29[137], which showed cross-reactivity to M. smeg Cfp29 and validated that Δ*dyP operon* and Δ*dyPop*Δ*cyDop* lack Cfp29 protein expression. A band for Cfp29 was re-visualized in a complemented strain expressing the DyP operon from its native promoter *(*Δ*dyPop::dyPop*) (Figure 1B).

We then sought to evaluate if phenotypes of the nanocompartment mutant in Mtb could be recapitulated in M. smeg. A mutant strain of the DyP operon in Mtb is more susceptible to pyrazinamide at pH 5.5 in the presence of hydrogen peroxide[140]. Nontuberculosis mycobacteria are more resistant to pyrazinamide, so we tested if M. smeg nanocompartment mutants were susceptible to H_2O_2 at a pH of 5.5 with a high concentration of pyrazinamide[142]. Our attempts at testing this condition in M. smeg were inconsistent due to large variability among experiments and between strains (data not shown). Thus, we tested if a strong inoculum effect in M. smeg could be leading to inconsistent results. We started cultures for WT, Δ*dyP operon*, Δ*dyPop*Δ*cyDop*, and Δ*dyPop::dyPop* at an OD_{600} of either 0.05, 0.08, or 0.10 in liquid media acidified to pH 5.5 with pyrazinamide and H_2O_2. After 22 hours, we plated for bacterial survival and observed drastic differences in the colony forming units (CFUs) between different starting inocula (Figure 1C). When cultures were started at an OD of 0.05, they died 1,000 to 10,000 fold depending on the strain after 22 hours, but, when started at an OD of 0.10, the bacteria

grew 1 to 10 fold after 22 hours. The nearly 5-6 logs of CFU difference between starting at an OD_{600} of 0.05 and 0.10 likely lead to our inconsistent results testing bacterial survival at pH 5.5 with H_2O_2 and pyrazinamide.

To evaluate if the inoculum effect was specific to acidic pH, we tested starting OD_{600}s of 0.05, 0.08, and 0.10 in WT M. smeg at neutral pH of 6.6 with H_2O_2 (Figure 1D). Under these conditions, there was a minimal inoculum effect with a four-fold difference between starting at OD_{600} of 0.05 and OD of 0.10 (Figure 1D). We proceeded with exposing WT, Δ*dyP operon*, Δ*cyD operon*, and Δ*dyPop*Δ*cyDop* to hydrogen peroxide at neutral pH and plating for bacterial survival (Figure 1E). The M. smeg strain lacking both nanocompartment operons (Δ*dyPop*Δ*cyDop*) was modestly attenuated, similar to the phenotype of the strain lacking the DyP operon in Mtb.[105]

Using the mrx-roGFP reporter that evaluates mycobacterial redox potential[138], the cytosol of DyP operon knockout strain in Mtb was found to be more oxidized at baseline and in the presence of acidic and oxidative stress[139]. Due to the mild attenuation of Δ*dyPop*Δ*cyDop* in the presence of hydrogen peroxide, we hypothesized that M. smeg Δ*dyPop*Δ*cyDop* cytosol would have the same phenotype. We electroporated the mrx-roGFP reporter into WT and Δ*dyPop*Δ*cyDop* M. smeg and exposed the cultures to hydrogen peroxide at pH 4.5. Although there was an oxidative shift of the redox potential in the presence of hydrogen peroxide, we did not observe any changes in the redox potential between the WT and nanocompartment mutant strain (Figure 1F).

3.3.2 M. smeg nanocompartment mutant colony morphology

The deletion of nanocompartment genes in M. smeg resulted in alterations in colony morphologies (Figure 2A). The Δ*dyP operon* and Δ*dyPop::dyPop* strains appeared similar to WT M. smeg, white-yellow in color with crinkly edges. However, the Δ*cyD operon* colonies were much smaller in size with a smooth appearance. The smooth colony morphology phenotype was not restored by complementation of the cyD operon from its native promoter (Figure 2A). The Δ*dyPop*Δ*cyDop* strain also did not present with the smooth colony phenotype. Rather, the double mutant contained a mixed population of small and large colonies (Figure 2B). When a large Δ*dyPop*Δ*cyDop* colony was collected, grown in liquid media, and plated on LB agar, the resulting colonies were all large , and the same size as typical WT M. smeg colonies (Figure 2C). When a small colony was propagated, it contained a mixture of small and large colonies (Figure 2C). We therefore reasoned that the large colonies may contain suppressor mutations of the small colony phenotype. To test this hypothesis, we started cultures from small colonies and passaged the culture daily for ten days (Figure 2D). We plated on LB agar at each passage to determine the proportion of small and large colonies. When a small colony was first grown to midlog phase in liquid media and plated on LB agar, around 10-20% of the culture consisted of large colonies (Figure 2D) After ten days, we observed 90-100% of the culture was dominated by large colonies (Figure 2D).

If large colonies were a suppressor of small colonies, we reasoned that we may expect to see different *in vitro* phenotypes between small and large colonies. We reasoned that there may be a growth defect between large and small colonies in liquid media given the difference in colony size, but WT, small, and large all doubled at roughly the same rate in LB broth (Figure 2E). We tested the minimum inhibitory concentration (MIC) of WT, small, and large to H_2O_2 at neutral pH but found no differences among

strains (Figure 2F). We sent WT, small Δ*dyPop*Δ*cyDop*, and large Δ*dyPop*Δ*cyDop* colonies for whole genome sequencing but did not observe any noticeable single nucleotide polymorphisms that could have obviously accounted for the difference in colony size (data not shown).

3.3.3 Macrophage infections with M. smeg nanocompartment mutants

To overcome our difficulty with in vitro experiments due to the inoculum effect, we sought to examine if the M. smeg nanocompartment mutants were more easily cleared in a macrophage infection. After isolating bone marrow derived macrophages (BMDMs) from C57BL/6 mice, we added WT M. smeg at MOIs of 1, 10, and 100 and plated for bacterial survival at 0 hours, 4 hours, and 20 hours to evaluate infection dynamics. Because we previously observed M. smeg growth in media used for differentiating and plating macrophages, we also tested the effect of adding gentamicin, which kills extracellular bacteria. The bacterial growth dynamics appeared similar between MOI 1, 10, and 100 with a small growth increase at 4 hours followed by the beginning of clearance from the macrophages at 20 hours (Figure 3A). At 20 hours, there was also about a ten-fold decrease in bacterial survival when gentamicin was added, supporting our findings that M. smeg can grow in macrophage media. Although the macrophages were thoroughly washed after phagocytosis of M. smeg, we suspect washing was not 100% efficient at removing all bacteria or that dying macrophages may release bacteria into the extracellular space.

We proceeded with infecting BMDMs at an MOI of 1 in the presence of gentamicin with WT, Δ*dyP operon*, Δ*dyPop::dyPop*, Δ*cyD operon*, Δ*cyDop::cyDop*, and Δ*dyPop*Δ*cyDop* M. smeg followed by plating for bacterial survival at 20 hours (Figure 3B). Interestingly, we observed that the ΔcyD operon was attenuated with a partial rescue in the complemented cyD operon strain (Figure 3B). Given that Δ*dyPop*Δ*cyDop* was not attenuated, we suspect the attenuation may be due to the smooth colony morphology of Δ*cyD operon* (Figure 2A).

3.3.4 M. abs nanocompartment mutant phenotypes

The lack of recapitulation of nanocompartment mutant phenotypes between Mtb and M. smeg led us to wonder if nanocompartments may be important in another mycobacterial pathogen. In M. abs, the predicted Cfp29/DyP nanocompartment is encoded by MAB_0699c/MAB0700c, and the predicted CyD/SrpI nanocompartment is encoded by MAB_0217c/MAB_0218c (Figure 4A). We generated knockouts of the DyP and CyD nanocompartments using ORBIT[141]. First, we evaluated growth by OD_{600} of WT, Δ*dyP operon*, and Δ*cyD operon* M. abs with and without H_2O_2 at neutral pH for 12 hours (Figure 4B). Although H_2O_2 attenuated the growth of the cultures slightly, there were no differences between WT and the nanocompartment mutants (Figure 4B).

We next sought to examine if the nanocompartment mutants would be attenuated at a condition that more closely mimics the phagosomal environment by exposing WT, Δ*dyP operon*, and Δ*cyD operon* to media acidified to pH 4.5 in the presence of H_2O_2 and plating for bacterial survival at 24 and 48 hours (Figure 4C). WT and the nanocompartment mutants all persisted to the same degree (Figure 4C). Intriguingly, the M. abs strains grew about ten-fold overnight in these harsh conditions. This is in contrast to Mtb, which persists under a pH of 4.5 with hydrogen peroxide but does not grow[141].

Due to the difficulty of testing phenotypes in acidic media in M. smeg, we evaluated if the inoculum effect would complicate M. abs experiments. We started WT M. abs cultures at OD_{600}s of 0.05, 0.08, and 0.10 in media acidified to pH 5.5 with H_2O_2 in the presence of absence of pyrazinamide and plated for bacterial survival (Figure 4D). At 24 hours, there was a 6-7 fold difference between cultures starting at an OD of 0.05 compared to 0.10. The fold difference was not affected by pyrazinamide, suggesting that the inoculum effect is not being driven by the antibiotic. In line with the known features of intrinsic antibiotic resistance in M. abs, the high concentration of pyrazinamide did not affect bacterial survival. Given the more modest inoculum effect in M. abs, we proceeded with exposing WT, Δ*dyP operon*, and Δ*cyD operon* M. abs to pH 5.5 with H_2O_2 in the presence and absence of pyrazinamide (Figure 4E). Plating for bacterial survival at 24 hours did not reveal any statistically significant differences among strains.

Lastly, we tested whether nanocompartments are important for M. abs bacterial survival during infection. We infected BMDMs at an MOI of 1 with WT, Δ*dyP operon*, and Δ*cyD operon* M. abs and plated for bacterial survival every day for three days (Figure 4F). We also treated half of the cells with IFN-γ[143], a cytokine known to be important for macrophage control of mycobacteria. WT, Δ*dyP operon*, and Δ*cyD operon* M. abs all persisted to the same degree, suggesting nanocompartments to not play a significant role in growth during infection of BMDMs in this organism.

3.3.5 Biochemistry of Mtb DyP

Genetic analysis of nanocompartment mutants in Mtb, M. smeg, and M. abs revealed that the strongest phenotypes in both broth and infection result from knockout of the DyP operon in Mtb. Thus, we were interested in following up on interesting observations previously made in Mtb. A transposon-insertion sequencing (TnSeq) screen revealed that both DyP and lipid metabolism genes were important for survival at a pH of 4.5 with H_2O_2, and Mtb Δ*dyP operon* is only susceptible to a pH of 4.5 with H_2O_2 if lipids are present in the media[139]. The dependency of the phenotype on lipids led us to the hypothesis that Mtb DyP may be able to detoxify lipid peroxides.

We generated lipid peroxides with an *in vitro* Fenton reaction by incubating arachidonic acid, H_2O_2, and iron. The lipid peroxide was isolated by a chloroform:methanol extraction and run on a TLC plate to visualize the oxidized fatty acid (Figure 5A). Although the arachidonic acid alone appeared to have some auto-oxidized lipid, we saw an increase in oxidized lipid in the condition containing H_2O_2 and iron (Figure 5A). After quantification of the lipid peroxide, we added arachidonic lipid peroxide to purified DyP protein and ABTS (2,2'-azino-bis(3-ethylbenzothiazoline-6-sulfonic acid), which was previously used for DyP peroxidase assays[139]. By measuring absorbance at 420nm, we did not observe any peroxidase activity in the presence of arachidonic acid peroxide above that of the arachidonic acid control (Figure 5B), but we did observe the expected peroxidase activity with H_2O_2[139].

The solubility of lipid peroxides proved challenging, so we also tested DyP peroxidase activity with two organic hydroperoxides: tert-butyl peroxide and cumene hydroperoxide. We exposed purified DyP to tert-butyl peroxide or cumene hydroperoxide, ranging from 1 to 1000μM (Figures 5C and 5D). We did not observe any oxidation of ABTS measured by absorbance as 420nm.

3.3.6 KatG and DyP redundancy in Mtb

In our previously conducted TnSeq in Mtb at pH 4.5 with H_2O_2, *katG* (*Rv1908c*) was found to be important for resistance to H_2O_2 in acidified media[142]. KatG is a catalase-peroxidase that can detoxify hydrogen peroxide and is important for full virulence in mice[144]. Interestingly, katG activates the tuberculosis drug isoniazid (INH). INH-resistant strains of Mtb have loss of function mutations in KatG[140], suggesting that DyP might be able to compensate for KatG in INH-resistant clinical isolates

To test if KatG and DyP play redundant roles, we generated single knockout strains lacking the DyP-Cfp29 operon *(*Δ*dyP operon*) or KatG (Δ*katG*) as well as a strain lacking both the DyP-Cfp29 operon and KatG (Δ*dyPoperon*Δ*katG*) in the Erdman Mtb strain. We infected BMDMs with WT, Δ*dyP operon*, Δ*katG*, and Δ*dyPoperon*Δ*katG* and plated for bacterial survival throughout four days of infection (Figure 6A). We did not observe any differences in bacterial CFU between strains (Figure 6A).

We next infected C57BL/6 mice with WT, Δ*dyP operon*, Δ*katG*, and Δ*dyPoperon*Δ*katG* Mtb with 250 CFUs via the aerosol route. We homogenized lungs and plated for bacterial survival on days 1, 10, 28, and 60 (Figure 6B). We observed a one log attenuation of Δ*katG* and Δ*dyPoperon*Δ*katG strains*, which aligns with previous mouse infections with katG mutants (cite). We did not observe any attenuation of Δ*dyPoperon* or an additional attenuation of Δ*dyPoperon*Δ*katG* (Figure 6B). Thus, it appears, at least in the Erdman strain, that DyP and KatG may play distinct roles during infection, and there may be additional factors that provide redundancy to defense against acid and oxidative stress.

3.4 Discussion

We generated mutants of the Cfp29-DyP and CyD-SrpI nanocompartments in M. smeg and M. abs, two nontuberculosis mycobacterial species. In M. smeg, we find that analysis of mutant phenotypes at acidic pH is difficult due to a strong inoculum effect, and this inoculum effect is not as persistent in M. abs. The DyP nanocompartment mutants in M. smeg and M. abs fail to recapitulate phenotypes seen in Mtb nanocompartment mutants, such as attenuation in oxidative stress at low pH, sensitivity to pyrazinamide in the presence of oxidative stress, and increased killing by macrophages[140]. Interestingly, an M. smeg strain lacking the CyD nanocompartment has a smooth colony morphology and is attenuated in macrophages. The requirement for fatty acids for observing attenuation of Mtb DyP mutants in the presence of H_2O_2 suggested to us that perhaps lipid peroxides may be the substrate for the Mtb nanocompartment. Additional efforts to characterize the biochemical properties of Mtb DyP by testing its ability to reduce lipid peroxides or organic hydroperoxides yielded negative data. We also show that DyP does not provide redundancy in the absence of KatG in Mtb in a macrophage or mouse infection.

The contribution of nanocompartments to bacterial physiology has been an unanswered question in the field. Few studies have analyzed phenotypes of genetic knockouts in nanocompartments. To our knowledge, these studies include the knockout of a nanocompartment containing ferritin-like proteins that resulted in sensitivity to hydrogen peroxide in Myxococcus xanthus[141], and our previous work on importance against defense against oxidative stress of DyP nanocompartment in Mtb.

Peroxidases in the DyP family have been shown to have low pH optima[143], and the DyP nanocompartment mutant in Mtb is susceptible to oxidative stress at a low pH. To

facilitate analysis of the function of nanocompartments in mycobacteria, we attempted to utilize the fast growing species M. smeg. However, a strong inoculum effect blocked our ability to rigorously examine the function of M. smeg nanocompartment mutants at low pH. The inoculum effect is defined as the large increase in minimum inhibitory concentration (MIC) of a compound when the number of bacteria inoculated is increased[145]. Typically, the inoculum effect is described in the context of antibiotics[145]. One common explanation for the inoculum effect is the decrease in effective concentration of the compound due to binding to bacterial surfaces or degradation from bacterial enzymes[146]. Another explanation for the inoculum effect is that the amount of compound per individual bacterium is changed when the inoculum is changed[146]. Our data suggest that the inoculum effect to hydrogen peroxide is potentiated by acidic pH. One potential explanation for the inoculum effect at acidic pH is that M. smeg can neutralize protons and alter the local pH. In Mtb, an example of proton buffering is the extracellular conversion of asparagine to aspartate to generate ammonia, which neutralizes acidic pH[145–147]. Given that the inoculum effect at acidic pH was stronger in M. smeg than M. abs, it would be interesting to screen for acid sensitive M. smeg and M. abs mutants.

Our negative data also highlight the differences in the contribution of nanocompartments among different mycobacterial species. From an evolutionary point of view, M. smeg, M. abs, and Mtb are evolutionarily distant. Further, both M. smeg and M. abs live in the environment, while Mtb is an obligate human intracellular pathogen. It is common for pathogens to have undergone genome reduction[147–149]. Accordingly, Mtb is predicted to encode around ~4000 genes, while M. smeg and M. abs are predicted to encode ~6700 and ~5000 genes, respectively. This difference in gene number and millions of years of evolution may perhaps translate to differences in genetic responses to oxidative stress. For instance, OxyR, a regulator of oxidative stress response in many bacteria, is absent in Mtb but is present in M. smeg and M. abs[150]. There are 28 sigma factors in M. smeg, 19 in M. abscessus, and 13 in Mtb[151,152]. M. smeg encodes three different katG catalase-peroxidase sequences in its genome, although only two of them appear to be functional proteins[153], and Mtb does not encode the CyD/SrpI nanocompartment. Our negative data searching for phenotypes in M. smeg and M. abs demonstrate the potential redundancy of oxidative stress genes in mycobacteria.

Nanocompartment mutants in M. smeg resulted in interesting colony morphologies. While the Δ*dyP operon* strain appeared normal, Δ*cyD operon* had a smooth colony morphology. Smooth and rough colony morphologies have been observed across many mycobacterial species[154], some of which include *Mycobacterium fortuim*, *Mycobacterium kansasii*, *Mycobacterium avium complex*, and *Mycobacterium abscessus*. Colony morphology is often attributed to the presence of glycopeptidolipids (GPLs) in smooth colony variants and absence of GPLs in rough colony variants[155]. Conventionally, rough colony variants lacking GPLs are thought to be more virulent[156]. In M. smeg, smooth colony variants have been attributed to both the overexpression of GPL biosynthetic locus[157] and mutating the nucleoid-associated protein Lsr2[157–159]. An interesting future direction would be to test for the presence of GPLs in M. smeg Δ*cyD operon* to evaluate if it is a conventional smooth colony phenotype. We found that expressing the cyD operon from its native promoter in the ΔcyD operon strain failed to complement the smooth colony morphology. Whether this is a failure of the

complemented strain to make functional nanocompartments has yet to be tested. The genes neighboring the CyD-SrpI nanocompartment locus in M. smeg are not well characterized, but colony morphology changes due to polar effects is a possibility. Deletion of the serine/threonine kinase PknL in M. smeg led to smooth colony variants that were not complemented by expressing PknL and were instead found to contain transposon insertions or mutations in Lsr2[159]. Thus, whole genome sequencing of Δ*cyD operon* smooth colony variants may be informative. Given that CyD is predicted to be important for sulfur mobilization, it may also be interesting to assay WT and Δ*cyD operon* for differences in sulfur-containing lipids[160].

Interestingly, the Δ*dyPop*Δ*cyDop* double nanocompartment mutant appears rough even though it is lacking the cyD operon. This leads us to believe that the attenuation of Δ*cyD operon* in macrophages may be due to its colony morphology, as Δ*dyPop*Δ*cyDop* was not attenuated in macrophages. To generate the double nanocompartment mutant, we electroporated Δ*dyP operon* bacteria that appeared phenotypically normal with the ORBIT plasmids and oligonucleotides to delete the cyD operon. It would be informative to do the reverse by starting with Δ*cyD operon* and perform the ORBIT protocol to generate the DyP operon deletion.

Although Δ*dyPop*Δ*cyDop* appeared rough, this mutant presented with a unique phenotype of small and large colony morphologies. In *Listeria monocytogenes*, deletion of PerR, a regulatory protein that initiates oxidative stress defense genes, results in "small" and "large" colonies[161]. Similar to our findings, the large colonies eventually dominate the culture[161]. The large colonies are more resistant to H_2O_2 and are more virulent in a mice, so it is concluded that the large colonies are suppressors of the small colonies[161], although the suppressor mutations have not been reported to our knowledge.

Since the M. smeg Δ*dyPop*Δ*cyDop* large colonies were the same size as WT colonies, we originally hypothesized that small colonies were the true phenotype of deleting both nanocompartments and large colonies were the result of suppressor mutations, similar to the findings of deleting PerR in *Listeria monocytogenes*[161]. However, we were unable to find differences in single nucleotide polymorphisms among strains by whole genome sequencing. Sequencing of strains did reveal that large colony cultures were nanocompartment mutant bacteria and not contaminated by WT M. smeg. We also did not observe any phenotypes between small and large colonies for conditions tested besides the colony size itself. Although the Δ*dyPop*Δ*cyDop* complemented strain was never constructed, it would be informative to complement the small colonies.

Another important future direction is the purification of nanocompartments from M. smeg and M. abs. We previously purified nanocompartments from Mtb by layering bacterial lysate on a sucrose gradient followed by ultracentrifugation[157]. It would be interesting to know which nanocompartments are expressed in M. smeg and M. abs and to what degree. It would also be interesting to evaluate if any conditions, such as acidic pH or oxidative stress, drive increased expression of nanocompartments.

The strongest nanocompartment phenotypes we have observed from generating nanocompartments in mycobacteria are mutants of the DyP operon in Mtb[157], so we aimed to further characterize the Mtb DyP nanocompartment. When TnSeq was performed in Mtb at pH 4.5 with hydrogen peroxide, many genes involved in lipid metabolism, including Mce1A, Ltp2, and FadE29, were top hits[158]. This led us to discover that a knockout of the DyP nanocompartment in Mtb is only attenuated at acidic pH in the

presence of hydrogen peroxide if lipids are in the media[160]. Thus, we wondered if DyP could act as a lipid peroxidase. Lipid peroxides form when reactive oxygen species undergo chemical reactions with polyunsaturated fatty acids or cholesterol[162]. Lipid peroxides inflict more damage on biomolecules than oxygen radicals because they are larger, more membrane permeable, and stable[162]. Malondialdehyde, an indicator of lipid peroxidation, is upregulated in the serum of patients with extrapulmonary tuberculosis[163], and redox sensitive transcription factors such as NF-kB and AP-1 are regulated by lipid peroxides[164]. The role that lipid peroxides play during infection and if there is a system to detoxify lipid peroxides in Mtb is still unknown.

We aimed to assay the ability for DyP to reduce oxidized lipids by incubating purified DyP protein with ABTS and lipid peroxide generated from arachidonic acid. We failed to quantify any lipid peroxidase activity under these conditions. In macrophages, Mtb preferentially internalizes arachidonic acid[165], but it is possible DyP has the ability to reduce other lipid peroxides that were not tested. Solubility of the lipid peroxide in aqueous buffer was worrisome, so we also tested the ability of DyP to use tert-butyl peroxide or cumene hydroperoxide as a substrate and generated negative data. It is hard to conclude if DyP only can reduce hydrogen peroxide or if the conditions of our in vitro peroxidase activity assay or lipid peroxide generation were not optimal. DyP from *Rhodococcus jostii* has been found to degrade nitrated lignin[161], a polymer found in plant cell walls, providing precedence for DyP to utilize substrates other than hydrogen peroxide.

Another Mtb phenotype we were interested in following up on was the observation from conducting TnSeq at pH 4.5 with hydrogen peroxide that KatG, a well-characterized catalase-peroxidase, is attenuated along under these conditions along with the DyP nanocompartment. KatG is of high interest in Mtb biology because it activates the prodrug isoniazid commonly used to treat tuberculosis infections. Isoniazid-resistant Mtb strains often contain loss of function mutants of KatG[162–165]. Therefore, we reasoned that DyP may provide redundancy for KatG in clinical strains lacking KatG function. In a macrophage infection, we observed that Δ*dyPoperon*, Δ*katG*, and Δ*dyPoperon*Δ*katG* in the Erdman background all grew to the same extent as WT. Previously, we observed an attenuation of the Δ*dyP operon* in BMDMs[142]; however, this was in the H37Rv Mtb strain. When infecting mice, we found the Δ*katG* strain to be attenuated about a log CFU in alignment with previous findings[144], but there was no additional impact of knocking out the DyP nanocompartment. We find this data to highlight the redundancy of oxidative stress defense genes in mycobacteria. Generating a TnSeq library in Δ*dyP operon* or Δ*katG* background would be informative in uncovering genetic components that provide redundancy to these peroxidases.

One of the biggest questions remaining about nanocompartments is determining why these proteins are encapsulated. Many peroxidases and cysteine desulfurases throughout bacterial phyla do not have a protein shell, so why are DyP, CyD, and other encapsulated proteins surrounded by a protein shell? One leading hypothesis is that encapsulation promotes stability of the cargo protein. If we had discovered strong phenotypes in M. smeg or M. abs nanocompartment mutants, our experimental plan was to test the function of encapsulation by generating genetic deletions of the shell protein and probing for the half-life of cargo protein by western blot.

Here, we show that deletion of nanocompartments in the nontuberculosis mycobacterial species M. smeg and M. abs do not phenocopy what we have previously observed in Mtb[18,19,167]. This highlights the differences that nanocompartments may play in different bacterial species. We also gathered negative data for the ability of Mtb DyP to detoxify lipid peroxides or provide redundancy for KatG. Nonetheless, nanocompartments have primarily been characterized biochemically. Hence, our genetic data provide insights into the roles of nanocompartments may play in bacterial physiology.

3.5 Materials and Methods

Bacterial strains and plasmids

M. smeg mc^{2}155, M. abs ATCC19977, or Mtb Erdman were used for all experiments. Bacteria were grown to midlog phase in Middlebrook 7H9 liquid medium supplemented with 10% albumin-dextrose-saline, 0.4% glycerol, and 0.05% Tween80. M. smeg and M. abs were plated on LB agar. Mtb was plated on solid 7H10 agar supplemented with Middlebrook OADC (BD Biosciences) and 0.4% glycerol. For complementation studies, the open reading frame of the DyP operon or CyD operon plus 1000bp upstream were cloned into pMV306kan via Gibson assembly. To measure redox state, a kanamycin cassette was cloned into pMV762-mrx-roGFP[164] via Gibson assembly and transformed into M. smeg strains. Erdman ΔkatG was a gift from Jeff Cox. Erdman Δ*dyP operon* and Δ*katG*Δ*dyPoperon* was made by specialized transduction with pMSG361 vector as previously described[166].

Knockout of nanocompartment genes in M. smeg and M. abs with ORBIT

Mutants were made in M. smeg and M. abs using ORBIT as described previously[141]. In summary, M. smeg and M. abs cultures containing pKM444 were grown overnight to midlog phase in 7H9 with 50μg/mL kanamycin for M. smeg and 150μg/mL kanamycin for M. abs. Cultures were back diluted to $OD6_{00}$=0.3, followed by addition of 500ng/mL anhydrotetracycline for 3 hours shaking at 37C. To prepare electrocompetent cells, the cells were washed three times with cold 10% glycerol and resuspended in 1/10 the original culture volume of cold 10% glycerol. 1μg ultramer containing flanking regions for the gene of interest and an attP site was mixed with 200ng of pKM464 and added to 400μL of electrocompetent cells. The mixture was electroporated at 2.5kV, 25μF, and 1000Ω. Electroporation was immediately recovered in 2mL 7H9 and shaken at 37C for 16-20 hours before plating on LB agar with 25μg/mL zeocin for M. smeg and 50μg/mL zeocin for M. abs. Mutants were confirmed by PCR and sequencing the genetic locus of interest. Mutants were cultured in the absence of kanamycin to recover clones that spontaneously lost pKM444.

Western blot

M. smeg strains were grown in 7H9 to midlog phase, pelleted, washed two times with PBS, and lysed in mycobacterial lysis buffer (50mM Tris-Hcl pH 7.5, 5mM EDTA, 0.6% SDS, 1mM PMSF). Samples were lysed in a bead beater, cell debris was removed, and total protein was quantified using Pierce BCA Protein Assay kit. 10μg of protein was ran on an SDS-PAGE Tris-HCl 4-20% criterion gel (Bio-Rad). Primary polyclonal antibody for Cfp29 was generated as described previously[20,96,169], and GroEL primary antibody was purchased from Enzo Life Sciences (ADI-SPS-875-D). Primary antibodies were used at

a dilution of 1:1000 in 5% bovine serum albumin in 1x Tris Buffered Saline + 0.1% Tween-20 (TBST). Goat anti-rabbit-HRP secondary antibody (Cell Signaling Technology #7074) was used at 1:5000 in 5% nonfat dry milk in TBST. Blots were developed by using Western Lightning Plus-ECL chemiluminescence substrate (Perkin-Elmer) and imaged on a ChemiDoc MP System (BioRad).

Exposure to acidic pH and oxidative stress

M. smeg or M. abs strains were grown to midlog phase, washed two times with respective media, and diluted to OD_{600}=0.10 unless otherwise specified in 10mL total volume of respective 7H9 pH 4.5-6.5. Cultures were shaken at 37C for specified time. CFUs were enumerated by dilution in phosphate buffered saline (PBS) + 0.05% Tween-80 and plating dilutions on LB agar.

Measurement of redox state

M. smeg strains were transformed with mrx1-roGFP. Bacteria were grown to midlog phase in 7H9, washed two times with 7H9 pH 4.5, and added to 96-well plates at an OD=0.5 in 200µL in designated media (7H9 pH 4.5 or pH 4.5 + 5mM H_2O_2). Plates were read every 10 minutes for 1 hour at excitation 390 and 490 and emission at 510 in a SpectraMax M2 plate reader. Redox homeostasis was calculated by emission ratios of 390/490 excitations.

Serial passaging of M. smeg small and large colonies

WT and small or large M. smeg Δ*dyPop*Δ*cyDop* colonies were grown to midlog phase in 3mL of 7H9 and plated for CFU enumeration on LB agar (day 0). Culture was diluted to OD_{600}=0.0015 in 10mL culture volume and grown to log phase overnight. Culture was plated for CFU enumeration on LB agar (day 1) and subsequently diluted to OD_{600}=0.0015. Process was repeated for 10 days total, and the number of small or large colonies was recorded in comparison to passaging of WT M. smeg.

In vitro generation of lipid peroxide and TLC plate

4mL of 50mM Na-acetate pHed to 4.5 with acetic acid was combined with 300mg of ammonium iron III sulfate , 46µg of arachidonic acid, and 0.5M H_2O_2. The reaction was incubated at room temperature for 3 hours followed by quenching with 1mL of 5% sulfuric acid. To extract the lipid, 2:1 chloroform:methanol was added in a volume of 5mL and mixed. The top aqueous phase was removed. Lipid peroxide in the organic phase was quantified with the PeroxiDetect Kit (Millipore-Sigma PD1-1KT) per manufacturer's instructions. Lipid peroxide was visualized by adding 3µL to a TLC plate ran in 93:7 hexane:isopropanol. The TLC plate was heated to 160C and visualized with UV light.

DyP purification

SUMO-His-tag Mtb DyP was expressed and purified from *E. coli* as described previously[165].

ABTS assays

312nM of purified DyP was combined with 250µM H_2O_2, 250µM lipid peroxide, or indicated concentration of tert-butyl or cumene hydroperoxide, and 250µM ABTS in

100mM sodium citrate buffer pH 4. The reaction was monitored by absorbance at 420nm for 20min in a SpectraMax M3 plate reader.

Infection of murine macrophages with M. smeg, M. abs, and Mtb

To generate bone marrow derived macrophages (BMDMs), femurs were removed from C57BL/6 mice and flushed with BMDM media (Dulbecco's Modified Eagle Medium (DMEM)+ 1% L-glutamine, 10% supernatant from 3T3-M-CSF cells, and 10% fetal bovine serum). Bone marrow was plated at $1x10^7$ cells per 15cm non-TC treated dish and differentiated for 6 days with feeding on day 3. Cells were frozen in BMDM media with 10% DMSO. Two days before infection, BMDMs were thawed and plated at $5x10^4$ cells per well in a 96-well plate. One day before infection, IFN-γ was added if specified. On the day of infection, either M. smeg, M. abs, or Mtb cultures were grown to midlog phase, washed two times in phosphate buffered saline (PBS), centrifuged at 500rpm for 5 minutes to remove clumps, and added to BMDMs in DMEM supplemented with 5% FBS and 5% horse serum at the designated multiplicity of infection (MOI). Phagocytosis occurred for 1 hour for M. smeg and 4 hours for Mtb. For M. abs, phagocytosis was initiated by centrifugation at 1200rpm for 10 minutes. BMDMs were washed with room temperature PBS two times before fresh BMDM media was added. Gentamicin was added at 50μg/mL when specified. For CFU, BMDMs were washed two times with PBS and lysed with 0.5% Triton-X in H_2O and incubated at 37C for 10 minutes. Lysed cells were serially diluted in PBS + 0.05% Tween-80 and plated on LB agar for M. smeg and M. abs and on 7H10 agar for Mtb.

Mouse infections

C57BL/6 mice were obtained from Jackson Laboratory, Bar Harbor, ME. Mice were infected via the aerosol route at 6 weeks of age with 250 CFUs of Mtb strains using a Glas-Col (Brazil, IN) full-body inhalation exposure system. On days 1, 10, 28, and 60, lungs were homogenized, serially diluted in PBS + 0.05% Tween 80, and plated on 7H10 agar for CFU enumeration. The number of mice per group was calculated by G*power, and five mice per group were used.

3.6 Figures

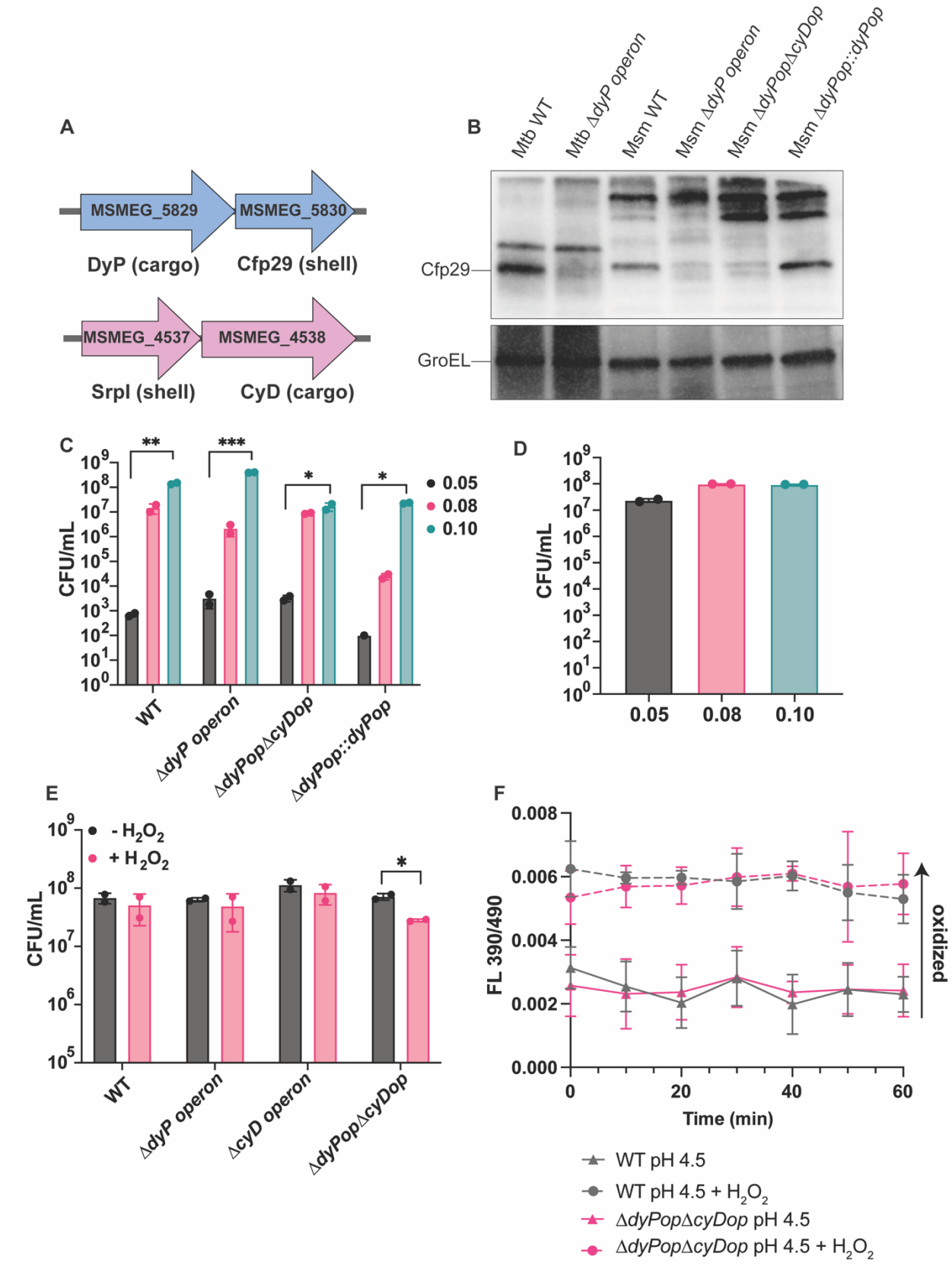
A
MSMEG_5829
MSMEG_5830
DyP (cargo)
Cfp29 (shell)
MSMEG_4537
MSMEG_4538
SrpI (shell)
CyD (cargo)
B
Mtb WT
Mtb ΔdyP operon
Msm WT
Msm ΔdyP operon
Msm ΔdyPopΔcyDop
Msm ΔdyPop::dyPop
Cfp29
GroEL
C
CFU/mL
0.05
0.08
0.10
WT
ΔdyP operon
ΔdyPopΔcyDop
ΔdyPop::dyPop
D
CFU/mL
0.05
0.08
0.10
E
- H2O2
+ H2O2
CFU/mL
WT
ΔdyP operon
ΔcyD operon
ΔdyPopΔcyDop
F
FL 390/490
oxidized
Time (min)
WT pH 4.5
WT pH 4.5 + H2O2
ΔdyPopΔcyDop pH 4.5
ΔdyPopΔcyDop pH 4.5 + H2O2

Figure 1. In vitro M. smeg nanocompartment phenotypes
(A) Schematic of the two nanocompartment operons in M. smeg (B) Western blot for Cfp29 and GroEL of WT and Δ*dyP operon* lysates from Mtb as a control in addition to M. smeg nanocompartment mutants and dyP complemented strain. (C) CFU of M. smeg nanocompartment strains at 21 hours with inoculum at either OD_{600}=0.05, 0.08, or 0.10 at a pH 5.5 with 2.5mM H_2O_2 and 200μg/mL PZA. (D) CFU of WT M. smeg at 15 hours with inoculum at either OD_{600}=0.05, 0.08, or 0.10 at a pH 6.6 with 1mM H_2O_2. (E) CFU of M. smeg nanocompartment mutants at 12 hours with inoculum at OD=0.10 at a pH 6.6 with 1mM H_2O_2. (F) Fluorescence emissions of WT or Δ*dyPop*Δ*cyDop* M. smeg expressing the mrx-roGFP reporter at pH 4.5 +/- 5mM H_2O_2 over the course of 60 minutes. p-Values were determined using unpaired t-test. *p<0.05, **p<0.01, ***p<0.001.

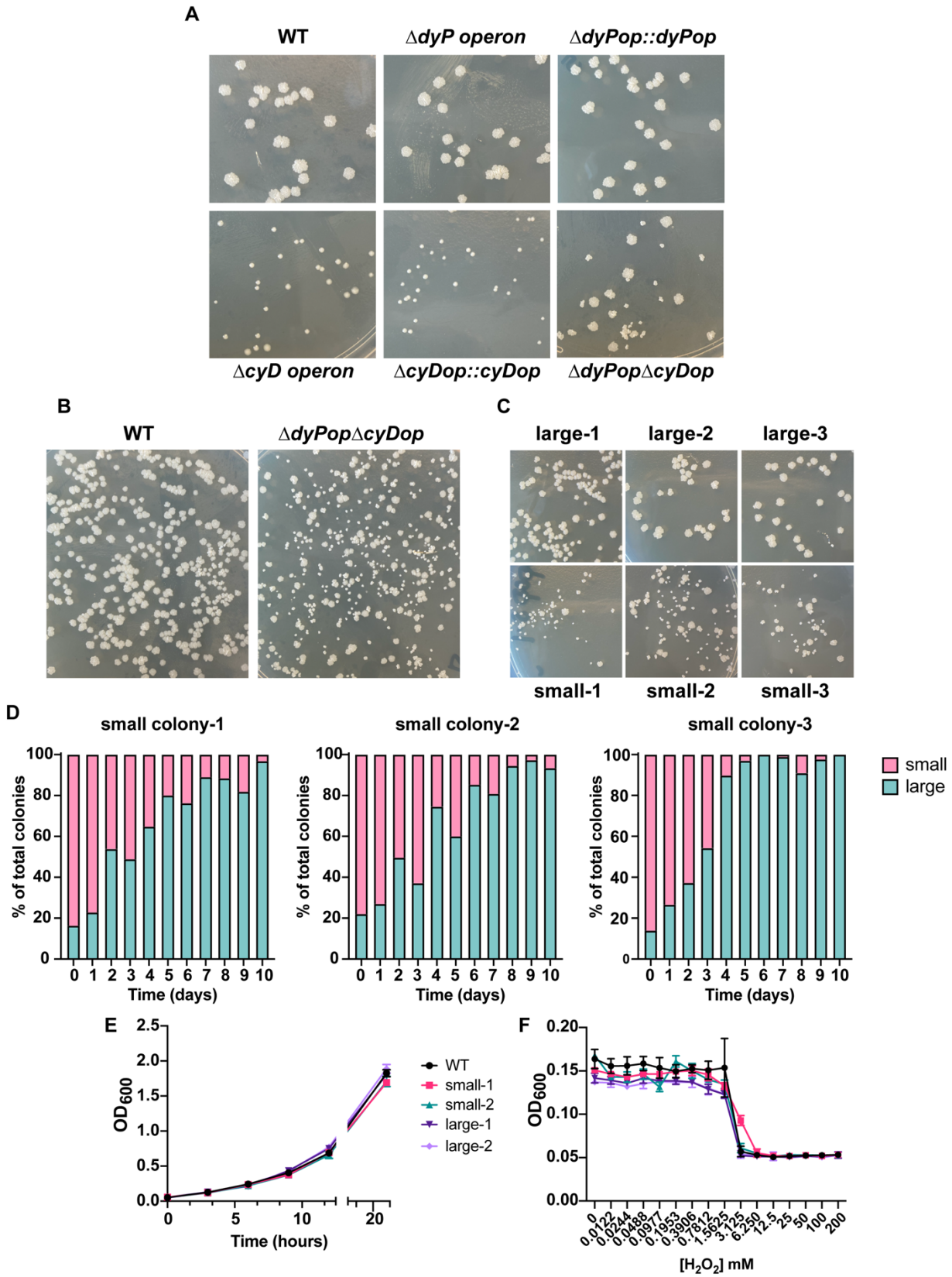
A
WT
ΔdyP operon
ΔdyPop::dyPop
ΔcyD operon
ΔcyDop::cyDop
ΔdyPopΔcyDop
B
WT
ΔdyPopΔcyDop
C
large-1
large-2
large-3
small-1
small-2
small-3
D
small colony-1
small colony-2
small colony-3
% of total colonies
Time (days)
small
large
E
OD600
Time (hours)
WT
small-1
small-2
large-1
large-2
F
OD600
[H2O2] mM

Figure 2. Colony morphologies in M. smeg nanocompartment mutants
(A) Images of colonies in M. smeg nanocompartment strains all imaged at the same zoom. (B) Images of colonies in M. smeg WT and Δ*dyPop*Δ*cyDop.* (C) Images of colonies propogated from either M. smeg large Δ*dyPop*Δ*cyDop* or small Δ*dyPop*Δ*cyDop* colonies. (D) Percentage of Δ*dyPop*Δ*cyDop* large or Δ*dyPop*Δ*cyDop* small colonies when passaging cultures daily for 10 days started from Δ*dyPop*Δ*cyDop* small colonies. (E) OD_{600} of M. smeg WT, Δ*dyPop*Δ*cyDop* large, and small strains in LB broth over the course of 20 hours. (F) Minimum inhibitory concentration (MIC) determination by OD_{600} of M. smeg WT, Δ*dyPop*Δ*cyDop* large, and small in 7H9 across a dilution series of H_2O_2 at 24 hours.

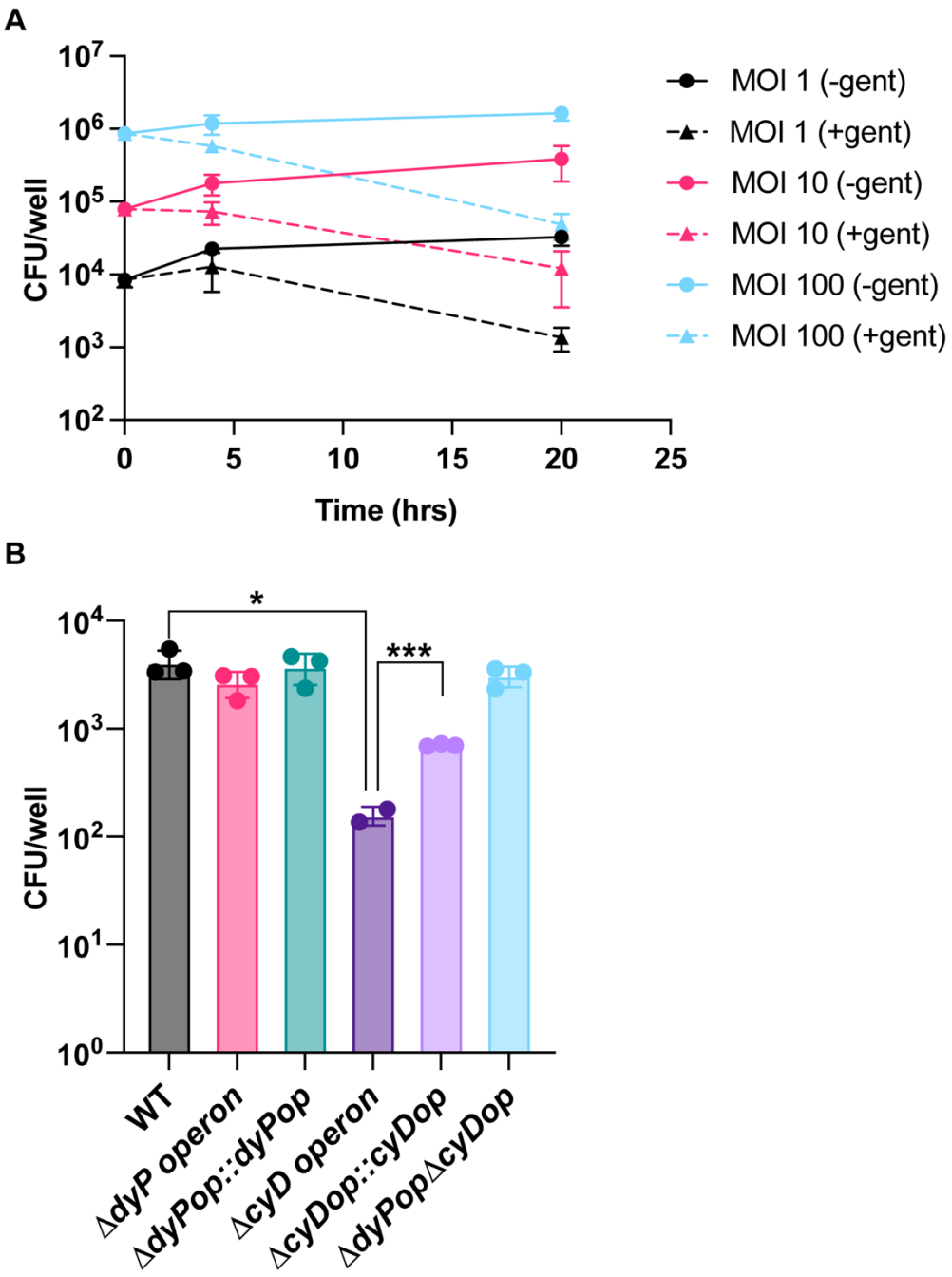

Figure 3. Macrophage infection with M. smeg nanocompartment mutants
(A) CFU from infection of C57BL/6 BMDMs with WT M. smeg at MOI of either 1, 10, or 100 with or without 50μg/mL gentimicin over the course of 20 hours. (B) CFU from infection of C57BL/6 BMDMs with M. smeg nanocompartment strains at MOI of 1 with 50μg/mL gentimicin at 20 hours. p-Values were determined using unpaired t-test. *p<0.05, **p<0.01, ***p<0.001.

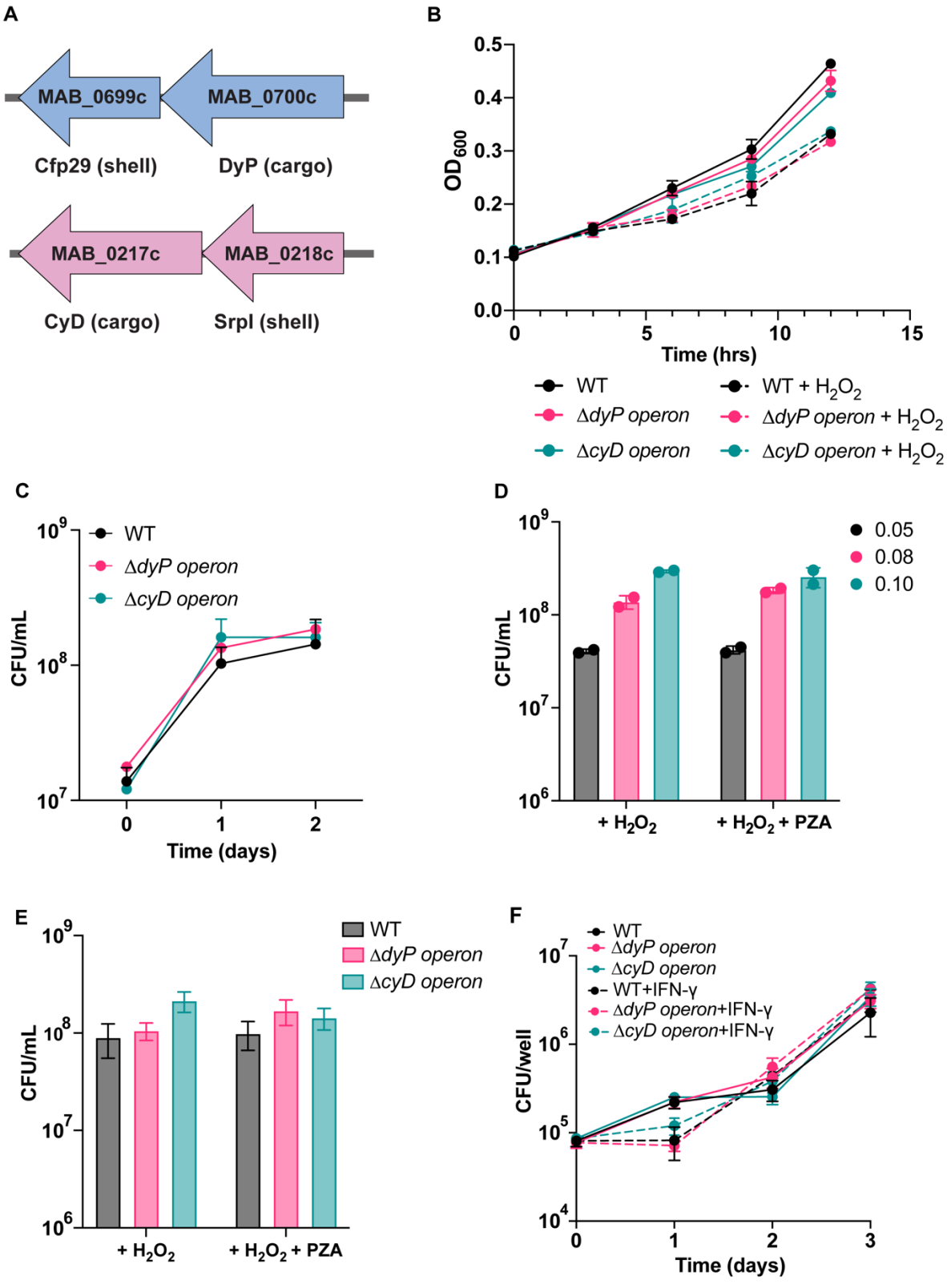
A
MAB_0699c
MAB_0700c
Cfp29 (shell)
DyP (cargo)
MAB_0217c
MAB_0218c
CyD (cargo)
SrpI (shell)
B
OD600
Time (hrs)
WT
ΔdyP operon
ΔcyD operon
WT + H2O2
ΔdyP operon + H2O2
ΔcyD operon + H2O2
C
CFU/mL
Time (days)
WT
ΔdyP operon
ΔcyD operon
D
CFU/mL
0.05
0.08
0.10
+ H2O2
+ H2O2 + PZA
E
CFU/mL
WT
ΔdyP operon
ΔcyD operon
+ H2O2
+ H2O2 + PZA
F
CFU/well
Time (days)
WT
ΔdyP operon
ΔcyD operon
WT+IFN-γ
ΔdyP operon+IFN-γ
ΔcyD operon+IFN-γ

Figure 4. Nanocompartment mutant phenotypes in M. abs
(A) Schematic of the two nanocompartment operons in M. abs. (B) OD_{600} of M. abs nanocompartment mutants in 7H9 pH 6.6 with 1mM H_2O_2 over the course of 12 hours. (C) CFU of M. abs nanocompartment mutants in 7H9 pH 4.5 with 2.5mM H_2O_2 at 24 hours (D) CFU of WT M. abs started at inoculum of OD_{600}=0.05, 0.08 or 0.10 in 7H9 pH 5.5 with 2.5mM H_2O_2 and 200μg/mL PZA at 24 hours (E) CFU of M. abs nanocompartment mutants started at inoculum of OD600=0.05 in 7H9 pH 5.5 with 2.5mM H_2O_2 and 200μg/mL PZA at 24 hours (F) CFU of infection of C57BL/6 BMDMs with M. abs nanocompartment mutants at MOI=1 +/- IFN-γ over the course of 3 days.

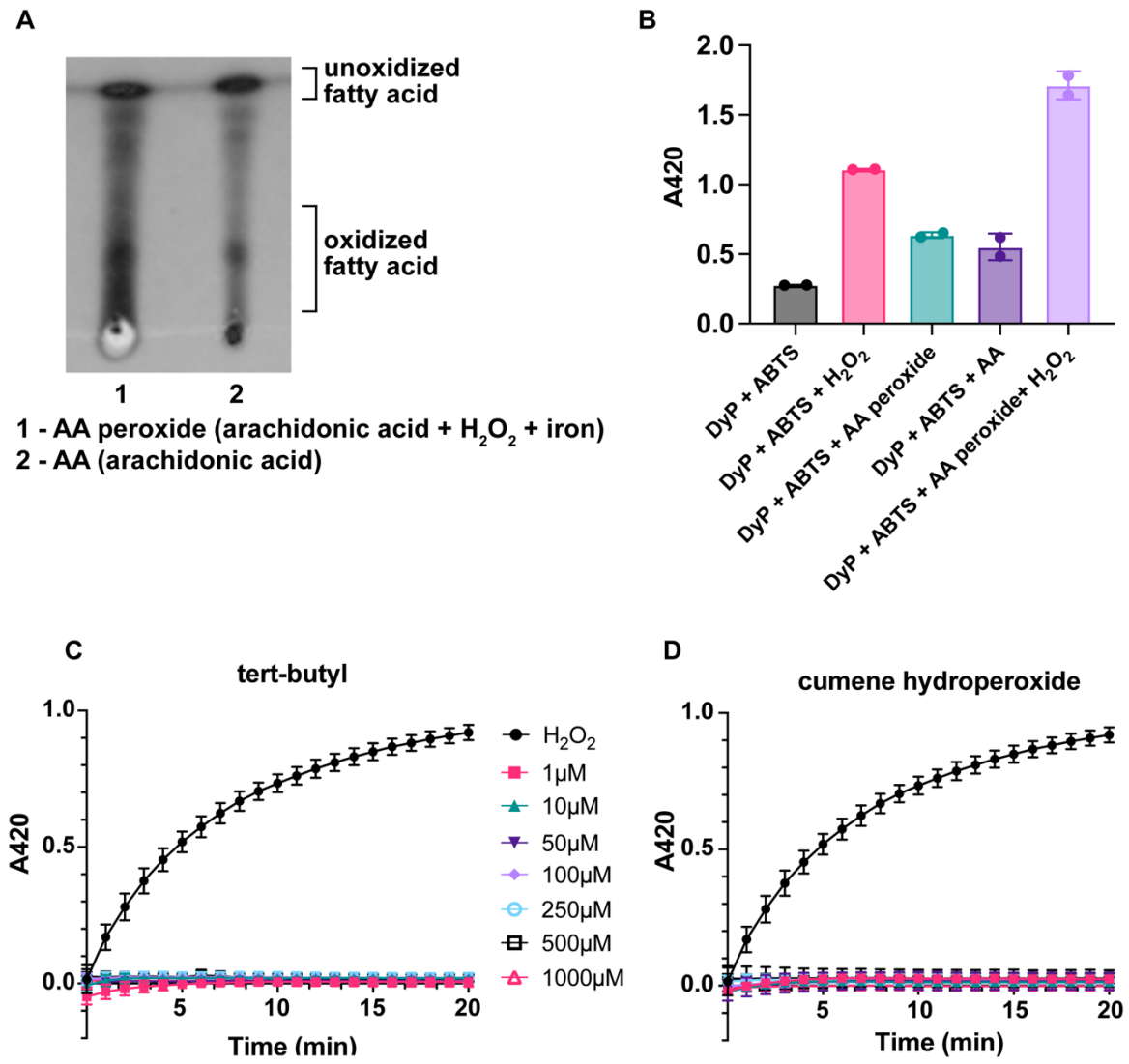

Figure 5. Lipid peroxides as a substrate for Mtb DyP
(A) TLC of (1) arachidonic acid lipid peroxide generated by incubation of arachidonic acid, H_2O_2, and iron and (2) arachidonic acid as a control. (B) Peroxidase activity of purified Mtb DyP using 250μM ABTS as a substrate along with either 250μM H_2O_2, arachidonic acid (AA) peroxide, arachidonic acid, or a control with AA peroxide and H_2O_2 as substrates measured by absorbance at 420nm after 20 minutes. Peroxidase activity of purified DyP using 250μM ABTS as a substrate, 250μM H_2O_2 as a positive control, and concentrations of 1μM-1000μM (C) tert-butyl or (D) cumene hydroperoxide measured by absorbance at 420nm over the course of 20 minutes.

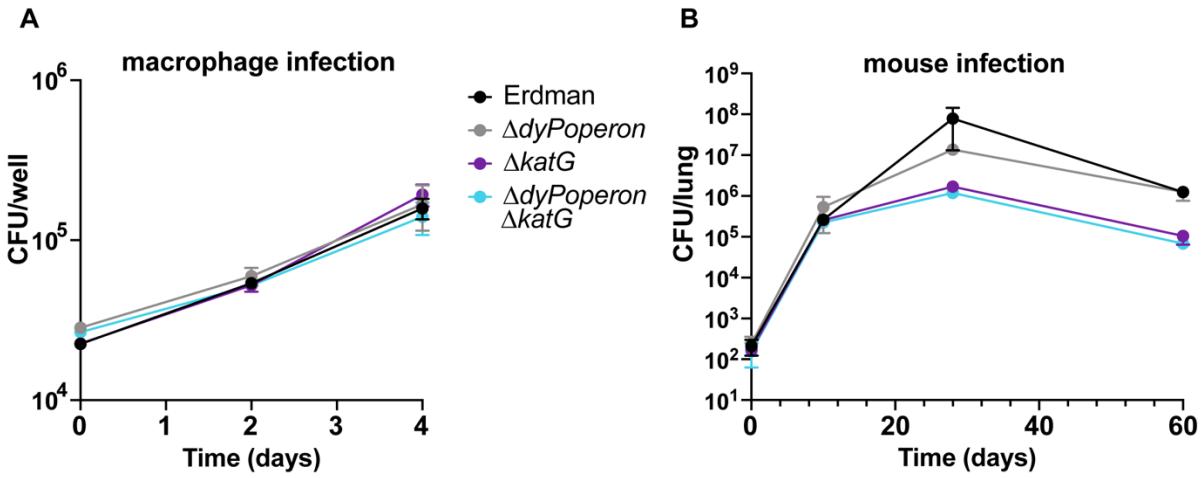

Figure 6. Testing redundancy of DyP and KatG during Mtb infection
(A) CFU from infection of C57BL/6 BMDMs at MOI=1 of Mtb WT, Δ*dyPoperon, ΔkatG, and ΔdyPoperonΔkatG* over the course of 4 days. (B) CFU from the lungs of C57BL/6 mice infected by aerosol with 250 CFUs of Mtb WT, Δ*dyPoperon, ΔkatG, and ΔdyPoperonΔkatG* at 1, 10, 28, and 60 days.

Chapter 4: Random barcode transposon-site sequencing in *Mycobacterium tuberculosis* to reveal the functions of unknown genes

Kayla M. Dinshaw, Katie A. Lien., Matthew Knight, Sorel Ounkap, Morgan Price, Hans Carlson, Nick Campbell-Kruger, Adam Deutschbauer, Sarah A. Stanley

4.1 Abstract

Mycobacterium tuberculosis (Mtb) is a bacterial human pathogen that can establish chronic infections in the lung. Although the genome of Mtb was sequenced nearly 25 years ago, the function of many individual genes and how they contribute to Mtb survival *in vivo* remains to be discovered. Large scale genetic approaches to understanding gene function are hindered by the limited throughput of traditional transposon sequencing strategies used in mycobacteria. To create a resource for determining the function of unknown genes, we generated a pooled random barcode transposon-site sequencing (RB-TnSeq) library in *Mycobacterium tuberculosis* (Mtb). A unique twenty-nucleotide barcode in the transposon allows for rapid, high throughput genetic screening without the laborious protocol of standard bacterial TnSeq screens. The Mtb RB-TnSeq library was exposed to a chemical library of carbon sources, nitrogen sources, and stressors. We performed 38 RB-TnSeq screens, which resulted in ~1700 statistically significant hits overall. To validate the results from the high-throughput genetic screens, we evaluated conditions with relevance to Mtb metabolism and antibiotic resistance. For instance, we found that the *nuo* operon, one of three loci encoding complex I of the electron transport chain, is required for growth on two carbon sources, propionate and asparagine. We propose D-lactate as a potential carbon source for Mtb to use during infection. Lastly, we characterize novel mutants that confer resistance to the tuberculosis antibiotic pretomanid. Results from these genetic screens have begun to reveal the function of unknown genes and will expand our knowledge of the genetics behind Mtb pathogenesis.

4.2 Introduction

Mycobacterium tuberculosis (Mtb) is a bacterium that infects the lungs and is the causative agent of tuberculosis, which is estimated to infect a quarter of the global population[167]. The success of Mtb as a human pathogen may be attributed to many unique features of mycobacterial physiology. Mtb is both intrinsically resistant to many antibiotics and acquires de novo resistance to clinically used antibiotics. As a result, antibiotic therapy for tuberculosis infections requires multiple antibiotics that present with harsh side effects. Depending on the strain, treatment can range from three to nine months in duration[168], resulting in patient non-adherence and the rise of multidrug resistant (MDR) and extensively drug resistant (XDR) strains.

To grow inside the host, Mtb assimilates macromolecules such as fatty acids, amino acids, and carbohydrates to use as carbon and nitrogen sources. Mtb has the genetic potential for the synthesis of essential amino acids, vitamins, and co-factors, and a large portion of the genome seemingly dedicated to lipid metabolism[167]. Mtb often resides in the phagosome of macrophages, which activate an arsenal of host defenses to attempt to eradicate the infection. For instance, the phagosome is acidified by the vacuolar-H(+)-ATPase, NOS2 catalyzes production of nitric oxide, and the NADPH oxidase generates a respiratory burst of superoxide. Although these immune processes

are successful at killing many pathogens, Mtb can persist and establish a chronic infection. Much of Mtb's intrinsic resistance to antibiotics and stress has been attributed to its thick and elaborate cell envelope, a multi-layered structure containing peptidoglycan, arabinogalactan, and mycolic acids. Understanding the molecular mechanisms behind drug susceptibility and resistance, metabolism, resistance against various stressors, and the mycobacterial cell wall will be imperative in combatting the global tuberculosis epidemic.

Mtb encodes ~4000 genes, a similar size to the model bacterium *Escherichia coli*[169], yet many genes remain unannotated as "hypothetical proteins" or annotated by homology to other bacteria, which is often inaccurate. The requirement for high-containment facilities and the slow growth of Mtb (21 days to grow a colony on solid agar) complicate laboratory experiments. Genetic screens are a common method of uncovering gene function. In bacteria, this can be accomplished by transposon insertion sequencing (TnSeq), which couples pooled transposon insertion mutagenesis with next-generation sequencing[170–173]. Transposon-mutant libraries are exposed to a condition of interest, and the enrichment or depletion of transposon mutants are used to infer gene function. TnSeq screens in Mtb have revealed essential genes in broth[18,19,174] and genes important for virulence in various mouse models[20,96,175]. TnSeq screens have also been conducted in biologically-relevant conditions, some of which include acid and oxidative stress[169], tuberculosis antibiotics[170], hypoxia[171], and growth on cholesterol[172,173]. A major limitation of TnSeq methods are the long and laborious protocols that include plating bacteria after exposure to conditions of interest, genomic fragmentation, DNA end-repair, adapter ligation, PCR, and the computationally intensive process of aligning of sequencing reads to the genome[173,174].

To combat the limitations of TnSeq, random barcode transposon-site sequencing (RB-TnSeq) was developed[174]. In RB-TnSeq, each transposon contains a unique twenty nucleotide barcode. One round of traditional TnSeq is performed on the initial library to identify the genetic location of each barcode. Then, barcode abundance can simply be quantified by PCR and deep sequencing of DNA barcodes (BarSeq). The main advantage of this technique is that it is rapid and thus high throughput. TnSeq requires microgram quantities of genomic DNA, while RB-TnSeq protocols only require 200 nanograms of genomic DNA. In addition, elimination of the need for arbitrary PCR to identify transposon-gene insertion sites limits potential bias introduced at this step. To demonstrate the high-throughput nature of RB-TnSeq, barcoded transposon libraries were generated in 32 diverse environmental bacterial species, and each library was exposed to a chemical library of carbon sources, nitrogen sources, and stress compounds[176]. This effort allowed annotation for nearly 12,000 unannotated genes. Large-scale fitness experiments and mouse colonization experiments with an RB-TnSeq library in the gut commensal bacterium *Bacteroides thetaiotaomicron* uncovered novel metabolic features and the dynamics of gut colonization[177,178].

Here, we generate an RB-TnSeq library in Mtb and expose the library to a variety of carbon sources, nitrogen sources, and stress compounds. We find the *nuo* operon, which encodes an NADH dehydrogenase, or complex I of the electron transport chain, is important for growth on specific carbon sources, propionate and asparagine. We uncover genes that are specific for growth on D-lactate and predict that D-lactate could be a carbon source for Mtb. Finally, we evaluate the role of a putative operon in resistance to

pretomanid, a recently approved antibiotic for drug resistant Mtb strains. These data from the high-throughput genetic screens have allowed us to begin to uncover novel aspects of Mtb biology.

4.3 Results

4.3.1 High-throughput fitness data with Mtb RB-TnSeq library

To create an RB-TnSeq library in Mtb, we generated a temperature-sensitive mycobacteriophage encoding a transposase under the T6 mycobacterial promoter, *Himar1* mariner transposon with unique twenty nucleotide barcodes, and a kanamycin resistance cassette (Supplementary Figure 1). Transduction of the Mtb laboratory strain H37Rv with the mycobacteriophage yielded an RB-TnSeq library with ~60k unique mutants in 2888 genes. TnSeq libraries in Mtb typically represent ~3300 genes[174], suggesting our library is unsaturated. Due to the difficulty of generating the RB-TnSeq library with expansive barcode diversity, we proceeded with conducting high-throughput genetic screens.

The H37Rv RB-TnSeq library was exposed to a chemical library of carbon sources, nitrogen sources, and antibiotics[176]. After growth to midlog phase, the RB-TnSeq library was diluted into smaller culture volumes in either Sauton's minimal media containing a singular carbon or nitrogen source or in 7H9, the standard Mtb liquid medium, with a stressor concentration that yields approximately 50% inhibition (Figure 1A). For the carbon and nitrogen chemical libraries, a condition was sent for sequencing if the culture doubled at least three times (OD_{600}>0.4) (Table 1 and Table 2). For stress compounds, IC50s were predetermined and used for a screen if the IC50 was above 0.2 mM (Table 3)**.** After reaching saturation, cultures were pelleted for genomic DNA extraction, followed by PCR amplification, and deep sequencing of DNA barcodes (BarSeq). The number of barcodes at the end of the experiment was compared to the number of barcodes at the beginning of the experiment, which is represented by the log2 fold change or "BarSeq fitness." Mutants in genes that confer a growth advantage have a positive BarSeq fitness, while mutants in genes that confer a growth disadvantage have a negative BarSeq fitness.

We have conducted successful RB-TnSeq screens for 18 carbon sources, 8 nitrogen sources, and 12 antibiotics (Figure 1B). To our knowledge, only 6 of the 38 screens we conducted have published TnSeq data. We first examined specific phenotypes, in a which a given gene only has a fitness defect in one or a few conditions[176]. For example, *Rv3010c*, a putative phosphofructokinase, was only attenuated for growth on the two BarSeq screens conducted on sugars - trehalose and D-glucose (Figure 1C). This suggests that *Rv3010c* is specifically involved in sugar metabolism, supporting its well-known role in glycolysis. The high-throughput fitness data yielded specific phenotypes for 118 genes.

We also evaluated cofitness, wherein multiple genes share the same fitness score across many conditions, suggesting the genes work together in a similar process or pathway[176]. *Rv3220c* and *Rv1626* are putative members of a bacterial two-component system, a signaling cascade comprised of a sensor histidine kinase that responds to an external stimulus by self-phosphorylation and subsequent phosphorylation and activation of a response regulator. Previous data demonstrate that the sensor histidine kinase *Rv3220c* self-phosphorylates and then phosphorylates the response regulator *Rv1626*

when expressed as purified proteins[179,180]. These two genes have a cofitness score of 0.802, supporting the biochemical data that these two genes do in fact interact (Figure 1D). To validate results from RB-TnSeq screening, we compared our data to previously published TnSeq screens. Comparison of the RB-TnSeq hits for exposure to isoniazid, a commonly used TB antibiotic, to a previously published TnSeq screen resulted in an overlap of the most significant hits (Figure 2A).

4.3.2 The *nuo* operon is required for growth on propionate

Lipids are a prominent carbon source for Mtb during infection, so we conducted RB-TnSeq screens on a variety of fatty acid carbon chain lengths, ranging from acetate (C2) to stearate (C18) (Figure 1B). Metabolism of branched-chain fatty acids, odd-chain fatty acids, and cholesterol results in the production of the three-carbon molecule propionyl-CoA. Propionyl-CoA is oxidized to pyruvate by the methylcitrate cycle through the action of methylcitrate synthase (*Rv1131*, *prpC),* methylcitrate dehydratase (*Rv1130, prpD*), and methyl-isocitrate lyase (*Rv1129c*, *icl1*)[179] (Figure 3B). Accordingly, top hits that conferred susceptibility to growth on propionate included *prpC*, *prpD*, and their regulator, *prpR* (Figure 3A). Propionyl-CoA can also be sunk into lipid synthesis of methyl-branched lipids such as phthiocerol dimycocerosate (PDIM) and sulfolipid-1[181].

Another top hit for growth on propionate was the *nuo* operon, encoded by genes *nuoA-nuoN* (*Rv3145-Rv3158*) (Figure 3C), which was not a hit for growth on the two-carbon fatty acid acetate (Figure 3D). The *nuo* operon encodes a large protein complex comprised of 14 subunits that comprises NADH dehydrogenase, complex I of the electron transport chain. Oxidative phosphorylation from the action of a highly branched electron transport chain and ATP synthase is an important energy generating pathway for mycobacteria and has recently been a target of interest for novel TB therapy[182]**.**

Nuo is a classical type I NADH dehydrogenase that oxidizes NADH to NAD+ using menaquionine as an electron acceptor. Nuo contributes to the proton motive force that drives ATP production by translocating protons to the outer membrane space. Interestingly, Mtb encodes two other NADH dehydrogenases, *ndh* (*Rv1854c*) and *ndhA* (*Rv0392c*). These NADH dehydrogenases differ in that they are type II NADH dehydrogenases and comprised of one subunit that lacks proton-pumping capabilities. Until recently, *ndh* was thought to be an essential gene because attempts at knocking out *ndh* were unsuccessful[183], and *ndh* was not represented in TnSeq libraries, including our RB-TnSeq library. However, *ndh* knockouts have now been generated in the CDC1551 strain[184] and in H37Rv in fatty-acid free media[185]. Transposon insertions have been found in *ndhA*[186], although questions remain as to the exact roles of these three NADH dehydrogenases. Notably, *ndhA* was not a BarSeq hit for any screen conducted thus far.

Using mutants with transposon insertions in *nuoA*, *nuoE*, *nuoG*, or *nuoM*, we confirmed that *nuo* mutants are attenuated for growth on 0.1% propionate as the sole carbon source by measuring OD_{600} over the course of 8 days (Figure 3E). As predicted by the RB-TnSeq data, the *nuo* mutants grew to the same degree as WT on 0.1% acetate, with WT and *nuo* mutants all reaching an OD_{600} of ~0.40 after 8 days in culture. (Figure 3F). When grown on a combination of 0.1% acetate and 0.1% propionate, the *nuo* mutants are attenuated compared to WT, with the *nuo* mutants growing to an OD_{600} of ~0.40, and WT growing to an OD_{600} of ~0.80 after 8 days (Figure 3G). Due to propionate toxicity, bacteria that cannot metabolize propionate, such as methylcitrate cycle mutants,

fail to grow in the presence of propionate and acetate[184]**.** Given that the *nuo* mutants still grew on acetate in the presence of propionate, we suspect that propionate is detoxified in the *nuo* mutants but is not able to be used as a carbon source to its full potential.

In addition to propionate, the fitness data revealed that *nuo* is also required for growth on asparagine as a carbon source (Figure 3H) but not with asparagine as a nitrogen source (Figure 3I) We reconfirmed this phenotype with the *nuo* transposon mutants by measuring the OD_{600} of WT and the *nuo* transposon mutants over 8 days (Figure 3J). Asparagine is metabolized to aspartate, releasing ammonia. Aspartate then undergoes transamination to form oxaloacetate. which can enter the TCA cycle. We hypothesize that both propionate and asparagine metabolism are conditions where the bacterial cell is under high metabolic stress and conservation of energy is important for optimum growth, stressing the importance of the proton gradient for ATP synthesis.

4.3.3 D-lactate as a potential carbon source for Mtb

In addition to lipids, Mtb grows on cellular metabolites as carbon sources. We observed growth and conducted RB-TnSeq screens on pyruvate, malic acid, D-lactate, and L-lactate (Figure 1B). Lactate exists in distinct D and L isomers that can be converted into pyruvate by stereo-specific enzymes. L-lactate is present in guinea pig granulomas[186] and is produced in immune cells during Mtb infection due to the Warburg effect, the metabolic shift from oxidative phosphorylation to aerobic glycolysis[187–190]. The top BarSeq hit for attenuated growth on L-lactate was *lld2 (Rv1872c)*, which has been characterized as a L-lactate dehydrogenase[191] and is under positive evolutionary selection in Mtb clinical strains[192].

D-lactate can be produced from lipid and protein metabolism, but like L-lactate, is largely produced as a product of carbohydrate metabolism. However, there has been little work investigating D-lactate as a carbon source for Mtb. Fragmentation of the glycolysis metabolites dihydroxyacetone phosphate (DHAP) and glyceraldehyde 3-phosphate (G3P) yields methylglyoxal, a reactive aldehyde that damages proteins and DNA. Methylglyoxal is subsequently detoxified via the glyoxalase system into D-lactate. Lipopolysaccharide (LPS) and interferon-gamma (IFNγ) stimulation increases methylglyoxal production in a macrophage cell line[193] and in primary mouse macrophages[194], and a murine alveolar macrophage cell line infected with Mtb had increased levels of methylglyoxal[195]. Thus, it is possible that Mtb encounters D-lactate *in vivo*.

The top two BarSeq hits for growth on D-lactate were *Rv1257c*, a putative oxidoreductase, and *Rv0487*, a hypothetical protein (Figure 4A). Using mutants with transposon insertions in *Rv1257c* and *Rv0487*, we confirmed that these mutants were specific for growth attenuation on D-lactate (Figure 4C), as they grew to the same OD_{600} as WT on L-lactate (Figure 4D). As expected, a transposon mutant in *lld2* was specifically attenuated for growth on L-lactate but not attenuated on D-lactate (Figures 4C and 4D).

Rv1257c and *Rv0487* have yet to be experimentally investigated in Mtb. *Rv1257c* contains a potential FAD oxidase domain (Figure 4B) and shares 40.1% amino acid sequence identity with *E. coli* glycolate oxidase subunit D (*glcD*), which is a member of a protein complex that oxidizes glycolate to glyoxylate. Interestingly, *E. coli* glycolate oxidase uses D-lactate as a substrate at similar kinetics to glycolate[196]. Thus, *Rv1257c* may act as a D-lactate dehydrogenase in Mtb.

By sequence alignment, *Rv0487* is predicted to contain a YbjN domain (Figure 4B). The YbjN gene family is most highly conserved in Enterobacteria, although the gene family appears in other bacterial families to a lesser extent[197]. The function of YbjN containing proteins is largely unknown; in *E. coli*, overexpression of YbjN suppresses multiple temperature sensitive mutations[198] and increases transcription of SOS stress response and toxin-antitoxin systems[199], leading to the hypothesis that YbjN may be involved in sensory transduction and stress response. Of the Mtb RB-TnSeq screens conducted thus far, *Rv0487* is only attenuated on D-lactate, suggesting a novel context for YbjN-domain containing proteins.

4.3.4 Mutants in *Rv1633-Rv1634* confer resistance to pretomanid

In addition to carbon and nitrogen sources, we conducted RB-TnSeq screens to find mutations that confer susceptibility and resistance to stressors, mainly antibiotics. In response to the rise of MDR and XDR Mtb strains, the WHO updated their guidelines in 2022 to include the BPaLM regimen[200]. This combination therapy consists of bedaquiline, pretomanid, linezolid, and moxifloxacin.

Pretomanid, also referred to as PA-824, is a nitroimidazole that inhibits mycolic acid synthesis, specifically the synthesis of ketomycolates[201]. Pretomanid is administered as a prodrug that requires activation by a deazaflavin-dependent nitroreductase (*Ddn*) that is involved in the redox cycling of the cofactor F420[202]. The nitroreduction of pretomanid releases nitric oxide, which is thought to provide an additional mechanism of action by inhibiting cytochrome oxidases in the electron transport chain[203]. Mutations that confer resistance to pretomanid have often been found in *ddn*, F420 synthesis genes (*fbiA-D*), and *fgd1*, which reduces the F420 cofactor[204–207]. In alignment with these previous findings, top hits for pretomanid resistant mutants in the RB-TnSeq screen included *ddn*, the *fbi* operon, and *fgd1* (Figure 5A).

We found that the putative two-gene operon *Rv1633-Rv1634* also conferred resistance to pretomanid (Figure 5B). *Rv1633* (*uvrB*) is a probable excinuclease in nucleotide excision repair, and *Rv1634* is a possible drug efflux membrane protein (Figure 5E). Transposon mutants in *Rv1633* and *Rv1634* showed an increase in the pretomanid IC50 (Figures 5C and 5D), with a transposon mutant in *Rv1634* showing a slightly more resistant phenotype compared to *Rv1633*. The WT IC50 to pretomanid of 0.30μg/mL was increased to 0.38μg/mL in *rv1633::tn* and increased to 0.62μg/mL in *rv1634::tn*. Plating for colony forming units (CFU) to determine bacterial survival supported these findings with a two-fold increase in pretomanid resistance (Figure 5F). Interestingly, these genes may function outside of the conventional F420 redox recycling pathway typically associated with pretomanid resistance.

4.4 Discussion

We performed 38 successful RB-TnSeq screens on a range of carbon sources, nitrogen sources, and antibiotics related to Mtb physiology. This high-throughput data allows generation of hypotheses about gene functions by applying specific phenotypes and cofitness measurements. We found that the *nuo* operon, encoding one of the three NADH dehydrogenases in Mtb, is specifically attenuated for growth on propionate and asparagine. From our current knowledge of metabolic pathways, there appears to be little overlap between propionate and asparagine metabolism. We hypothesize that Nuo is

important when the cell is under high metabolic stress because its proton-pumping capabilities allows for energy conservation due to the contribution to the proton motive force. It is well-appreciated that Mtb is a metabolically flexible bacterium, and these data highlight how the apparent redundancy of three NADH dehydrogenases allows for growth on different carbon sources. It would be interesting to add radiolabeled propionate to bacterial cultures and evaluate the fate of the radiolabeled carbon in the *nuo* transposon mutants.

Complementation of the *nuo* operon will also be informative. In *E. coli*, disruption of each *nuo* gene results in disassembly or destabilization of the entire Nuo complex[208]. However, it is unknown if this observation translates to *Mtb*, and which *nuo* genes contribute most to the growth defects on propionate and asparagine. Given that the BarSeq fitness for all *nuo* genes was similar (Figure 3C) and transposon mutants in *nuoA*, *nuoG*, *nuoE*, and *nuoM* all phenocopy (Figures 3E-3G), we suspect that the entire *nuo* operon may be required for growth on propionate and asparagine.

It will likewise be informative to infect mice with *nuo* transposon mutants and complemented strains. IV infection of SCID or BALB/c mice with a H37Rv Δ*nuoG* strain results in increased mouse survival[209]. In the immunocompetent BALB/c mice, the Δ*nuoG* mutant has decreased lung bacterial burden at 10 and 20 weeks post infection[209]. Another study performed IV infection of C57BL/6 mice with a CDC1551 Δ*nuoAN* strain and found no changes in survival or lung bacterial burden[184]. Thus, we plan to evaluate if the *nuo* mutants are attenuated in mice in an aerosol infection, which more closely mimics the natural route of infection.

Specific phenotypes also revealed two mutants that are specific for growth on D-lactate, *Rv0487* and *Rv1257c*. D-lactate dehydrogenases have long been elusive in Mtb. To our knowledge, the sole enzyme with D-lactate hydrogenase activity to have been characterized in Mtb is the flavohemoglobin *FHb* (*Rv0385*), which was shown biochemically to oxidize D-lactate to pyruvate by the action of FAD and heme cofactors[210]. A follow up study on *FHb* revealed an additional biochemical function as a disulfide oxidoreductase[211]. In our dataset, *Rv0385* did not have significant BarSeq fitness for growth on D-lactate. Based on sequence homology to *E. coli*, we predict that *Rv1257c* may be the predominant D-lactate dehydrogenase in Mtb for utilization of D-lactate as a carbon source. However, biochemical studies are needed to support this hypothesis.

Rv0487 is predicted to contain a YbjN domain. Although the YbjN gene family is highly conserved in Enterobacteria, little has been uncovered about this gene family's exact function. In *E. coli*, overexpression of *YbjN* results in a myriad of effects: transcriptional changes in stress responses and metabolism, acid resistance, biofilm formation, and reduced motility[199]. *AmyR*, a YbjN containing protein in the plant pathogen *Erwinia amylovora,* is a regulator of a virulence factor that produces exopolysaccharide[212]. Given the known pleiotropic effects of mutating YbjN-domain containing proteins, it is intriguing that *Rv0487* is specifically attenuated for growth on D-lactate in our dataset.

Although we observe growth of Mtb on D-lactate in broth, *in vivo* experiments will be imperative in understanding if Mtb uses D-lactate as a carbon source during infection. Infection of macrophages and mice lacking GloI, which are unable to detoxify methylgloxyal and thus predicted to have less host D-lactate available to Mtb, will be

informative. Future work also includes complementation of the transposon mutants in *Rv1257c* and *Rv0487*.

The last specific phenotype we followed up on was concerning the TB antibiotic pretomanid, which is included in newer drug-resistant TB regimens. We identified that mutants in *Rv1633* and *Rv1634* confer resistance to pretomanid. Transposon mutants in *Rv1633* and *Rv1634* result in a two-fold increase in pretomanid resistance, which we hypothesize may act as a stepping-stone to develop even higher resistance *in vivo*. *Rv1633* encodes UvrB, which is involved in nucleotide excision repair that removes bulky lesions from DNA. Thus, a potential explanation is that this strain acquires more mutants overall and has a higher probability of acquiring *de novo* pretomanid resistance. However, if this were the case, we may expect to see *Rv1633* confer to resistance to other antibiotics. The cumulation of all the RB-TnSeq data thus far suggest that mutation of *Rv1633* is specific for pretomanid (Figure 5B) and mutants in the other nucleotide excision repair proteins, such as UvrA, UvrC, and UvrD, were not BarSeq hits on pretomanid.

Rv1634 encodes a putative drug efflux membrane protein. This presents a counter-intuitive situation. Typically, a loss of function mutant in a drug efflux protein drives susceptibility to an antibiotic. However, we observe that a mutant in *Rv1634* drives resistance to pretomanid. One potential explanation is that pretomanid enters the cell through this drug efflux membrane protein, but mass spectrometry experiments are needed to test this hypothesis. Additionally, complementation of the *Rv1633-Rv1634* operon is required to uncover which of the two genes, or both, is driving the pretomanid resistance phenotype. Given that *Rv1634* has a stronger phenotype than *Rv1633*, it is possible that the phenotype of *Rv1633* mutants is a polar effect.

A major limitation of our RB-TnSeq screens is that the library is unsaturated. Maintaining large barcode diversity throughout the library construction processes presented an enormous challenge. Even if the library were saturated, we would lack representation of essential genes, which comprise ~15-20% of the genome. To address this caveat of transposon libraries, CRISPRi libraries have been developed in Mtb and screened against TB antibiotics[30]. Nonetheless, we are conducting more RB-TnSeq screens on a larger panel of general and TB antibiotics as well as TB-specific stressors such as oxidative stress, nitrosative stress, and acidic pH. There is much to still be uncovered considering Mtb biology, and these screens will provide a useful resource for understanding mycobacterial genetics and improve our knowledge for developing novel TB antibiotic therapies.

4.5 Materials and Methods

Bacterial strains and culture

The Mtb strain H37Rv was used for generation of the BarSeq library and for all experiments. Transposon mutants (*nuoA::tn*, *nuoE::tn*, *nuoG::tn*, *nuoM::tn*, *rv0487::tn*, *rv1257c::tn*, *rv1872c::tn*, *rv1633:tn*, *rv1634::tn*) were picked from an arrayed transposon library generated at the Broad Institute. For all experiments, Mtb was grown to midlog phase in Middlebrook 7H9 liquid medium supplemented with 10% albumin-dextrose-saline, 0.4% glycerol, and 0.05% Tween80. When plated, Mtb was grown on solid 7H10 agar supplemented with Middlebrook OADC (BD Biosciences) and 0.4% glycerol. For growth on carbon and nitrogen sources, Sauton's media was prepared as previously described[123], except tyloxapol was substituted for Tween-80.

Generation of random barcode transposon-site sequencing library
PacI Digestion
10µg of phae159 cosmid and 10µg of BarSeq plasmid were PacI digested overnight at 37C followed by heat inactivation for 10 minutes at 75C. Phae159 digestion was purified by addition of 1:10 volume of 3M sodium acetate and 2.5 volumes of 100% ethanol. Mixture was incubated at -20C for 10 minutes. DNA was pelleted, washed with 70% ethanol, and air-dried for 5 minutes. Pellet was resuspended in 15µL TE buffer. BarSeq plasmid digestion was purified by DNA cleanup and concentrator kit and eluted in 15µL of TE buffer.

T4 Ligation
3µg digested phae159 cosmid and 1.5µg digested BarSeq plasmid were incubated with 100 units of T4 Ligase, HC at 16C for 4 hours. The reaction was ethanol precipitated as described above and resuspended in 20µL TE buffer.

In vitro lambda packaging and E. coli transduction
10µL of ligated phae159+BarSeq plasmid was added to 25µL of MaxPlax Packaging extract and incubated at 30C for 90 minutes. Another 25µL of MaxPlax Packaging extract was added to reaction mixture and incubated at 30C for another 90 minutes. 500µL of PD buffer (10mM Tris-HCl pH 8.3, 100mM NaCl, and 10mM MgCl2) was added to stop the reaction followed by addition of 25µL chloroform. The packaging reaction was then titered to estimate the efficiency of the reaction. Packaged lambda phage was incubated with stbl3 E. coli at 37C for 1.25 hours with no shaking and gentle vortexing every 15 minutes. Bacteria were then pelleted at 3500rpm for 5 minutes and resuspended in LB broth. Bacteria were plated on 24.5cm2 LB+50µg/mL kanamycin plates to achieve 60,000 colony forming units per plate. A total of 1x106 cfus were plated. The next day, colonies were collected by scraping into LB broth and phagemid was purified by midi-prep.

Electroporation of BarSeq phagemid into M. smegmatis to generate mycobacteriophage
Electrocompetent *M. smegmatis* was prepared by washing 2L of *M. smegmatis* grown to OD=0.2 with ice cold 10% glycerol and resuspending in a final volume of 20mL 10% ice cold glycerol. 400µL of electrocompetent *M. smegmatis* and 200ng of BarSeq phagemid were added to 0.2cm electroporation cuvettes. Cuvettes were incubated on ice for 10 minutes before electroporation pulse of 2.5 kV, 25 µF, and 1000Ω. 2mL of LB broth was immediately added to the electroporation cuvette, transferred to 15mL conicals, followed by incubation at 37C for 2 hours with no shaking. 8mL of top agar (2mM CaCl2, 0.6% agarose, melted and cooled to 55C) was added, and seeded onto two 7H10 plates. Plates were incubated at 30C for 3 days for plaque formation. A total of 100 electroporations were conducted to make the RB-TnSeq library.

Mycobacteriophage collection and concentration
Phage was collected by adding 3mL MP buffer (50mM Tris pH 7.6, 150mM NaCl, 10 mM $MgCl_2$, and 2mM $CaCl_2$) to each 7H10 plate and rocked at 4C overnight. The liquid on each plate was collected, pooled into 50mL conicals, and centrifuged at 4000 RPM for 20

minutes to pellet any bacteria. The supernatant was then passed through a 0.22μm filter. To concentrate phage, a 20%PEG-8000/2.5M NaCl mixture was incubated with the phage at a 7.5mL PEG-NaCl to 30mL phage ratio on ice for 2 hours. The phage was pelleted at 15,000rpm for 30min at 4C. Phage was resuspended in MP buffer and subsequently titered.

Mycobacterium tuberculosis transduction

1L of Mtb was grown to OD_{600}=0.8, washed two times with MP buffer, and resuspended in a final volume of 9mL MP buffer. 1mL of phage (concentration between $1x10^{11}$ and $1x10^{12}$ pfu/mL) was added to the bacteria and incubated at 37C for 18hours without shaking. Transduction was then washed two times and resuspended in 10mL PBS+0.05% Tween80. The transduction was plated on 7H10+50μg/mL kanamycin + 0.05% Tween80 24cm^2 plates and incubated at 37C for 21 days. Colonies were collected by scraping into 7H9 broth. Bacterial clumps were dissolved by sonication and light vortexing, and the RB-TnSeq library was aliquoted into cryovials for storage at -80C.

RB-TnSeq fitness assays

Mtb RB-TnSeq library was grown from frozen stocks in 7H9+50μg/mL kanamycin in roller bottles for 5 days. For day 0 barcode abundance, 5mL of culture was pelleted and stored at -80C for eventual genomic DNA extraction. For carbon source experiments, the culture was washed 2x with Sauton's minimal media minus carbon (no glycerol). For nitrogen source experiments, the culture was washed 2x with Sauton's minimal media minus nitrogen (no asparagine and no ammonium iron citrate). For antibiotic and stress experiments, the culture was washed 2x with 7H9. Cultures were started at OD=0.05 in 10mL in inkwells in duplicate and shaken at 37C. For carbon and nitrogen sources, the cultures were pelleted for genomic DNA extraction when the culture reached saturation (OD=0.8-1) or had at least doubled three times (OD=0.4). For antibiotic and stress experiments, cultures were pelleted at day 5.

Mtb genomic DNA extraction

10mL of midlog phase culture was pelleted and frozen at -80C. When thawed, pellet was resuspended in 440μL RB buffer (25mM Tris-HCl pH 7.9, 10mM EDTA, and 50mM D-glucose) with 1mg/mL lysozyme and 0.2mg/mL RNase A and incubated at 37C overnight. 100μL 10% SDS and 50μL 10mg/mL proteinase K were added and incubated at 55C for 30 minutes. 200μL 5M NaCl was added followed by gentle mixing. 160μL of pre-heated cetrimide saline solution (4.1g NaCl and 10g of cetrimide (hexadecyltrimethylammonium bromide) in 90mL H_2O) was added and incubated at 65C for 10 minutes. 1mL of chloroform:isoamyl alcohol (24:1) was added and inverted to mix. Mixture was centrifuged at 14,000 rpm for 10 minutes, and 800μL of aqueous layer was transferred to a new tube. 560μL (0.7x volume) isopropanol was added and mixed to precipitate DNA. Tubes were centrifuged at 14,000 rpm for 10 minutes, DNA pellet was washed with 700μL 70% ethanol, and centrifuged at 14,000rpm for 5 minutes. Pellets were air-dried and covered in 50μL water. DNA was stored at 4C overnight to allow for DNA pellets to dissolve.

Data analysis of RB-TnSeq

TnSeq sequencing and data analysis, BarSeq, computation of gene fitness values, t scores, specific phenotypes, cofitness, and quality metrics were done as described previously[26]. Genes were considered to have significant BarSeq fitness if the |log2 fold change|>01 and |t-like statistic| > 4.

Growth curves for carbon sources

Mtb strains were grown to midlog phase in 7H9, washed two times with Sauton's media minus carbon, and diluted to OD=0.05 in 10mL in inkwells in media containing the respective carbon source (0.1% propionate, 0.1% acetate, 10mM asparagine, 10mM D-lactate, or 10mM L-lactate). OD_{600} was measured on days 0, 4, and day 8.

Determination of antibiotic IC50s in 96 well-plates

Mtb strains were grown to midlog phase in 7H9 and washed two times with fresh 7H9. Mtb was added to 96 well-plates containing two-fold dilutions of antibiotics for a final starting OD_{600} of 0.05 in 100µL. Plates were incubated in a standing incubator in a sealed-tupperware with a water-wet rag to prevent evaporation for 10 days. OD_{600} was measured using a SpectraMax M2 Microplate Reader. IC50s were determined by a nonlinear regression on GraphPad Prism.

Determination of pretomanid resistance in culture

Mtb strains were grown to midlog phase in 7H9 and washed two times with fresh 7H9. Mtb was added to inkwell bottles containing 0, 0.30, or 0.45 µg/mL pretomanid for a final starting OD_{600} of 0.05 in 10mL. Cultures were shaken at 37C for 5 days. CFUs were determined by diluting bacteria into PBS+0.05% Tween-80 and plating serial dilutions on 7H10.

4.6 Figures

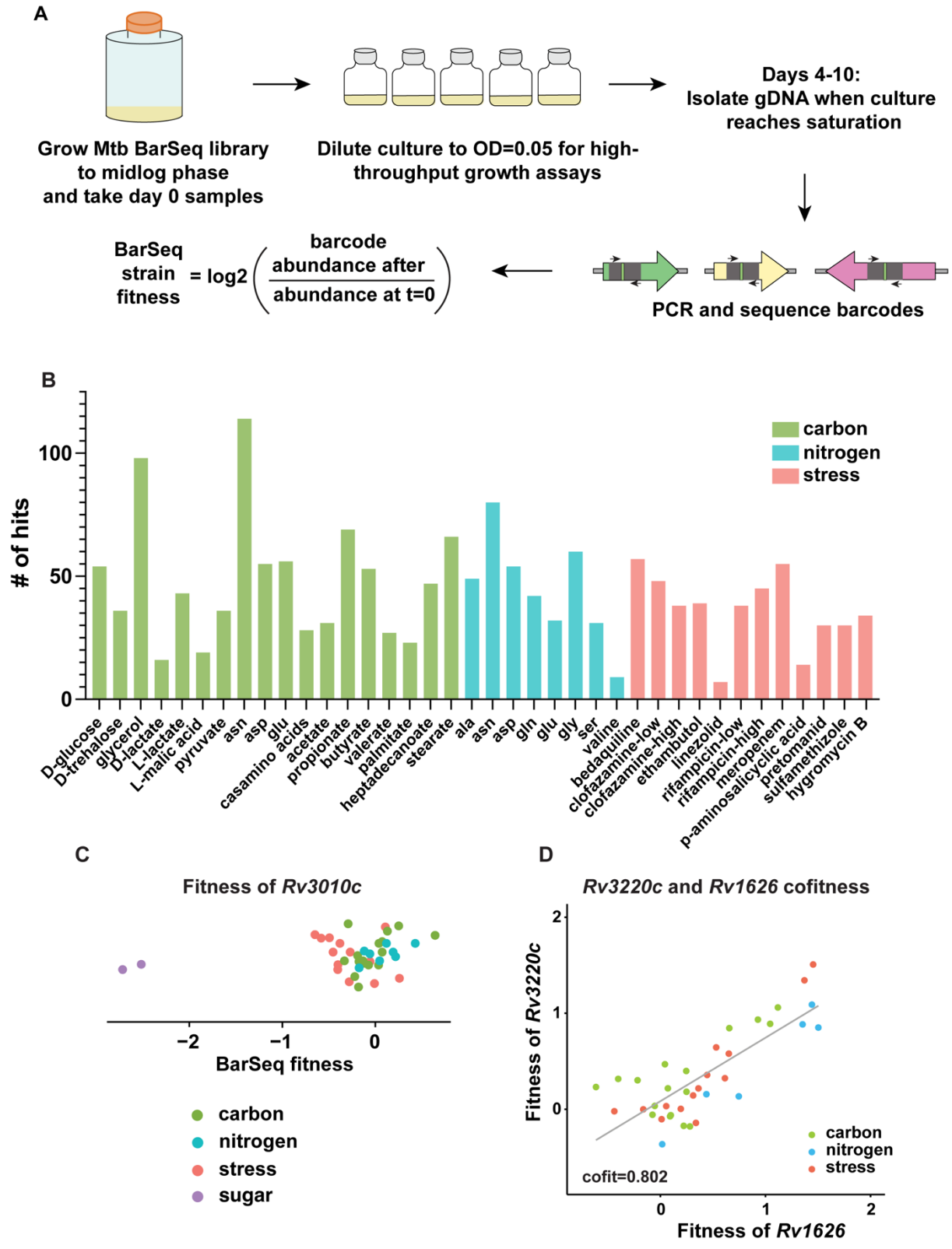
A
Grow Mtb BarSeq library to midlog phase and take day 0 samples
Dilute culture to OD=0.05 for high-throughput growth assays
Days 4-10: Isolate gDNA when culture reaches saturation
PCR and sequence barcodes
BarSeq strain fitness = log2 (barcode abundance after / abundance at t=0)
B
# of hits
carbon
nitrogen
stress
D-glucose
D-trehalose
glycerol
D-lactate
L-lactate
L-malic acid
pyruvate
asn
asp
glu
casamino acids
acetate
propionate
butyrate
valerate
palmitate
heptadecanoate
stearate
ala
asn
asp
gln
glu
gly
ser
valine
bedaquiline
clofazamine-low
clofazamine-high
ethambutol
linezolid
rifampicin-low
rifampicin-high
meropenem
p-aminosalicylic acid
pretomanid
sulfamethizole
hygromycin B
C
Fitness of Rv3010c
BarSeq fitness
carbon
nitrogen
stress
sugar
D
Rv3220c and Rv1626 cofitness
Fitness of Rv3220c
Fitness of Rv1626
cofit=0.802
carbon
nitrogen
stress

Figure 1. RB-TnSeq screens, specific phenotypes, and cofitness
(A) Schematic for RB-TnSeq screen experimental set-up. (B) Number of statistically significant hits for each successful condition categorized by carbon, nitrogen, or stress. (C) BarSeq fitness (log2 fold change) for *Rv3010c*, a putative phosphofructokinase. (D) Cofitness data for *Rv3220c* and *Rv1626*, which are hypothesized to work together in a bacterial two component system.

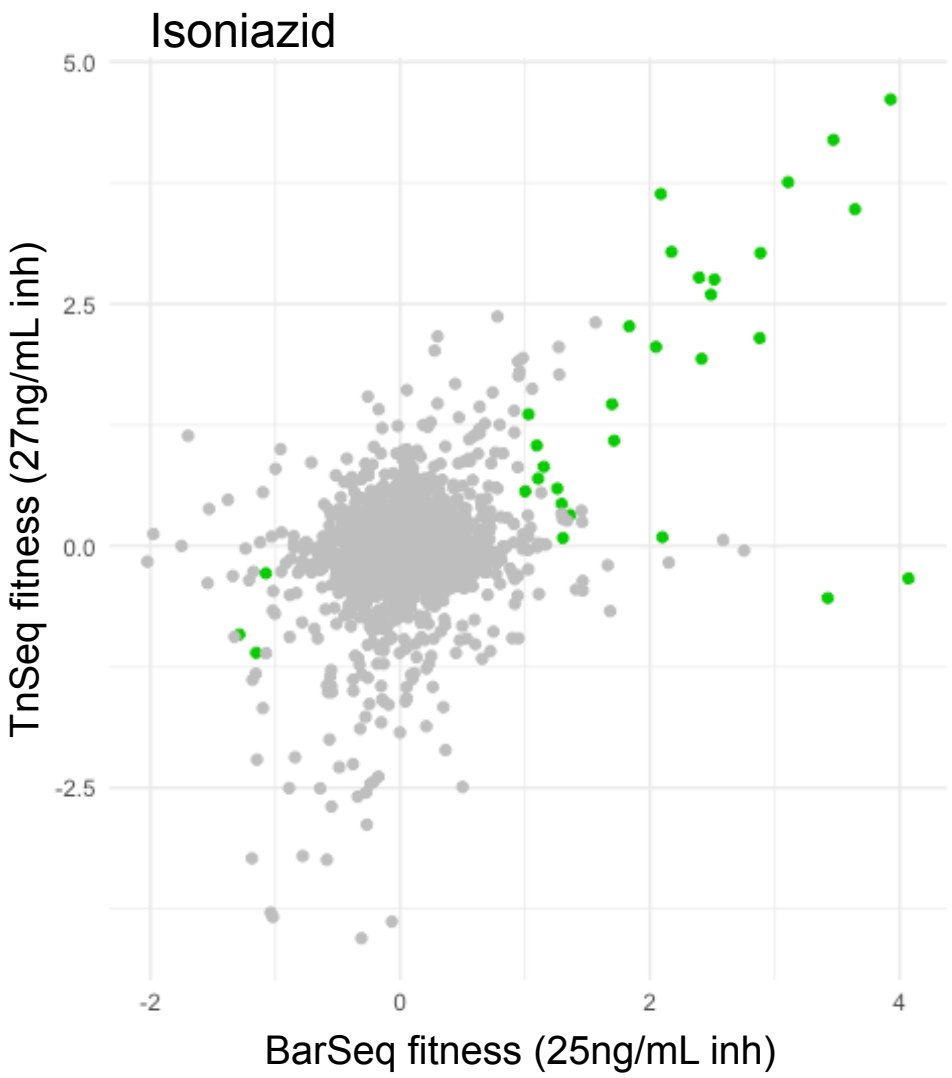

Figure 2. Comparison of TnSeq and BarSeq fitness
TnSeq fitness with 27ng/mL isoniazid[23] plotted against BarSeq fitness with 25ng/mL isoniazid. Statistically significant hits for BarSeq fitness are in green. BarSeq data are considered significant if |log2fold change| > 1 and |t-like statistic| > 4.

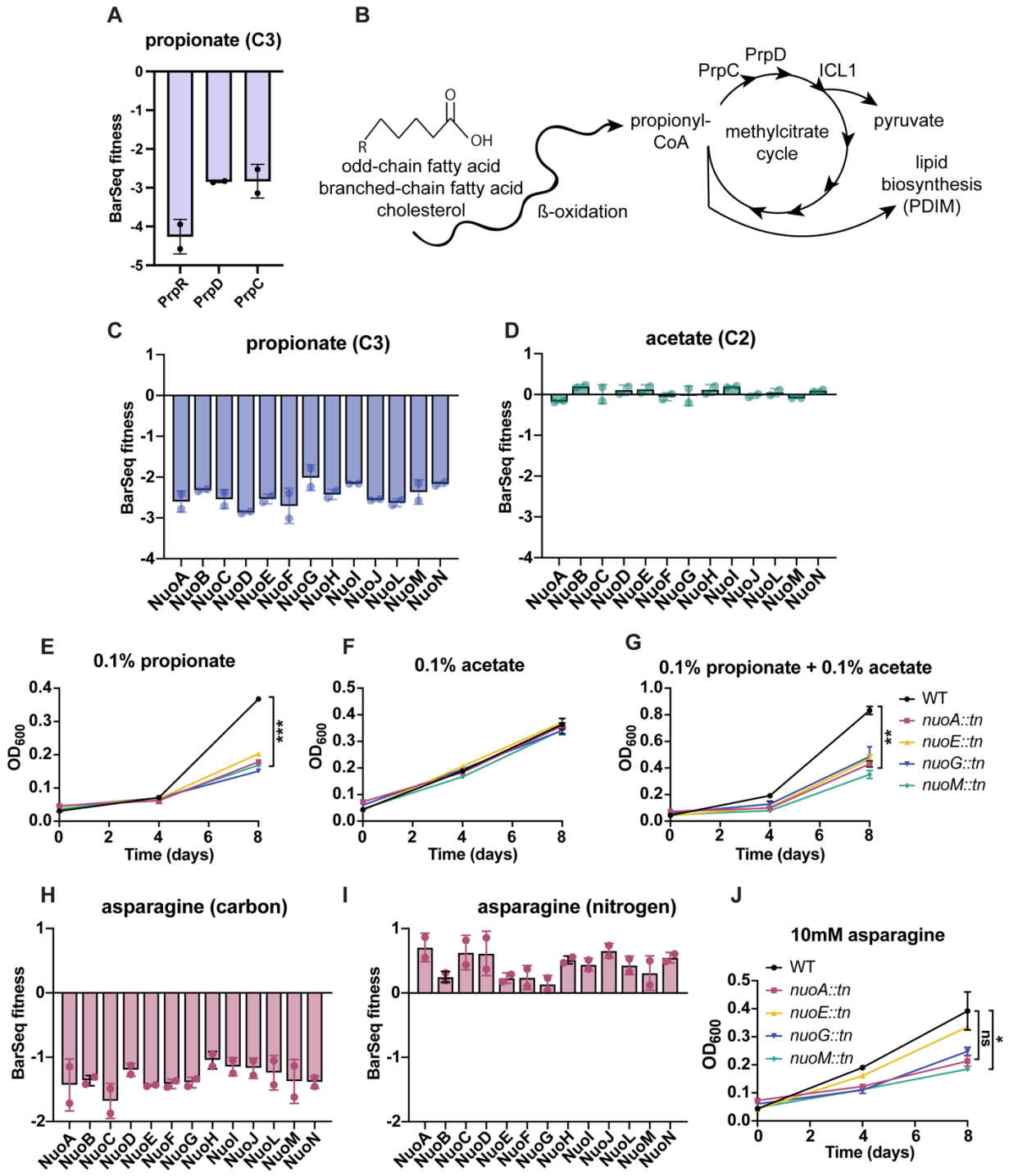

Figure 3. Nuo mutants are attenuated on propionate and asparagine

(A) BarSeq fitness of methylcitrate cycle genes on propionate. (B) Schematic of propionate detoxification. BarSeq fitness of the *nuo* operon for growth on (C) propionate and (D) acetate. OD_{600} of WT and *nuo* transposon mutants for growth on (E) 0.1% propionate (F) 0.1% acetate, and (G) 0.1% propionate and 0.1% acetate on days 0, 4, and 8. BarSeq fitness for the *nuo* operon on (H) asparagine as a carbon source and (I) asparagine as a nitrogen source. (J) Growth of WT and *nuo* transposon mutants on 10mM

asparagine as a carbon source on days 0, 4, and 8. p-Values were determined using unpaired t-test. *p<0.05, **p<0.01, ***p<0.001

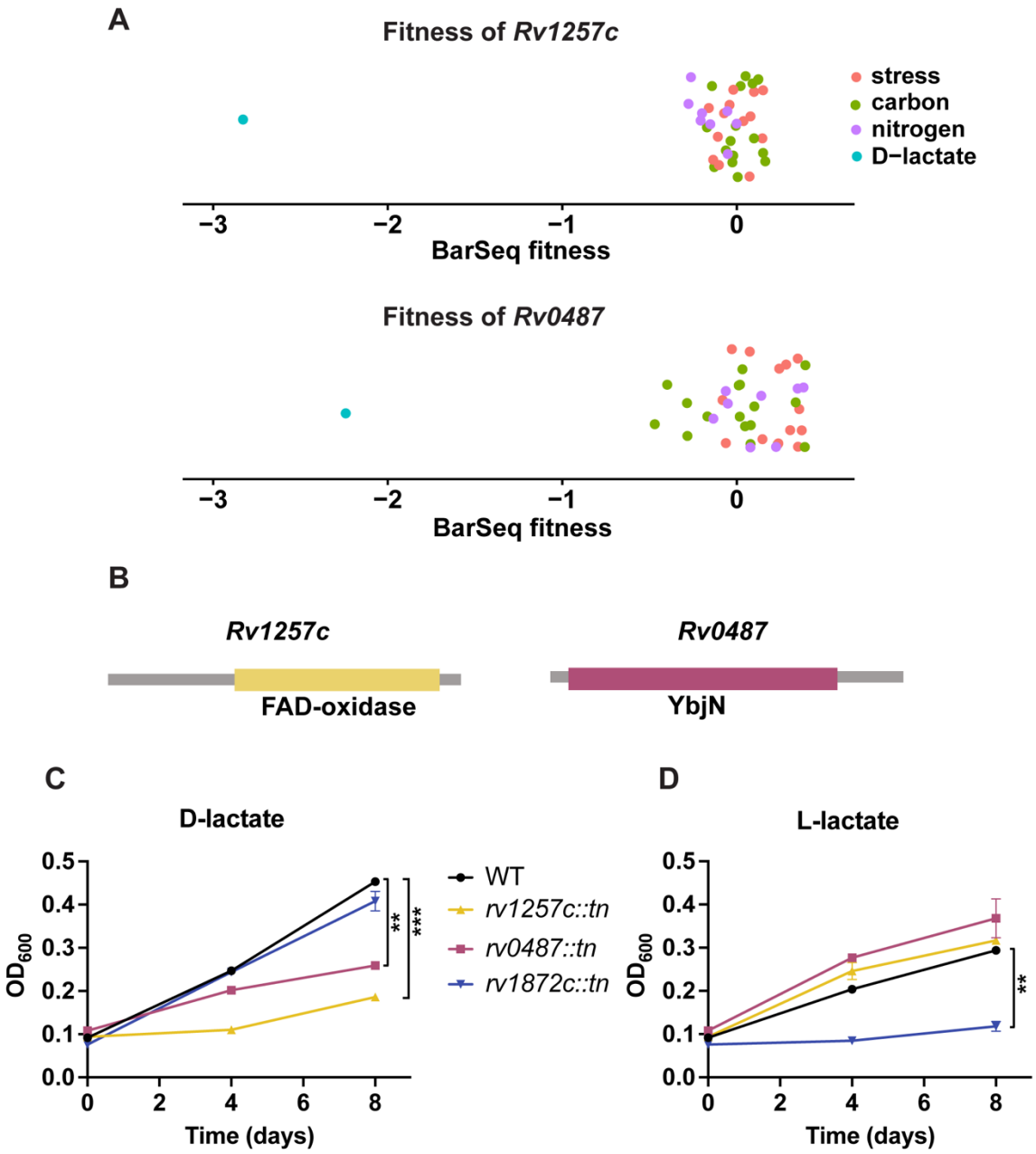

Figure 4. Mutants attenuated for growth on lactate
(A) BarSeq fitness (log2 fold change) of all RB-TnSeq screens for *Rv1257c* and *Rv0487.* (B) Predicted domains determined by Interpro for *Rv1257c* and *Rv0487*. OD_{600} of WT, *rv1257c::tn, rv0487::tn, rv1872c::tn* on (C) 10mM D-lactate and (D) 10mM L-lactate on days 0, 4, and 8. p-Values were determined using unpaired t-test. **p<0.01, ***p<0.001.

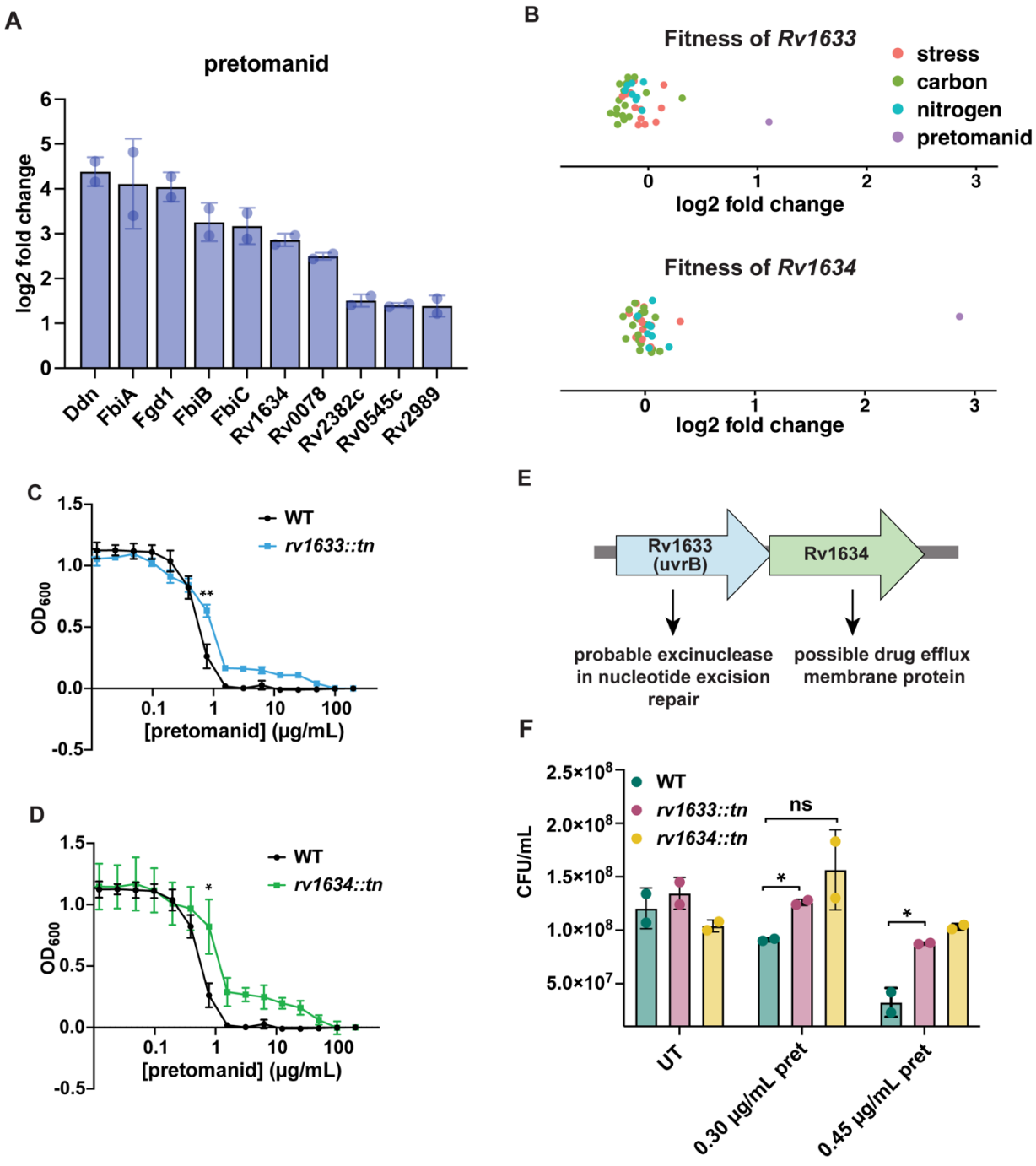

Figure 5. Rv133-Rv1634 confers resistance to pretomanid
(A) Top 10 BarSeq hits for pretomanid resistance (B) BarSeq fitness (log2 fold change) of all RB-TnSeq screens for *Rv1257c* and *Rv0487*. OD_{600} in 96 well-plates of WT and (C) *rv1633::tn* and (D) *rv1634::tn* after exposure to two-fold dilutions of pretomanid for 10 days. (E) *Rv1633 (uvrB)* and *Rv1634* (possible drug efflux membrane protein) are hypothesized to be in an operon. (F) CFU enumeration of WT, *rv1633::tn*, and *rv1634::tn* after exposure to either 0, 0.30, or 0.45µg/mL pretomanid in inkwell cultures for 5 days. p-Values were determined using unpaired t-test. *p<0.05, **p<0.01.

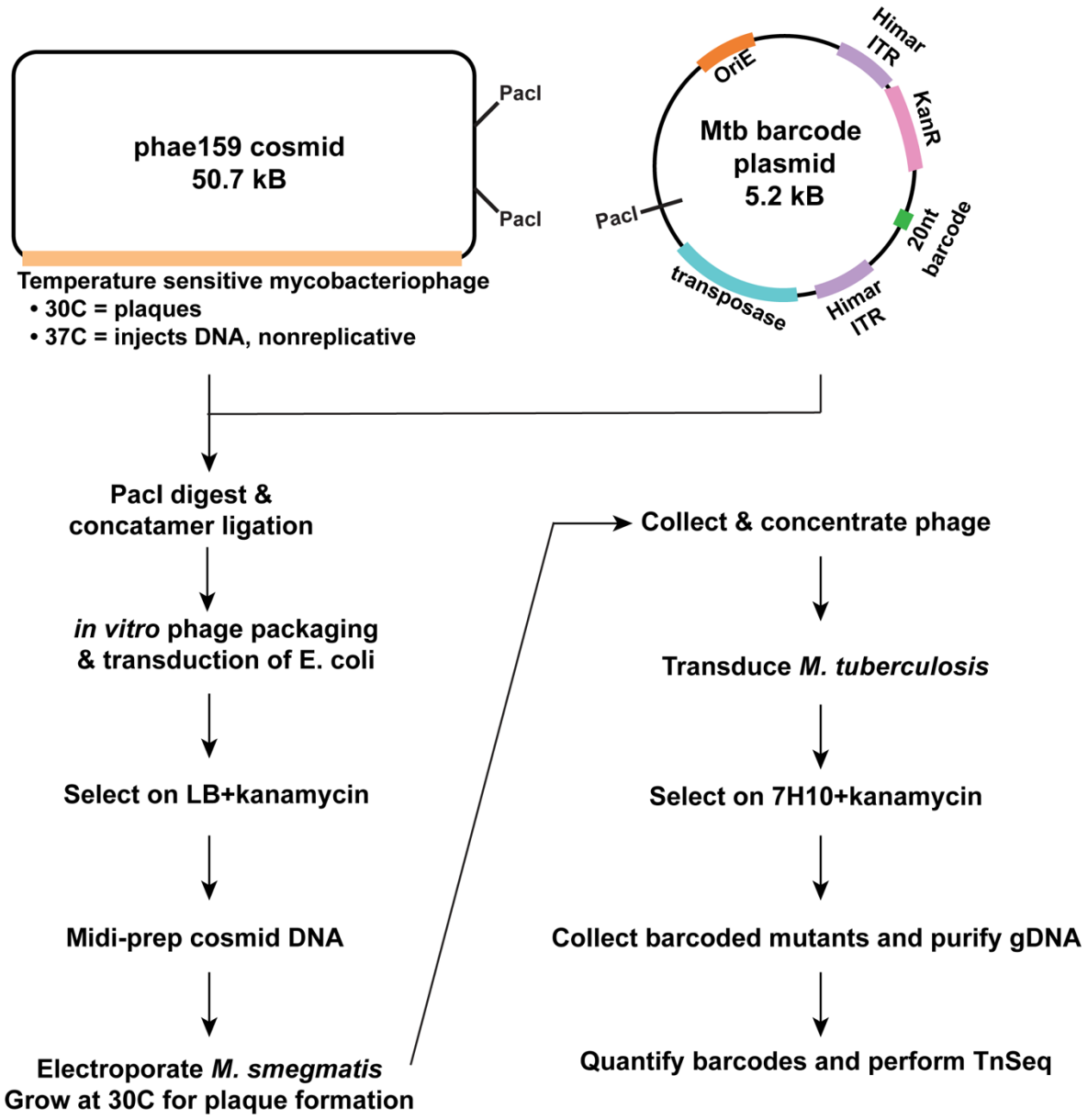

Figure S1. Protocol for construction of RB-TnSeq library in Mtb
In summary, temperature-sensitive phae159 cosmid was combined with a BarSeq plasmid containing the transposase, *Himar1* mariner barcoded transposons, and a kanamycin resistant cassette via PacI digest and concatemer ligation. The ligated cosmid was packaged into lambda phage and transduced into *E. coli* to be midi-prepped. Barcoded phagemid was electroporated into Mycobacterium smegmatis and incubated at 30C for lytic phage plaque formation. Once the phage was collected and concentrated, it was transduced into Mtb and plates were incubated at 37C. After 21 days, colonies were scraped from plates and pooled to create the RB-TnSeq library, which was subsequently gDNA purified and sent for TnSeq and BarSeq.

Table 1: Carbon source RB-TnSeq experiments
Table of carbon sources tested for RB-TnSeq screens. "Growth" is designated "YES" only if the culture doubled three times to reach an OD_{600}>0.4.

Compound	Condition	Concentration	units	Growth?	OD600	Time point (day)
D-Glucose	carbon	0.20	%	YES	0.699	10
D-Trehalose dihydrate	carbon	10	mM	YES	0.438	10
Sodium D-Lactate	carbon	10	mM	YES	0.59	10
Sodium L-Lactate	carbon	10	mM	YES	0.378	10
Sodium pyruvate	carbon	10	mM	YES	0.355	10
Glycerol	carbon	0.2	%	YES	0.798	8
L-Malic acid	carbon	10	mM	YES	0.496	10
L-Aspartic acid	carbon	10	mM	YES	0.516	10
L-Glutamic acid	carbon	10	mM	YES	0.467	10
L-Asparagine	carbon	10	mM	YES	0.532	10
Casamino acids	carbon	1	mg/mL	YES	0.308	10
Sodium acetate	carbon	0.1	%	YES	0.591	10
Sodium propionate	carbon	0.1	%	YES	0.83	10
Sodium butyrate	carbon	10	mM	YES	0.733	10
Valeric acid	carbon	10	mM	YES	1.006	10
Palmitic acid	carbon	100	µM	YES	0.392	16
Heptadecanoic acid	carbon	250	µM	YES	0.46	16
Sodium stearate	carbon	100	µM	YES	0.404	16
D-Fructose	carbon	10	mM	NO		
Sucrose	carbon	10	mM	NO		
L-Arabinose	carbon	10	mM	NO		
D-Arabinose	carbon	10	mM	NO		
D-Maltose monohydrate	carbon	10	mM	NO		
L-Sorbose	carbon	10	mM	NO		
D-Xylose	carbon	10	mM	NO		
D-Galactose	carbon	10	mM	NO		
D-Raffinose pentahydrate	carbon	10	mM	NO		

L-Rhamnose monohydrate	carbon	10	mM	NO
a-Cyclodextrin	carbon	10	mM	NO
D-Ribose	carbon	10	mM	NO
L-Fucose	carbon	10	mM	NO
a-Ketoglutaric acid disodium salt hydrate	carbon	10	mM	NO
5-Keto-D-Gluconic Acid potassium salt	carbon	10	mM	NO
Itaconic Acid	carbon	10	mM	NO
D-Glucuronic Acid	carbon	10	mM	NO
D-Gluconic Acid sodium salt	carbon	10	mM	NO
D-Glucose-6-Phosphate sodium salt	carbon	10	mM	NO
Sodium Fumarate dibasic	carbon	10	mM	NO
D-Cellobiose	carbon	10	mM	NO
2-Deoxy-D-Ribose	carbon	10	mM	NO
Trisodium citrate dihydrate	carbon	10	mM	NO
Citric Acid	carbon	10	mM	NO
Sodium D,L-Lactate	carbon	10	mM	NO
Sodium succinate dibasic hexahydrate	carbon	10	mM	NO
Sodium Formate	carbon	10	mM	NO
Xylitol	carbon	10	mM	NO
Glycolic Acid	carbon	10	mM	NO
D-Mannitol	carbon	10	mM	NO
4-Hydroxybenzoic Acid	carbon	10	mM	NO
m-Inositol	carbon	10	mM	NO

D-Galacturonic Acid monohydrate	carbon	10	mM	NO
Potassium oxalate monohydrate	carbon	10	mM	NO
Ethanol	carbon	10	mM	NO
D-Sorbitol	carbon	10	mM	NO
D,L-Malic Acid	carbon	10	mM	NO
Tween 20	carbon	0.5	%	NO
L-Arginine	carbon	10	mM	NO
L-Histidine	carbon	10	mM	NO
L-Lysine	carbon	10	mM	NO
L-Serine	carbon	10	mM	NO
L-Threonine	carbon	10	mM	NO
L-Glutamine	carbon	10	mM	NO
L-Cysteine hydrochloride monohydrate	carbon	10	mM	NO
Glycine	carbon	10	mM	NO
L-Proline	carbon	10	mM	NO
L-Alanine	carbon	10	mM	NO
L-Valine	carbon	10	mM	NO
L-Isoleucine	carbon	10	mM	NO
L-Leucine	carbon	10	mM	NO
L-Methionine	carbon	10	mM	NO
L-Phenylalanine	carbon	10	mM	NO
L-tyrosine disodium salt	carbon	10	mM	NO
L-Tryptophan	carbon	10	mM	NO
D-Serine	carbon	10	mM	NO
D-Alanine	carbon	10	mM	NO
Gly-DL-Asp	carbon	10	mM	NO
Gly-Glu	carbon	10	mM	NO
L-Citrulline	carbon	10	mM	NO
Carnitine Hydrochloride	carbon	10	mM	NO
Gelatin	carbon	0.2	mg/mL	NO
Putrescine Dihydrochloride	carbon	10	mM	NO
N-Acetyl-D-Glucosamine	carbon	10	mM	NO

D-Glucosamine Hydrochloride	carbon	10	mM	NO
Parabanic Acid	carbon	10	mM	NO
Adenosine	carbon	1	mM	NO
Adenine hydrochloride hydrate	carbon	2	mM	NO
Uridine	carbon	10	mM	NO
Thymidine	carbon	5	mM	NO
Inosine	carbon	2.5	mM	NO
Cytidine	carbon	10	mM	NO
Thymine	carbon	2	mM	NO
Cytosine	carbon	2.5	mM	NO
Glucuronamide	carbon	10	mM	NO
D-Salicin	carbon	10	mM	NO
Beta-Lactose	carbon	10	mM	NO
D-Mannose	carbon	10	mM	NO
Sodium octanoate	carbon	10	mM	NO
D-Tagatose	carbon	10	mM	NO

Table 2: Nitrogen source RB-TnSeq experiments
Table of nitrogen sources tested for RB-TnSeq screens. "Growth" is designated "YES" only if the culture doubled three times to reach an OD_{600}>0.4.

Compound	Condition	Concentration	units	Growth?	OD600	Time point (day)
L-alanine	nitrogen	10	mM	YES	1.031	10
L-asparagine	nitrogen	10	mM	YES	1.109	10
L-aspartic acid	nitrogen	10	mM	YES	0.774	10
L-glutamine	nitrogen	10	mM	YES	0.573	10
L-glutamic acid	nitrogen	10	mM	YES	0.402	10
Glycine	nitrogen	10	mM	YES	0.727	10
L-serine	nitrogen	10	mM	YES	0.821	10
L-valine	nitrogen	10	mM	YES	0.377	10
L-Arginine	nitrogen	10	mM	NO		
L-Histidine	nitrogen	10	mM	NO		
L-Lysine	nitrogen	10	mM	NO		
L-Threonine	nitrogen	10	mM	NO		
L-Cysteine hydrochloride monohydrate	nitrogen	10	mM	NO		
L-Proline	nitrogen	10	mM	NO		
L-Valine	nitrogen	10	mM	NO		
L-Isoleucine	nitrogen	10	mM	NO		
L-Leucine	nitrogen	10	mM	NO		
L-Methionine	nitrogen	10	mM	NO		
L-Phenylalanine	nitrogen	10	mM	NO		
L-tyrosine disodium salt	nitrogen	10	mM	NO		
L-Tryptophan	nitrogen	10	mM	NO		
D-Serine	nitrogen	10	mM	NO		
D-Alanine	nitrogen	10	mM	NO		
Gly-DL-Asp	nitrogen	10	mM	NO		
Gly-Glu	nitrogen	10	mM	NO		
L-Citrulline	nitrogen	10	mM	NO		
Carnitine Hydrochloride	nitrogen	10	mM	NO		
Gelatin	nitrogen	0.2	mg/mL	NO		
Putrescine Dihydrochloride	nitrogen	10	mM	NO		
N-Acetyl-D-Glucosamine	nitrogen	10	mM	NO		
D-Glucosamine Hydrochloride	nitrogen	10	mM	NO		

Parabanic Acid	nitrogen	10	mM	NO
Adenosine	nitrogen	10	mM	NO
Adenine hydrochloride hydrate	nitrogen	10	mM	NO
Uridine	nitrogen	10	mM	NO
Thymidine	nitrogen	5	mM	NO
Inosine	nitrogen	2.5	mM	NO
Cytidine	nitrogen	10	mM	NO
Thymine	nitrogen	2	mM	NO
Cytosine	nitrogen	2.5	mM	NO
Glucuronamide	nitrogen	10	mM	NO

Table 3: Antibiotic/stress RB-TnSeq experiments
Table of antibiotics tested for RB-TnSeq screens. “No inhibition” designates IC50>0.2mM.

Compound	Condition	Concentration	units	OD600	Time point (day)
Bedaquiline	antibiotic/stress	0.15	µg/mL	0.513	5
Clofazimine-low	antibiotic/stress	0.072	µg/mL	0.532	5
Clofazimine-high	antibiotic/stress	0.45	µg/mL	0.219	5
Ethambutol	antibiotic/stress	0.75	µg/mL	0.458	5
Linezolid	antibiotic/stress	0.44	µg/mL	0.323	5
Rifampicin-low	antibiotic/stress	0.00045	µg/mL	0.757	5
Rifampicin-high	antibiotic/stress	0.014	µg/mL	0.433	5
Meropenem	antibiotic/stress	9.6	µg/mL	0.549	5
para-aminosalicyclic acid	antibiotic/stress	0.086	µg/mL	0.550	5
Pretomanid	antibiotic/stress	0.213	µg/mL	0.268	5
Sulfamethizole	antibiotic/stress	7.02	µg/mL	0.490	5
HygromycinB	antibiotic/stress	5.01	µg/mL	0.341	5
Cisplatin	antibiotic/stress	no inhibition			
Allopurinol	antibiotic/stress	no inhibition			
Trimethoprim	antibiotic/stress	no inhibition			
Spiramycin	antibiotic/stress	no inhibition			
Nalidixic sodium salt	antibiotic/stress	no inhibition			
Penicillin g	antibiotic/stress	no inhibition			

Chapter 5: Summary of results and future directions

5.1 Characterization of mycobacterial nanocompartments

5.1.1 Summary of results

In chapters two and three, we aimed to characterize the role of an understudied bacterial organelle, the encapsulin nanocompartment, in mycobacteria. Encapsulin nanocompartments are comprised of a proteinaceous shell that surrounds an enzymatic cargo protein, and nanocompartments are predicted to be widespread throughout bacterial phyla, including mycobacteria[93]. *Mycobacterium tuberculosis* (Mtb) encodes one nanocompartment comprised of the enzymatic cargo protein DyP and its shell protein Cfp29. We show that Mtb generates nanocompartments containing DyP and Cfp29 when grown in standard growth medium. Using a biochemical assay for peroxidase activity, we demonstrate that DyP detoxifies hydrogen peroxide. A DyP nanocompartment deletion mutant in Mtb is susceptible to hydrogen peroxide at acidic pH, yet this phenotype is dependent on lipids in the media. We hypothesized that DyP may also utilize lipid peroxides as a substrate, but we were unable to observe peroxidase activity using arachidonic acid peroxide or organic hydroperoxides as substrates. The DyP nanocompartment mutant in Mtb is also susceptible to pyrazinamide in broth and in a mouse infection model.

Mycobacterium smegmatis (M. smeg) and *Mycobacterium abscessus* (M. abs) are two nontuberculosis mycobacterial species predicted to encode homologs to the DyP nanocompartment in Mtb. Interestingly, M. smeg and M. abs are predicted to encode another nanocompartment, comprised of the cysteine desulfurase CyD surrounded by a shell protein SrpI. We generated nanocompartment deletion mutants in M. smeg and M. abs but failed to recapitulate the phenotypes observed in Mtb, such as susceptibility to hydrogen peroxide at acidic pH and susceptibility to pyrazinamide. These experiments in M. smeg were difficult due to a strong inoculum effect at acidic pH. However, we observed unique colony morphologies in nanocompartment mutants in M. smeg.

5.1.2 Future directions

Generating deletions of nanocompartment genes in M. smeg resulted in interesting colony morphologies that warrant additional exploration. For instance, the M. smeg mutant lacking the CyD nanocompartment that yields a smooth colony morphology. It would be informative to examine cell envelope lipids, especially the presence of glycopeptidolipids. Additionally, whole genome sequencing of the CyD nanocompartment mutant would be useful in determining if known loci that confer smooth colony morphology are altered. The identification of nanocompartment shell proteins as dominant antigens suggest that nontuberculosis mycobacteria express nanocompartments at the protein level[135,139], but an important future direction involves isolating endogenous nanocompartments from M. smeg and M. abs and using mass spectrometry to determine their composition.

One of the main unanswered questions in the study of nanocompartments concerns the function of encapsulation. It is hypothesized that encapsulation of a cargo protein enhances its stability, which has been supported by the observation that encapsulation confers protein stability under heat and protease exposure [92]. A future direction would be to test the function of encapsulation in bacterial cells by generating

genetic deletions of the shell protein and probing for the half-life of cargo protein by western blot.

Another unanswered question is whether nanocompartments can function extracellularly. We find that Mtb DyP enzymatic activity has a pH optima ~4, which matches the pH of the phagolysosome and not that of the bacterial cytosol. Furthermore, nanocompartments are often found in the cell culture supernatant. Given that no known protein machinery can export molecules as large as a nanocompartment, it is predicted that extracellular nanocompartments are released from dying bacteria. In the future, it would be interesting to test if nanocompartments can function cell non-autonomously to promote bacterial survival.

5.2 Random-barcode transposon site sequencing in Mycobacterium tuberculosis

5.2.1 Summary of results

To elucidate the function of unknown genes in Mtb, we generated a random barcode transposon-site sequencing (RB-TnSeq) library and exposed it to a chemical library of carbon sources, nitrogen sources, and stressors. Overall, we conducted 38 successful RB-TnSeq screens with only a handful having pre-existing TnSeq data. By examining genes that have specific phenotypes, we found that the Nuo complex, which encodes NADH dehydrogenase, or complex I of the electron transport chain, is important for growth on propionate and asparagine. Mtb encodes three different NADH dehydrogenases, so it is insightful to determine which metabolic conditions rely on the Nuo complex. Given that Nuo is the only NADH dehydrogenase in Mtb with proton-pumping capabilities, we hypothesize that metabolism of propionate and asparagine result in an environment where the conservation of energy is important for bacterial growth.

From our RB-TnSeq data, we observed growth of Mtb on D-lactate as a carbon source. D-lactate is largely a product of carbohydrate metabolism and subsequent methylglyoxal detoxification, yet, to our knowledge, D-lactate has not been investigated as a carbon source for Mtb, and D-lactate hydrogenases have long been elusive in Mtb. We confirmed that the top two hits from our RB-TnSeq screen for growth on D-lactate, *Rv1257c* and *Rv0487*, are unable to grow on D-lactate. Based on homology to *Escherichia coli,* we hypothesize that *Rv1257c* may act as a D-lactate dehydrogenase.

Finally, we investigated the role of a novel operon, *Rv1633-Rv1634*, and its role in conferring pretomanid resistance in Mtb. Pretomanid has recently been approved for treating drug-resistant tuberculosis. Most characterized pretomanid-resistant mutants are involved in the biochemical activation of pretomanid prodrug. However, *Rv1633* encodes UvrB, involved in nucleotide excision repair, and *Rv1634* is a predicted drug efflux protein. Given that a mutant in *Rv1634* displays a stronger pretomanid-resistance phenotype than a mutant in *Rv1633*, we suspect that the phenotype of mutants in *Rv1633* may be due to a polar effect, and mutating *Rv1634* drives pretomanid resistance. Typically, a loss of function mutant in a drug efflux protein would confer susceptibility to an antibiotic. Yet, we observe that mutating *Rv1634* drives resistance to pretomanid. Our leading hypothesis is that pretomanid may enter the bacterial cell through *Rv1634*.

5.2.2 Future directions

The RB-TnSeq screens conducted this far in Mtb have allowed us to generate interesting hypotheses about the functions of genes. However, more mechanistic studies are now needed to test our hypotheses. For example, it will be important to biochemically assay that ability for *Rv1257c* to use D-lactate as a substrate. Likewise, to test our hypothesis that pretomanid can enter the cell through *Rv1634*, it will be important to conduct mass spectrometry to evaluate intracellular levels of pretomanid when *Rv1634* is mutated. Furthermore, complementation of mutant phenotypes is crucial for validating our results. We also plan to conduct mouse infections with our mutants of interest to evaluate their contribution to Mtb survival *in vivo*.

In the future, we will conduct more RB-TnSeq screens on tuberculosis-specific stressors such as oxidative stress, nitrosative stress, and acidic pH. We will also expose our RB-TnSeq library to a wider array of general and tuberculosis specific antibiotics. The more data that is generated from high-throughput genetic screens, the easier it will be to form hypothesizes about gene function. Elucidating the function of genes required for the survival of Mtb *in vivo* will be imperative in developing future treatments for tuberculosis.

References

1. World Health Organization. *Global Tuberculosis Report 2023*. (World Health Organization, 2023).
2. Houben, R. M. G. J. & Dodd, P. J. The Global Burden of Latent Tuberculosis Infection: A Re-estimation Using Mathematical Modelling. *PLoS Med.* **13**, e1002152 (2016).
3. Stephenson, L. & Byard, R. W. An atlas overview of characteristic features of tuberculosis that may be encountered at autopsy. *Forensic Sci. Med. Pathol.* **16**, 143–151 (2020).
4. Fedrizzi, T. *et al.* Genomic characterization of Nontuberculous Mycobacteria. *Sci. Rep.* **7**, 45258 (2017).
5. Gagneux, S. Ecology and evolution of Mycobacterium tuberculosis. *Nature Reviews Microbiology* vol. 16 202–213 Preprint at https://doi.org/10.1038/nrmicro.2018.8 (2018).
6. Jang, J., Becq, J., Gicquel, B., Deschavanne, P. & Neyrolles, O. Horizontally acquired genomic islands in the tubercle bacilli. *Trends Microbiol.* **16**, 303–308 (2008).
7. Price, J. V. & Vance, R. E. The macrophage paradox. *Immunity* **41**, 685–693 (2014).
8. Wang, J. *et al.* Insights on the emergence of Mycobacterium tuberculosis from the analysis of Mycobacterium kansasii. *Genome Biol. Evol.* **7**, 856–870 (2015).
9. Cole, S. T. *et al.* Deciphering the biology of Mycobacterium tuberculosis from the complete genome sequence. *Nature* **393**, 537–544 (1998).
10. Camilli, A., Merrell, D. S. & Mekalanos, J. J. CHAPTER 4 - Strategies to Identify Bacterial Pathogenicity Factors. in *Principles of Bacterial Pathogenesis* (ed. Groisman, E. A.) 133–177 (Academic Press, San Diego, 2001).
11. Cox, J. S., Chen, B., McNeil, M. & Jacobs, W. R., Jr. Complex lipid determines tissue-specific replication of Mycobacterium tuberculosis in mice. *Nature* **402**, 79–83 (1999).
12. Camacho, L. R., Ensergueix, D., Perez, E., Gicquel, B. & Guilhot, C. Identification of a virulence gene cluster of Mycobacterium tuberculosis by signature-tagged transposon mutagenesis. *Mol. Microbiol.* **34**, 257–267 (1999).
13. Converse, S. E. *et al.* MmpL8 is required for sulfolipid-1 biosynthesis and *Mycobacterium tuberculosis* virulence. *Proc. Natl. Acad. Sci. U. S. A.* **100**, 6121–6126 (2003).
14. Rosas-Magallanes, V. *et al.* Signature-tagged transposon mutagenesis identifies novel Mycobacterium tuberculosis genes involved in the parasitism of human macrophages. *Infect. Immun.* **75**, 504–507 (2007).
15. Sassetti, C. M., Boyd, D. H. & Rubin, E. J. Genes required for mycobacterial growth defined by high density mutagenesis. *Mol. Microbiol.* **48**, 77–84 (2003).
16. Rengarajan, J., Bloom, B. R. & Rubin, E. J. From The Cover: Genome-wide requirements for Mycobacterium tuberculosis adaptation and survival in macrophages. *Proceedings of the National Academy of Sciences* **102**, 8327–8332 (2005).
17. Sassetti, C. M. & Rubin, E. J. Genetic requirements for mycobacterial survival during infection. *Proc. Natl. Acad. Sci. U. S. A.* **100**, 12989–12994 (2003).
18. Griffin, J. E. *et al.* High-resolution phenotypic profiling defines genes essential for mycobacterial growth and cholesterol catabolism. *PLoS Pathog.* **7**, 1–9 (2011).

19. DeJesus, M. A. *et al.* Comprehensive Essentiality Analysis of the Mycobacterium tuberculosis Genome via Saturating Transposon Mutagenesis. *MBio* **8**, 1–17 (2017).
20. Smith, C. M. *et al.* Host-pathogen genetic interactions underlie tuberculosis susceptibility in genetically diverse mice. *Elife* **11**, (2022).
21. Lien, K. A. *et al.* A nanocompartment system contributes to defense against oxidative stress in Mycobacterium tuberculosis. *Elife* **10**, (2021).
22. Rittershaus, E. S. C. *et al.* A Lysine Acetyltransferase Contributes to the Metabolic Adaptation to Hypoxia in Mycobacterium tuberculosis. *Cell Chem Biol* **25**, 1495-1505.e3 (2018).
23. Xu, W. *et al.* Chemical Genetic Interaction Profiling Reveals Determinants of Intrinsic Antibiotic Resistance in Mycobacterium tuberculosis. *Antimicrob. Agents Chemother.* **61**, (2017).
24. Long, J. E. *et al.* Identifying essential genes in Mycobacterium tuberculosis by global phenotypic profiling. *Methods Mol. Biol.* **1279**, 79–95 (2015).
25. Dejesus, M. A., Ambadipudi, C., Baker, R., Sassetti, C. & Ioerger, T. R. TRANSIT-A Software Tool for Himar1 TnSeq Analysis. (2015) doi:10.1371/journal.pcbi.1004401.
26. Wetmore, K. M. *et al.* Rapid Quantification of Mutant Fitness in Diverse Bacteria by Sequencing Randomly Bar-Coded Transposons. *MBio* **6**, e00306-15 (2015).
27. Choudhary, E., Thakur, P., Pareek, M. & Agarwal, N. Gene silencing by CRISPR interference in mycobacteria. *Nat. Commun.* **6**, 6267 (2015).
28. Rock, J. M. *et al.* Programmable transcriptional repression in mycobacteria using an orthogonal CRISPR interference platform. (2017) doi:10.1038/nmicrobiol.2016.274.
29. Bosch, B. *et al.* Genome-wide gene expression tuning reveals diverse vulnerabilities of M. tuberculosis. *Cell* **184**, 4579-4592.e24 (2021).
30. Li, S. *et al.* CRISPRi chemical genetics and comparative genomics identify genes mediating drug potency in Mycobacterium tuberculosis. *Nat Microbiol* **7**, 766–779 (2022).
31. Modlin, S. J. *et al.* Structure-Aware Mycobacterium tuberculosis Functional Annotation Uncloaks Resistance, Metabolic, and Virulence Genes. *mSystems* **6**, e0067321 (2021).
32. Nathan, C. F., Murray, H. W., Wiebe, M. E. & Rubin, B. Y. Identification of interferon-gamma as the lymphokine that activates human macrophage oxidative metabolism and antimicrobial activity. *J. Exp. Med.* **158**, 670–689 (1983).
33. Miller, R. A. & Britigan, B. E. Role of oxidants in microbial pathophysiology. *Clin. Microbiol. Rev.* **10**, 1–18 (1997).
34. Bogdan, C., Röllinghoff, M. & Diefenbach, A. Reactive oxygen and reactive nitrogen intermediates in innate and specific immunity. *Curr. Opin. Immunol.* **12**, 64–76 (2000).
35. Piddington, D. L. *et al.* Cu,Zn superoxide dismutase of Mycobacterium tuberculosis contributes to survival in activated macrophages that are generating an oxidative burst. *Infect. Immun.* **69**, 4980–4987 (2001).
36. Harth, G. & Horwitz, M. A. Export of recombinant Mycobacterium tuberculosis superoxide dismutase is dependent upon both information in the protein and mycobacterial export machinery. A model for studying export of leaderless proteins by pathogenic mycobacteria. *J. Biol. Chem.* **274**, 4281–4292 (1999).

37. Zhang, Y., Lathigra, R., Garbe, T., Catty, D. & Young, D. Genetic analysis of superoxide dismutase, the 23 kilodalton antigen of Mycobacterium tuberculosis. *Mol. Microbiol.* **5**, 381–391 (1991).
38. Mishra, S. & Imlay, J. Why do bacteria use so many enzymes to scavenge hydrogen peroxide? *Arch. Biochem. Biophys.* **525**, 145–160 (2012).
39. Marcinkeviciene, J. A., Magliozzo, R. S. & Blanchard, J. S. Purification and characterization of the Mycobacterium smegmatis catalase-peroxidase involved in isoniazid activation. *J. Biol. Chem.* **270**, 22290–22295 (1995).
40. Manca, C., Paul, S., Barry, C. E., 3rd, Freedman, V. H. & Kaplan, G. Mycobacterium tuberculosis catalase and peroxidase activities and resistance to oxidative killing in human monocytes in vitro. *Infect. Immun.* **67**, 74–79 (1999).
41. Wengenack, N. L., Jensen, M. P., Rusnak, F. & Stern, M. K. Mycobacterium tuberculosis KatG is a peroxynitritase. *Biochem. Biophys. Res. Commun.* **256**, 485–487 (1999).
42. Hillas, P. J., del Alba, F. S., Oyarzabal, J., Wilks, A. & Ortiz De Montellano, P. R. The AhpC and AhpD antioxidant defense system of Mycobacterium tuberculosis. *J. Biol. Chem.* **275**, 18801–18809 (2000).
43. Bryk, R., Griffin, P. & Nathan, C. Peroxynitrite reductase activity of bacterial peroxiredoxins. *Nature* **407**, 211–215 (2000).
44. Newton, G. L. & Fahey, R. C. Mycothiol biochemistry. *Arch. Microbiol.* **178**, 388–394 (2002).
45. Buchmeier, N. A., Newton, G. L., Koledin, T. & Fahey, R. C. Association of mycothiol with protection of Mycobacterium tuberculosis from toxic oxidants and antibiotics. *Mol. Microbiol.* **47**, 1723–1732 (2003).
46. Chan, J., Fan, X. D., Hunter, S. W., Brennan, P. J. & Bloom, B. R. Lipoarabinomannan, a possible virulence factor involved in persistence of Mycobacterium tuberculosis within macrophages. *Infect. Immun.* **59**, 1755–1761 (1991).
47. Armstrong, J. A. & Hart, A. *RESPONSE OF CULTURED MACROPHAGES TO MYCOBAC-TERIUM TUBERCULOSIS, WITH OBSERVATIONS ON FUSION OF LYSOSOMES WITH PHAGOSOMES*. https://rupress.org/jem/article-pdf/134/3/713/471805/713.pdf.
48. MacMicking, J. D., Taylor, G. A. & McKinney, J. D. Immune control of tuberculosis by IFN-gamma-inducible LRG-47. *Science* **302**, 654–659 (2003).
49. Vandal, O. H., Nathan, C. F. & Ehrt, S. Acid resistance in Mycobacterium tuberculosis. *Journal of Bacteriology* vol. 191 4714–4721 Preprint at https://doi.org/10.1128/JB.00305-09 (2009).
50. Turk, V., Turk, B. & Turk, D. Lysosomal cysteine proteases: facts and opportunities. *EMBO J.* **20**, 4629–4633 (2001).
51. Vandal, O. H., Pierini, L. M., Schnappinger, D., Nathan, C. F. & Ehrt, S. A membrane protein preserves intrabacterial pH in intraphagosomal Mycobacterium tuberculosis. *Nat. Med.* **14**, 849–854 (2008).
52. Vandal, O. H. *et al.* Acid-susceptible mutants of mycobacterium tuberculosis share hypersusceptibility to cell wall and oxidative stress and to the host environment. *J. Bacteriol.* **191**, 625–631 (2009).

53. Buchmeier, N. *et al.* A parallel intraphagosomal survival strategy shared by Mycobacterium tuberculosis and Salmonella enterica. *Mol. Microbiol.* **35**, 1375–1382 (2002).
54. Fisher, M. A., Plikaytis, B. B. & Shinnick, T. M. Microarray analysis of the Mycobacterium tuberculosis transcriptional response to the acidic conditions found in phagosomes. *J. Bacteriol.* **184**, 4025–4032 (2002).
55. Rohde, K. H., Abramovitch, R. B. & Russell, D. G. Mycobacterium tuberculosis invasion of macrophages: linking bacterial gene expression to environmental cues. *Cell Host Microbe* **2**, 352–364 (2007).
56. Gouzy, A., Healy, C., Black, K. A., Rhee, K. Y. & Ehrt, S. Growth of *Mycobacterium tuberculosis* at acidic pH depends on lipid assimilation and is accompanied by reduced GAPDH activity. *Proc. Natl. Acad. Sci. U. S. A.* **118**, (2021).
57. de Carvalho, L. P. S. *et al.* Metabolomics of Mycobacterium tuberculosis reveals compartmentalized co-catabolism of carbon substrates. *Chem. Biol.* **17**, 1122–1131 (2010).
58. Pethe, K. *et al.* A chemical genetic screen in Mycobacterium tuberculosis identifies carbon-source-dependent growth inhibitors devoid of in vivo efficacy. *Nat. Commun.* **1**, 57 (2010).
59. Schnappinger, D. *et al.* Transcriptional Adaptation of Mycobacterium tuberculosis within Macrophages: Insights into the Phagosomal Environment. *J. Exp. Med.* **198**, 693–704 (2003).
60. Timm, J. *et al.* Differential expression of iron-, carbon-, and oxygen-responsive mycobacterial genes in the lungs of chronically infected mice and tuberculosis patients. *Proc. Natl. Acad. Sci. U. S. A.* **100**, 14321–14326 (2003).
61. Kalscheuer, R., Weinrick, B., Veeraraghavan, U., Besra, G. S. & Jacobs, W. R. Trehalose-recycling ABC transporter LpqY-SugA-SugB-SugC is essential for virulence of Mycobacterium tuberculosis. *Proc. Natl. Acad. Sci. U. S. A.* **107**, 21761–21766 (2010).
62. Marrero, J., Rhee, K. Y., Schnappinger, D., Pethe, K. & Ehrt, S. Gluconeogenic carbon flow of tricarboxylic acid cycle intermediates is critical for Mycobacterium tuberculosis to establish and maintain infection. *Proceedings of the National Academy of Sciences* **107**, 9819–9824 (2010).
63. Amalia, F. *et al.* The Role of Amino Acids in Tuberculosis Infection: A Literature Review. *Metabolites* **12**, (2022).
64. Bloch, H. & Segal, W. Biochemical differentiation of Mycobacterium tuberculosis grown in vivo and in vitro. *J. Bacteriol.* **72**, 132–141 (1956).
65. McKinney, J. D. *et al.* Persistence of Mycobacterium tuberculosis in macrophages and mice requires the glyoxylate shunt enzyme isocitrate lyase. *Nature* **406**, 735–738 (2000).
66. Muñoz-Elías, E. J. & McKinney, J. D. Mycobacterium tuberculosis isocitrate lyases 1 and 2 are jointly required for in vivo growth and virulence. *Nat. Med.* **11**, 638–644 (2005).
67. Muñoz-Elías, E. J., Upton, A. M., Cherian, J. & McKinney, J. D. Role of the methylcitrate cycle in Mycobacterium tuberculosis metabolism, intracellular growth, and virulence. *Mol. Microbiol.* **60**, 1109–1122 (2006).

68. Gouzy, A., Poquet, Y. & Neyrolles, O. *Nitrogen Metabolism in Mycobacterium Tuberculosis Physiology and Virulence*. vol. 12 http://dx.doi.org/10.1038/nrmicro3349 (2014).
69. Niederweis, M. Nutrient acquisition by mycobacteria. *Microbiology* **154**, 679–692 (2008).
70. Song, H. & Niederweis, M. Uptake of sulfate but not phosphate by Mycobacterium tuberculosis is slower than that for Mycobacterium smegmatis. *J. Bacteriol.* **194**, 956–964 (2012).
71. Viljoen, A. J., Kirsten, C. J., Baker, B., van Helden, P. D. & Wiid, I. J. F. The role of glutamine oxoglutarate aminotransferase and glutamate dehydrogenase in nitrogen metabolism in Mycobacterium bovis BCG. *PLoS One* **8**, e84452 (2013).
72. Giffin, M. M., Raab, R. W., Morganstern, M. & Sohaskey, C. D. Mutational analysis of the respiratory nitrate transporter NarK2 of Mycobacterium tuberculosis. *PLoS One* **7**, e45459 (2012).
73. Beste, D. J. V. *et al.* 13C-flux spectral analysis of host-pathogen metabolism reveals a mixed diet for intracellular Mycobacterium tuberculosis. *Chem. Biol.* **20**, 1012–1021 (2013).
74. Gouzy, A. *et al.* Mycobacterium tuberculosis nitrogen assimilation and host colonization require aspartate. (2013) doi:10.1038/nchembio.1355.
75. Gouzy, A. *et al.* Mycobacterium tuberculosis Exploits Asparagine to Assimilate Nitrogen and Resist Acid Stress during Infection. doi:10.1371/journal.ppat.1003928.
76. Tailleux, L. *et al.* Probing host pathogen cross-talk by transcriptional profiling of both Mycobacterium tuberculosis and infected human dendritic cells and macrophages. *PLoS One* **3**, e1403 (2008).
77. El-Benna, J., Dang, P. M.-C., Gougerot-Pocidalo, M. A., Marie, J. C. & Braut-Boucher, F. p47phox, the phagocyte NADPH oxidase/NOX2 organizer: structure, phosphorylation and implication in diseases. *Exp. Mol. Med.* **41**, 217–225 (2009).
78. Nathan, C. Neutrophils and immunity: challenges and opportunities. *Nat. Rev. Immunol.* **6**, 173–182 (2006).
79. Segal, A. W. How neutrophils kill microbes. *Annu. Rev. Immunol.* **23**, 197–223 (2005).
80. Chan, J., Xing, Y., Magliozzo, R. S. & Bloom, B. R. Killing of virulent Mycobacterium tuberculosis by reactive nitrogen intermediates produced by activated murine macrophages. *J. Exp. Med.* **175**, 1111–1122 (1992).
81. Ehrt, S. & Schnappinger, D. Mycobacterial survival strategies in the phagosome: Defence against host stresses. *Cellular Microbiology* vol. 11 1170–1178 Preprint at https://doi.org/10.1111/j.1462-5822.2009.01335.x (2009).
82. Nambi, S. *et al.* The oxidative stress network of Mycobacterium tuberculosis reveals coordination between radical detoxification systems HHS Public Access. *Cell Host Microbe* **17**, 829–837 (2015).
83. Voskuil, M. I., Bartek, I. L., Visconti, K. & Schoolnik, G. K. The response of mycobacterium tuberculosis to reactive oxygen and nitrogen species. *Front. Microbiol.* **2**, 105 (2011).
84. Singh, R. & Eltis, L. D. The multihued palette of dye-decolorizing peroxidases. (2015) doi:10.1016/j.abb.2015.01.014.

85. Brown, M. E., Barros, T. & Chang, M. C. Y. Identification and characterization of a multifunctional dye peroxidase from a lignin-reactive bacterium. *ACS Chem. Biol.* **7**, 2074–2081 (2012).
86. Uchida, T., Sasaki, M., Tanaka, Y. & Ishimori, K. A Dye-Decolorizing Peroxidase from Vibrio cholerae. *Biochemistry* **54**, 6610–6621 (2015).
87. Contreras, H. *et al.* Characterization of a Mycobacterium tuberculosis Nanocompartment and Its Potential Cargo Proteins * and the. (2014) doi:10.1074/jbc.M114.570119.
88. Ferousi, C. *et al.* Iron assimilation and utilization in anaerobic ammonium oxidizing bacteria. *Curr. Opin. Chem. Biol.* **37**, 129–136 (2017).
89. Kerfeld, C. A., Aussignargues, C., Zarzycki, J., Cai, F. & Sutter, M. Bacterial microcompartments. *Nat. Rev. Microbiol.* **16**, 277–290 (2018).
90. Uebe, R. & Schüler, D. Magnetosome biogenesis in magnetotactic bacteria. *Nat. Rev. Microbiol.* **14**, 621–637 (2016).
91. Giessen, T. W. *et al.* Large protein organelles form a new iron sequestration system with high storage capacity. *Elife* **8**, (2019).
92. Nichols, R. J., Cassidy-Amstutz, C., Chaijarasphong, T. & Savage, D. F. Critical Reviews in Biochemistry and Molecular Biology Encapsulins: molecular biology of the shell. (2017) doi:10.1080/10409238.2017.1337709.
93. Giessen, T. W. & Silver, P. A. Widespread distribution of encapsulin nanocompartments reveals functional diversity. *Nature Microbiology* **2**, 1–11 (2017).
94. Nichols, R. J. *et al.* Discovery and characterization of a novel family of prokaryotic nanocompartments involved in sulfur metabolism. *Elife* **10**, (2021).
95. McHugh, C. A. *et al.* A virus capsid-like nanocompartment that stores iron and protects bacteria from oxidative stress. *EMBO J.* **33**, 1896–1911 (2014).
96. Zhang, Y. J. *et al.* Tryptophan biosynthesis protects mycobacteria from CD4 T-Cell-mediated Killing. *Cell* **155**, 1296–1308 (2013).
97. Weldingh, K. & Andersen, P. Immunological evaluation of novel Mycobacterium tuberculosis culture filtrate proteins. *FEMS Immunol. Med. Microbiol.* **23**, 159–164 (1999).
98. Rosenkrands, I. *et al.* Identification and characterization of a 29-kilodalton protein from Mycobacterium tuberculosis culture filtrate recognized by mouse memory effector cells. *Infect. Immun.* **66**, 2728–2735 (1998).
99. Cassidy-Amstutz, C. *et al.* Identification of a Minimal Peptide Tag for in Vivo and in Vitro Loading of Encapsulin. (2016) doi:10.1021/acs.biochem.6b00294.
100. Ahmad, M. *et al.* Identification of DypB from Rhodococcus jostii RHA1 as a lignin peroxidase. *Biochemistry* **50**, 5096–5107 (2011).
101. Bhaskar, A. *et al.* Reengineering redox sensitive GFP to measure mycothiol redox potential of Mycobacterium tuberculosis during infection. *PLoS Pathog.* **10**, e1003902 (2014).
102. Griffin, J. E. *et al.* Cholesterol catabolism by Mycobacterium tuberculosis requires transcriptional and metabolic adaptations. *Chem. Biol.* **19**, 218–227 (2012).
103. van Opijnen, T. & Camilli, A. Transposon insertion sequencing: a new tool for systems-level analysis of microorganisms. *Nat. Rev. Microbiol.* **11**, 435–442 (2013).

104. Li, Z., Kelley, C., Collins, F., Rouse, D. & Morris, S. Expression of katG in Mycobacterium tuberculosis is associated with its growth and persistence in mice and guinea pigs. *J. Infect. Dis.* **177**, 1030–1035 (1998).
105. Pym, A. S., Saint-Joanis, B. & Cole, S. T. Effect of katG mutations on the virulence of Mycobacterium tuberculosis and the implication for transmission in humans. *Infect. Immun.* **70**, 4955–4960 (2002).
106. Seifert, M., Catanzaro, D., Catanzaro, A. & Rodwell, T. C. Genetic mutations associated with isoniazid resistance in Mycobacterium tuberculosis: a systematic review. *PLoS One* **10**, e0119628 (2015).
107. DeVito, J. A. & Morris, S. Exploring the structure and function of the mycobacterial KatG protein using trans-dominant mutants. *Antimicrob. Agents Chemother.* **47**, 188–195 (2003).
108. Mo, L. *et al.* Three-dimensional model and molecular mechanism of Mycobacterium tuberculosis catalase-peroxidase (KatG) and isoniazid-resistant KatG mutants. *Microb. Drug Resist.* **10**, 269–279 (2004).
109. Wei, C.-J., Lei, B., Musser, J. M. & Tu, S.-C. Isoniazid activation defects in recombinant Mycobacterium tuberculosis catalase-peroxidase (KatG) mutants evident in InhA inhibitor production. *Antimicrob. Agents Chemother.* **47**, 670–675 (2003).
110. Nieto R, L. M. *et al.* Virulence of Mycobacterium tuberculosis after Acquisition of Isoniazid Resistance: Individual Nature of katG Mutants and the Possible Role of AhpC. *PLoS One* **11**, e0166807 (2016).
111. Kim, M.-J. *et al.* Caseation of human tuberculosis granulomas correlates with elevated host lipid metabolism. *EMBO Mol. Med.* **2**, 258–274 (2010).
112. Russell, D. G. Mycobacterium tuberculosis and the intimate discourse of a chronic infection. *Immunol. Rev.* **240**, 252–268 (2011).
113. Russell, D. G., Huang, L. & VanderVen, B. C. Immunometabolism at the interface between macrophages and pathogens. *Nat. Rev. Immunol.* **19**, 291–304 (2019).
114. Nazarova, E. V. *et al.* The genetic requirements of fatty acid import by Mycobacterium tuberculosis within macrophages. *Elife* **8**, (2019).
115. Sankaranarayanan, S. *et al.* Serum albumin acts as a shuttle to enhance cholesterol efflux from cells. *J. Lipid Res.* **54**, 671–676 (2013).
116. van der Vusse, G. J. Albumin as fatty acid transporter. *Drug Metab. Pharmacokinet.* **24**, 300–307 (2009).
117. Abdelmagid, S. A. *et al.* Comprehensive profiling of plasma fatty acid concentrations in young healthy Canadian adults. *PLoS One* **10**, e0116195 (2015).
118. Kempker, R. R. *et al.* Lung Tissue Concentrations of Pyrazinamide among Patients with Drug-Resistant Pulmonary Tuberculosis. *Antimicrob. Agents Chemother.* **61**, (2017).
119. Jakobson, C. M. & Tullman-Ercek, D. Dumpster Diving in the Gut: Bacterial Microcompartments as Part of a Host-Associated Lifestyle. *PLoS Pathog.* **12**, e1005558 (2016).
120. Snijder, J. *et al.* Assembly and mechanical properties of the cargo-free and cargo-loaded bacterial nanocompartment encapsulin. *Biomacromolecules* **17**, 2522–2529 (2016).

121. Rosenberg, O. S. *et al.* Substrates Control Multimerization and Activation of the Multi-Domain ATPase Motor of Type VII Secretion. *Cell* **161**, 501–512 (2015).
122. Ehrt, S. *et al.* Controlling gene expression in mycobacteria with anhydrotetracycline and Tet repressor. *Nucleic Acids Res.* **33**, e21 (2005).
123. Larsen, M. H., Biermann, K. & Jacobs, W. R., Jr. Laboratory maintenance of Mycobacterium tuberculosis. *Curr. Protoc. Microbiol.* **Chapter 10**, Unit 10A.1 (2007).
124. Lyons, T. W., Reinhard, C. T. & Planavsky, N. J. The rise of oxygen in Earth's early ocean and atmosphere. *Nature* **506**, 307–315 (2014).
125. Fasnacht, M. & Polacek, N. Oxidative Stress in Bacteria and the Central Dogma of Molecular Biology. *Front Mol Biosci* **8**, 671037 (2021).
126. Falzon, D., Zignol, M., Bastard, M., Floyd, K. & Kasaeva, T. The impact of the COVID-19 pandemic on the global tuberculosis epidemic. *Front. Immunol.* **14**, 1234785 (2023).
127. Sparks, I. L., Derbyshire, K. M., Jacobs, W. R., Jr & Morita, Y. S. Mycobacterium smegmatis: The Vanguard of Mycobacterial Research. *J. Bacteriol.* **205**, e0033722 (2023).
128. Lee, M.-R. *et al.* Mycobacterium abscessus Complex Infections in Humans. *Emerg. Infect. Dis.* **21**, 1638–1646 (2015).
129. Li, G. *et al.* Antimicrobial susceptibility of standard strains of nontuberculous mycobacteria by microplate Alamar Blue assay. *PLoS One* **8**, e84065 (2013).
130. Charles L. Daley, Jonathan M. Iaccarino, Jr, Christoph Lange, Emmanuelle Cambau, Richard J. Wallace, Claire Andrejak, Erik C. B&ouml, van Ingen Dirk Wagner, T. J. B. D. E. G. L. G. G. A. H. S. L. K. P. L. T. K. M. K. N. O. M. S. J. E. S. E. T. J. & Winthrop, K. L. Treatment of Nontuberculous Mycobacterial Pulmonary Disease: An Official ATS/ERS/ESCMID/IDSA Clinical Practice Guideline. https://www.idsociety.org/practice-guideline/nontuberculous-mycobacterial-ntm-diseases/.
131. Das, M., Dewan, A., Shee, S. & Singh, A. The Multifaceted Bacterial Cysteine Desulfurases: From Metabolism to Pathogenesis. *Antioxidants (Basel)* **10**, (2021).
132. Nicholson, M. L. & Laudenbach, D. E. Genes encoded on a cyanobacterial plasmid are transcriptionally regulated by sulfur availability and CysR. *J. Bacteriol.* **177**, 2143–2150 (1995).
133. Chen, Y., Holtman, C. K., Magnuson, R. D., Youderian, P. A. & Golden, S. S. The complete sequence and functional analysis of pANL, the large plasmid of the unicellular freshwater cyanobacterium Synechococcus elongatus PCC 7942. *Plasmid* **59**, 176–192 (2008).
134. Hunter, S. W., Rivoire, B., Mehra, V., Bloom, B. R. & Brennan, P. J. The major native proteins of the leprosy bacillus. *J. Biol. Chem.* **265**, 14065–14068 (1990).
135. Britton, W. J., Hellqvist, L., Ivanyi, J. & Basten, A. Immunopurification of radiolabelled antigens of Mycobacterium leprae and Mycobacterium bovis (bacillus Calmette-Guerin) with monoclonal antibodies. *Scand. J. Immunol.* **26**, 149–159 (1987).
136. Ivanyi, J. *et al.* Definition of species specific and cross-reactive antigenic determinants of Mycobacterium leprae using monoclonal antibodies. *Clin. Exp. Immunol.* **52**, 528–536 (1983).
137. Winter, N. *et al.* Characterization of the gene encoding the immunodominant 35 kDa protein of Mycobacterium leprae. *Mol. Microbiol.* **16**, 865–876 (1995).

138. Gelber, R. H. *et al.* Effective vaccination of mice against leprosy bacilli with subunits of Mycobacterium leprae. *Infect. Immun.* **58**, 711–718 (1990).
139. Abdellrazeq, G. S. *et al.* A Mycobacterium avium subsp. paratuberculosis relA deletion mutant and a 35 kDa major membrane protein elicit development of cytotoxic T lymphocytes with ability to kill intracellular bacteria. *Vet. Res.* **49**, 53 (2018).
140. Bannantine, J. P., Huntley, J. F. J., Miltner, E., Stabel, J. R. & Bermudez, L. E. The Mycobacterium avium subsp. paratuberculosis 35 kDa protein plays a role in invasion of bovine epithelial cells. *Microbiology* **149**, 2061–2069 (2003).
141. Murphy, K. C. *et al.* ORBIT: a New Paradigm for Genetic Engineering of Mycobacterial Chromosomes. *MBio* **9**, (2018).
142. Boshoff, H. I. & Mizrahi, V. Expression of Mycobacterium smegmatis pyrazinamidase in Mycobacterium tuberculosis confers hypersensitivity to pyrazinamide and related amides. *J. Bacteriol.* **182**, 5479–5485 (2000).
143. Flynn, J. L. *et al.* An essential role for interferon gamma in resistance to Mycobacterium tuberculosis infection. *J. Exp. Med.* **178**, 2249–2254 (1993).
144. Ng, V. H., Cox, J. S., Sousa, A. O., MacMicking, J. D. & McKinney, J. D. Role of KatG catalase-peroxidase in mycobacterial pathogenesis: countering the phagocyte oxidative burst. *Mol. Microbiol.* **52**, 1291–1302 (2004).
145. Brook, I. Inoculum effect. *Rev. Infect. Dis.* **11**, 361–368 (1989).
146. Udekwu, K. I., Parrish, N., Ankomah, P., Baquero, F. & Levin, B. R. Functional relationship between bacterial cell density and the efficacy of antibiotics. *J. Antimicrob. Chemother.* **63**, 745–757 (2009).
147. Weinert, L. A. & Welch, J. J. Why Might Bacterial Pathogens Have Small Genomes? *Trends Ecol. Evol.* **32**, 936–947 (2017).
148. ten Bokum, A. M. C., Movahedzadeh, F., Frita, R., Bancroft, G. J. & Stoker, N. G. The case for hypervirulence through gene deletion in Mycobacterium tuberculosis. *Trends Microbiol.* **16**, 436–441 (2008).
149. Stinear, T. P. *et al.* Insights from the complete genome sequence of Mycobacterium marinum on the evolution of Mycobacterium tuberculosis. *Genome Res.* **18**, 729–741 (2008).
150. Deretic, V., Song, J. & Pagán-Ramos, E. Loss of oxyR in Mycobacterium tuberculosis. *Trends Microbiol.* **5**, 367–372 (1997).
151. Hurst-Hess, K. *et al.* Mycobacterial SigA and SigB Cotranscribe Essential Housekeeping Genes during Exponential Growth. *MBio* **10**, (2019).
152. Sachdeva, P., Misra, R., Tyagi, A. K. & Singh, Y. The sigma factors of Mycobacterium tuberculosis: regulation of the regulators. *FEBS J.* **277**, 605–626 (2010).
153. Iwao, Y. & Nakata, N. Roles of the three Mycobacterium smegmatis katG genes for peroxide detoxification and isoniazid susceptibility. *Microbiol. Immunol.* **62**, 158–167 (2018).
154. Fregnan, G. B. & Smith, D. W. Description of various colony forms of mycobacteria. *J. Bacteriol.* **83**, 819–827 (1962).
155. Barrow, W. W., Ullom, B. P. & Brennan, P. J. Peptidoglycolipid nature of the superficial cell wall sheath of smooth-colony-forming mycobacteria. *J. Bacteriol.* **144**, 814–822 (1980).

156. Schaefer, W. B., Davis, C. L. & Cohn, M. L. Pathogenicity of transparent, opaque, and rough variants of Mycobacterium avium in chickens and mice. *Am. Rev. Respir. Dis.* **102**, 499–506 (1970).
157. Kocíncová, D. *et al.* Spontaneous transposition of IS1096 or ISMsm3 leads to glycopeptidolipid overproduction and affects surface properties in Mycobacterium smegmatis. *Tuberculosis* **88**, 390–398 (2008).
158. Chen, J. M. *et al.* Roles of Lsr2 in colony morphology and biofilm formation of Mycobacterium smegmatis. *J. Bacteriol.* **188**, 633–641 (2006).
159. Báez-Ramírez, E. *et al.* Elimination of PknL and MSMEG_4242 in Mycobacterium smegmatis alters the character of the outer cell envelope and selects for mutations in Lsr2. *Cell Surf* **7**, 100060 (2021).
160. Rivera-Marrero, C. A., Ritzenthaler, J. D., Newburn, S. A., Roman, J. & Cummings, R. D. Molecular cloning and expression of a novel glycolipid sulfotransferase in Mycobacterium tuberculosis. *Microbiology* **148**, 783–792 (2002).
161. Rea, R., Hill, C. & Gahan, C. G. M. Listeria monocytogenes PerR mutants display a small-colony phenotype, increased sensitivity to hydrogen peroxide, and significantly reduced murine virulence. *Appl. Environ. Microbiol.* **71**, 8314–8322 (2005).
162. Yin, H., Xu, L. & Porter, N. A. Free Radical Lipid Peroxidation: Mechanisms and Analysis. *Chem. Rev.* **111**, 5944–5972 (2011).
163. Goyal, N., Kashyap, B., Singh, N. P. & Kaur, I. R. Neopterin and oxidative stress markers in the diagnosis of extrapulmonary tuberculosis. *Biomarkers* **22**, 648–653 (2017).
164. Yadav, U. C. S. & Ramana, K. V. Regulation of NF-í µí¼ B-Induced Inflammatory Signaling by Lipid Peroxidation-Derived Aldehydes. *Oxid. Med. Cell. Longev.* **2013**, 11 (2013).
165. Laval, T. *et al.* De novo synthesized polyunsaturated fatty acids operate as both host immunomodulators and nutrients for Mycobacterium tuberculosis. *Elife* **10**, (2021).
166. Glickman, M. S., Cox, J. S. & Jacobs, W. R., Jr. A novel mycolic acid cyclopropane synthetase is required for cording, persistence, and virulence of Mycobacterium tuberculosis. *Mol. Cell* **5**, 717–727 (2000).
167. Tuberculosis. https://www.who.int/news-room/fact-sheets/detail/tuberculosis.
168. CDCTB. Treatment for TB Disease. *Centers for Disease Control and Prevention* https://www.cdc.gov/tb/topic/treatment/tbdisease.htm (2024).
169. Blattner, F. R. *et al.* The complete genome sequence of Escherichia coli K-12. *Science* **277**, 1453–1462 (1997).
170. Gawronski, J. D., Wong, S. M. S., Giannoukos, G., Ward, D. V. & Akerley, B. J. Tracking insertion mutants within libraries by deep sequencing and a genome-wide screen for Haemophilus genes required in the lung. *Proc. Natl. Acad. Sci. U. S. A.* **106**, 16422–16427 (2009).
171. Langridge, G. C. *et al.* Simultaneous assay of every Salmonella Typhi gene using one million transposon mutants. *Genome Res.* **19**, 2308–2316 (2009).
172. Goodman, A. L. *et al.* Identifying genetic determinants needed to establish a human gut symbiont in its habitat. *Cell Host Microbe* **6**, 279–289 (2009).
173. van Opijnen, T., Bodi, K. L. & Camilli, A. Tn-seq: high-throughput parallel sequencing for fitness and genetic interaction studies in microorganisms. *Nat. Methods* **6**, 767–772 (2009).

174. Zhang, Y. J. *et al.* Global assessment of genomic regions required for growth in Mycobacterium tuberculosis. *PLoS Pathog.* **8**, e1002946 (2012).
175. Meade, R. K. *et al.* Genome-wide screen identifies host loci that modulate Mycobacterium tuberculosis fitness in immunodivergent mice. *G3* **13**, (2023).
176. Price, M. N. *et al.* Mutant phenotypes for thousands of bacterial genes of unknown function. *Nature* **557**, 503–509 (2018).
177. Liu, H. *et al.* Functional genetics of human gut commensal Bacteroides thetaiotaomicron reveals metabolic requirements for growth across environments. *Cell Rep.* **34**, 108789 (2021).
178. Kennedy, M. S. *et al.* Dynamic genetic adaptation of Bacteroides thetaiotaomicron during murine gut colonization. *Cell Rep.* **42**, 113009 (2023).
179. Morth, J. P., Gosmann, S., Nowak, E. & Tucker, P. A. A novel two-component system found in Mycobacterium tuberculosis. *FEBS Lett.* **579**, 4145–4148 (2005).
180. Mehta, D., Koottathazhath, A. & Ramesh, A. Discovery of ANTAR-RNAs and their Mechanism of Action in Mycobacteria. *J. Mol. Biol.* **432**, 4032–4048 (2020).
181. Lee, W., VanderVen, B. C., Fahey, R. J. & Russell, D. G. Intracellular Mycobacterium tuberculosis exploits host-derived fatty acids to limit metabolic stress. *J. Biol. Chem.* **288**, 6788–6800 (2013).
182. Iqbal, I. K., Bajeli, S., Akela, A. K. & Kumar, A. Bioenergetics of Mycobacterium: An Emerging Landscape for Drug Discovery. *Pathogens* **7**, (2018).
183. Awasthy, D., Ambady, A., Narayana, A., Morayya, S. & Sharma, U. Roles of the two type II NADH dehydrogenases in the survival of Mycobacterium tuberculosis in vitro. *Gene* **550**, 110–116 (2014).
184. Vilchèze, C., Weinrick, B., Leung, L. W. & Jacobs, W. R., Jr. Plasticity of Mycobacterium tuberculosis NADH dehydrogenases and their role in virulence. *Proc. Natl. Acad. Sci. U. S. A.* **115**, 1599–1604 (2018).
185. Beites, T. *et al.* Plasticity of the Mycobacterium tuberculosis respiratory chain and its impact on tuberculosis drug development. *Nat. Commun.* **10**, 4970 (2019).
186. Somashekar, B. S. *et al.* Metabolic profiling of lung granuloma in Mycobacterium tuberculosis infected guinea pigs: ex vivo 1H magic angle spinning NMR studies. *J. Proteome Res.* **10**, 4186–4195 (2011).
187. Kumar, R. *et al.* Immunometabolism of Phagocytes During Mycobacterium tuberculosis Infection. *Front Mol Biosci* **6**, 105 (2019).
188. Gleeson, L. E. *et al.* Cutting Edge: Mycobacterium tuberculosis Induces Aerobic Glycolysis in Human Alveolar Macrophages That Is Required for Control of Intracellular Bacillary Replication. *J. Immunol.* **196**, 2444–2449 (2016).
189. Braverman, J., Sogi, K. M., Benjamin, D., Nomura, D. K. & Stanley, S. A. HIF-1α Is an Essential Mediator of IFN-γ-Dependent Immunity to Mycobacterium tuberculosis. *J. Immunol.* **197**, 1287–1297 (2016).
190. Shi, L. *et al.* Infection with Mycobacterium tuberculosis induces the Warburg effect in mouse lungs. *Sci. Rep.* **5**, 18176 (2015).
191. Billig, S. *et al.* Lactate oxidation facilitates growth of Mycobacterium tuberculosis in human macrophages. *Sci. Rep.* **7**, 6484 (2017).
192. Stanley, S. *et al.* Ongoing evolution of the Mycobacterium tuberculosis lactate dehydrogenase reveals the pleiotropic effects of bacterial adaption to host pressure. *PLoS Pathog.* **20**, e1012050 (2024).

193. Dhananjayan, K. *et al.* Activation of Macrophages and Microglia by Interferon-γ and Lipopolysaccharide Increases Methylglyoxal Production: A New Mechanism in the Development of Vascular Complications and Cognitive Decline in Type 2 Diabetes Mellitus? *J. Alzheimers. Dis.* **59**, 467–479 (2017).
194. Prantner, D. *et al.* Classically activated mouse macrophages produce methylglyoxal that induces a TLR4- and RAGE-independent proinflammatory response. *J. Leukoc. Biol.* **109**, 605–619 (2021).
195. Rachman, H. *et al.* Critical role of methylglyoxal and AGE in mycobacteria-induced macrophage apoptosis and activation. *PLoS One* **1**, e29 (2006).
196. Lord, J. M. Glycolate oxidoreductase in Escherichia coli. *Biochim. Biophys. Acta* **267**, 227–237 (1972).
197. Bartho, J. D. *et al.* The crystal structure of Erwinia amylovora AmyR, a member of the YbjN protein family, shows similarity to type III secretion chaperones but suggests different cellular functions. *PLoS One* **12**, e0176049 (2017).
198. Chen, X., Shen, D. & Zhou, B. Analysis of the temperature-sensitive mutation of Escherichia coli pantothenate kinase reveals YbjN as a possible protein stabilizer. *Biochem. Biophys. Res. Commun.* **345**, 834–842 (2006).
199. Wang, D. *et al.* The orphan gene ybjN conveys pleiotropic effects on multicellular behavior and survival of Escherichia coli. *PLoS One* **6**, e25293 (2011).
200. WHO announces landmark changes in treatment of drug-resistant tuberculosis. https://www.who.int/news/item/15-12-2022-who-announces-landmark-changes-in-treatment-of-drug-resistant-tuberculosis.
201. Stover, C. K. *et al.* A small-molecule nitroimidazopyran drug candidate for the treatment of tuberculosis. *Nature* **405**, 962–966 (2000).
202. Gurumurthy, M. *et al.* Substrate specificity of the deazaflavin-dependent nitroreductase from Mycobacterium tuberculosis responsible for the bioreductive activation of bicyclic nitroimidazoles. *FEBS J.* **279**, 113–125 (2012).
203. Singh, R. *et al.* PA-824 kills nonreplicating Mycobacterium tuberculosis by intracellular NO release. *Science* **322**, 1392–1395 (2008).
204. Haver, H. L. *et al.* Mutations in genes for the F420 biosynthetic pathway and a nitroreductase enzyme are the primary resistance determinants in spontaneous in vitro-selected PA-824-resistant mutants of Mycobacterium tuberculosis. *Antimicrob. Agents Chemother.* **59**, 5316–5323 (2015).
205. Manjunatha, U. H. *et al.* Identification of a nitroimidazo-oxazine-specific protein involved in PA-824 resistance in Mycobacterium tuberculosis. *Proc. Natl. Acad. Sci. U. S. A.* **103**, 431–436 (2006).
206. Choi, K. P., Bair, T. B., Bae, Y. M. & Daniels, L. Use of transposon Tn5367 mutagenesis and a nitroimidazopyran-based selection system to demonstrate a requirement for fbiA and fbiB in coenzyme F(420) biosynthesis by Mycobacterium bovis BCG. *J. Bacteriol.* **183**, 7058–7066 (2001).
207. Battaglia, S. *et al.* Characterization of Genomic Variants Associated with Resistance to Bedaquiline and Delamanid in Naive Mycobacterium tuberculosis Clinical Strains. *J. Clin. Microbiol.* **58**, (2020).
208. Erhardt, H. *et al.* Disruption of individual nuo-genes leads to the formation of partially assembled NADH:ubiquinone oxidoreductase (complex I) in Escherichia coli. *Biochim. Biophys. Acta* **1817**, 863–871 (2012).

209. Velmurugan, K. *et al.* Mycobacterium tuberculosis nuoG is a virulence gene that inhibits apoptosis of infected host cells. *PLoS Pathog.* **3**, e110 (2007).
210. Gupta, S. *et al.* An Unconventional Hexacoordinated Flavohemoglobin from Mycobacterium tuberculosis*. *J. Biol. Chem.* **287**, 16435–16446 (2012).
211. Thakur, N. *et al.* New Insights Into the Function of Flavohemoglobin in Mycobacterium tuberculosis: Role as a NADPH-Dependent Disulfide Reductase and D-Lactate-Dependent Mycothione Reductase. *Front. Cell. Infect. Microbiol.* **11**, 796727 (2021).
212. Wang, D., Korban, S. S., Pusey, P. L. & Zhao, Y. AmyR is a novel negative regulator of amylovoran production in Erwinia amylovora. *PLoS One* **7**, e45038 (2012).